Chapter I

Introduction

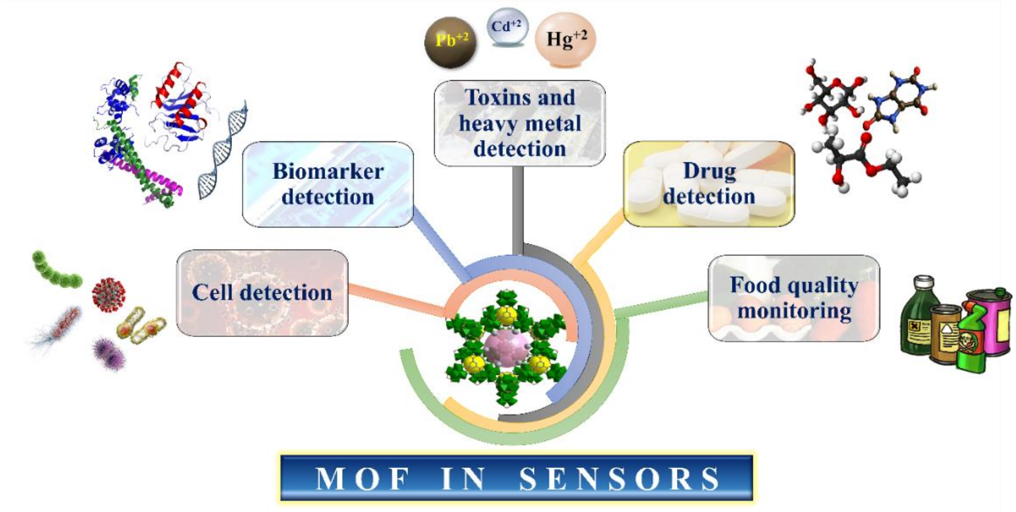

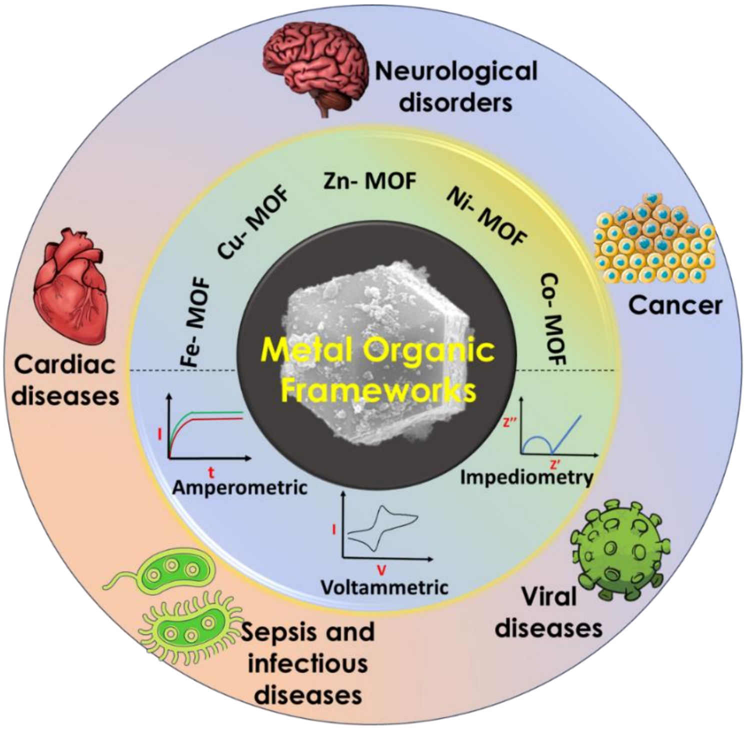

Shubhangi et al., Talanta 2024, 266, Part 2, 125124

Shubhangi et al., WIRES Nanomedicine and. Nanobiotecnology 2024, 16:e1980

1. General Introduction

Despite all of the medical advancements and sophisticated methods, universal healthcare is becoming a significant issue among all of the problems we face today. As a result, a healthy life for all people, regardless of age, is emphasized as a crucial component of sustainable development in the United Nations General Assembly's developmental plan, "Transforming our world: the 2030 agenda for sustainable development." On the other hand, disease outbreaks are getting more frequent in our globe. Because of a shift in lifestyle, a significant number of new cases of metabolic illnesses, such as obesity, diabetes, and even cancer, are now being found in younger populations. Despite the rapid development of improved drugs and cures, the number of new cases of cancer and the deaths associated with it are increasing annually. In the modern world, drug overdose and drug resistance-related illnesses are becoming serious issues. By identifying these cases as soon as feasible, the significant impact of such problems might be lessened. The diagnostic tools that identify these illnesses can also be used to document health problems for future monitoring, which is necessary for medication regimens.

A number of tools have been created to address these health concerns and are frequently employed in clinical sample analysis. Hospitals perform these biochemical tests using devices such as spectrophotometers, chromatography, and colorimetry. All of these tools search for biomarkers, which are molecules of biological or chemical origin linked to a specific condition. The concentration of these compounds changes beyond the clinical range in sick conditions. Therefore, the creation of POC devices can make advantage of these biomarkers. Despite their great strength, these devices have several drawbacks. They require a costly setup with skilled staff, a lengthy procedure, and a high sample volume. These restrictions impede the devices' portability, on-site detection, and speedy diagnosis.

To avoid such limitations in diagnosis, miniaturized devices have been developed to detect the biomarkers. Miniaturization of the devices would make them robust, reliable under emergency cases, and can be carried to remote locations easily.

1.1. Introduction to Biosensors

According to the International Union of Pure and Applied Chemistry, biosensor can be defined as "a device that uses specific biochemical reactions mediated by isolated enzymes, immune-systems, tissues, organelles or whole cells to detect chemical compounds usually by electrical, thermal, or optical signals".

A biosensor is a bio-analytical instrument that uses a variety of chemical or biological molecules with certain characteristics found in the sensing matrix to identify an analyte. The three main components of a biosensor are a processor, a transduction system, and biorecognition. Enzymes, antibodies, aptamers, entire cells, and other chemical or biological components that can interact with the analyte selectively are examples of biorecognition elements. Together with the biorecognition element, the transducer transforms this biorecognition event into a quantifiable signal. The transducer transforms the signal into various quantifiable forms after detecting changes in pH, temperature, charge, mass, etc.

An amplifier in the biosensor's following section reduces signal background noise and boosts weak signals so the analyte may be measured. After analyzing the data, the processor shows it on the digital display so that it can be further processed. New signal amplification techniques are integrated into the biosensor to attain better analytical results as a result of technological advancements.

Since its invention in 1956, biosensors have experienced remarkable growth and improvement. Clark created the first oxygen electrode sensor, which served as the basis for further studies in this field. This work served as the foundation for Yellow Spring Instruments' 1975 development of the YSI Model 23 Analyzer, the first commercially available glucose biosensor. In the ensuing decades, a plethora of novel commercial sensors, including as subcutaneous implantable in vivo glucose monitoring electrodes and self-testing blood glucose strips, inundated the market based on the biosensor's premise in order to detect glucose and other clinically significant molecules.

1.2. Classification of Biosensors

1.2.1. Biosensors can be classified based on the application of external labels, i.e. agents to facilitate the analytical performances of the sensors.

A. Label-free biosensors

Label-free biosensors are those that can detect the analyte without the use of an external label. No external label is required for sensing activity if the analyte is a redox-active molecule or if the biosensing matrix is made especially to interact with or catalyze the analyte. The majority of label-free biosensors are derived from potentiometry or impedimetric biosensors. Based on the shift in the resonant frequency of the matrix components, Maramatshu et al. created an unlabeled biosensor for the detection of immunoglobulin IgG. The sensor could distinguish between IgA and IgG. Using a label-free biosensor has the benefit of directly sensing the analyte, without the need for an immobilization step using a secondary antibody or tagged molecule.

B. Labeled biosensors

Biosensors are referred to as labeled biosensors when they use external labels to detect the analyte. The twofold confirmation of an analyte's existence is a benefit of utilizing a labeled tag. Additionally, a labeled tag (such as a fluorescence tag) can identify the presence of a single molecule in a sample, something that unlabeled biosensors find difficult to accomplish. The most widely used labels are fluorescently tagged DNA probes and different enzymes, such as horseradish peroxidase and alkaline phosphatase (ALP). Pallela et al. employed AuNP-polymer-antibody to capture the cell in order to create a labeled biosensor for the detection of metastatic cancer cells. For dual confirmation of the presence of cells, a secondary hydrazine-AuNP-Ab2 tag was employed, in which the analytical signal was produced by the catalysis of H_2O_2 by hydrazine. The disadvantages of using a tagged molecule lies in their sensitivity towards various environmental conditions (e.g. fluorescent tags are sensitive to incident light and interference from commonly coexisting molecules).

1.2.2. Sensors can also be classified on the basis of the type of transducer used, as discussed further:

A. Optical Biosensors

An optical biosensor is a type of biosensor that detects changes in the target analyte's optical characteristics. UV-Vis. adsorption and reflectance, fluorescence, phosphorescence, luminescence, surface plasmon resonance, internal reflection, and other photometric characteristics are frequently employed in optical biosensors. When physical or chemical changes occur in the analyte sample, an optical biosensor detects the change in the altered phase, polarization, or frequency of the input light. There are two primary types of optical biosensors: one that detects variations in the biomolecules' inherent optical characteristics, frequently as a result of interaction with a particular target molecule. This class is inexpensive and follows easy steps because it doesn't require the usage of any labels or optical probes.

SPR-based biosensors, interferometer-based biosensors (such as Mach-Zehnder, Young's, Hartman, and backscattering interferometers), optical waveguide-based biosensors, optical-resonator-based biosensors, optical-fiber-based biosensors, photonic crystal biosensors, etc. comprise the majority of non-labeled optical biosensors. In this, a fluorescent tag is affixed to the molecule of interest in the second class of labeled biosensors. The additional process of identifying the molecules is the class is the major drawback, though. However, a single analyte molecule in the sample, such as the circulating tumor cells, may be detectable by label-based biosensors due to their extremely high sensitivity. On the basis of optical measurements of analytes, new affordable wearable technology for ongoing health monitoring are being developed in recent times.

B. Mechanical/ Piezoelectric biosensors

Another class of biosensors are mechanical/piezoelectric biosensors, which can sense the analyte by measuring the change in its mechano-physical properties like pressure, acceleration, temperature, strain, or force applied. Piezoelectric materials like bernalite, quartz, Rochelle salt, etc. vibrate under the influence of an electric field depending on the thickness and nature of the material. Each piezoelectric material vibrates with a certain resonating frequency, which is measured by the biosensor. The change in the resonating frequency is proportional to the mass added/removed from the sensing surface, which can be calculated using the **Sauerbrey** equation. The piezoelectric sensors can reach upto a resolution of 1 µg. Quartz crystal microbalance (QCM) is the most widely used mechanical biosensor capable of sensing an analyte in solid, liquid and gaseous phases. The biggest advantage that they offer is that the analyte can be sensed directly, without using any label. However, environmental factors like humidity can affect the sensing activity of these biosensors. Unlike others, the biggest advantage that they offer is excellent mass resolutions (nanoelectromechanical system have achieved a zeptogram resolution), label-free detection, ease to study the interaction between a biological entity and small molecules, and capability to fabricate small microfluidics devices.

C. Electrochemical biosensors

The 'Physical Chemistry and Analytical Chemistry' division of the International Union of Pure and Applied Chemistry (IUPAC), defined the electrochemical biosensors as follows: "an electrochemical biosensor is a self-contained integrated device, which is capable of providing specific quantitative or semi-quantitative analytical information using a biological recognition element (biochemical receptor) which is retained in direct spatial contact with an electrochemical transduction element.

The biorecognition event in electrochemical biosensors was transformed into a detectable signal in the form of a measurable current, potential, or change in conductivity. Because of their affordability, ease of manufacture, and potential for downsizing, electrochemical biosensors are the most widely utilized biosensors among the aforementioned categories. Electrochemical biosensors can function in a very tiny sample volume, in contrast to optical and mechanical biosensors. Very LOD values are the main benefit of employing them, though. Additionally, they are not affected by fluorophores, chromophores, or other particles, which is typically the case with optical ones. They may therefore be more effective in identifying bacteria, cancerous cells, entire cells, etc.

Electrochemical biosensors are classified into three major categories: (i) Amperometry, that measures variations in current; (ii) Potentiometry, that measures a change in charge accumulation and potential; and (iii) Conductometry or impedimetric that measures the change in conducting behaviors of sensing sample.

(I) **Amperometry:** This kind of electrochemical biosensors function by measuring the current when a voltage is applied across the electrodes. The electrodes are held at a constant potential, and the changes in the current are measured as a function of the analyte concentration present in it. When a constant potential is applied, the current in the three-electrode system can be explained using the Butler-Volmer equation.

(II) **Potentiometry:** In such biosensors, the accumulated charge potential at the working electrode is measured in comparison to the reference electrode, when no current flows between them. This kind of system gives information about the charged molecules present in the solution, where the concentration of the analyte and the potential is governed by the Nernst equation.

(III) **Conductometry/ Impedimetric:** Unlike the above-mentioned techniques, the impedimetric biosensors do not measure the charged ion concentration, but measure the impedance of the cell across the working and counter electrode. Impedimetric biosensor does not require any detection tag, hence it is generally used for label-free detection of an analyte. This is also used to study protein or another biomolecule immobilization over the electrode surface. This can also be used for miniaturization of detection devices and can be integrated for chip development.

1.3. Role of nanomaterials in the development of biosensors

Because of their distinct geometric and electrical characteristics, nanomaterials improve a biosensor's analytical capabilities. They behave differently than the individual atoms that make them up, and they also alter their properties when they are present in close proximity to another complementary substance to form a composite. These materials are very promising for developing biosensors with increased efficiency because of their altered geometric and electrical properties. A bigger catalytic surface is produced by a higher surface to volume ratio, and this is used to reduce the size of the detection equipment without sacrificing sensitivity. The creation of point-of-care detection modules can greatly benefit from this trait, which does away with the necessity for large devices and the drawbacks that come with them. The following outcomes are the consequence of functionalizing the sensing surface with nanomaterials: Larger active surface area resulting into better sensitivity.

a) An increase in the conductivity results in a fast transfer of electrons between the electrode and the reaction center.

b) An increase in the catalytic activity results in the oxidation/reduction of analyte at a lower potential, which helps distinguish structurally similar molecules in sensing.

c) Surface modification results in limited interaction of interfering molecules with the electrode and increases the selectivity.

d) A large surface area also leads to fast diffusion and pre-concentration of target molecule onto the electrode surface.

Different class of nanomaterials can be explored for biosensor development based on their surface, chemical, and electronic properties. In our work, we have focused primarily on a specific class of materials, which are MOFs (Metal organic framework).

2. Introduction to MOFs

MOFs are a diverse class of multifunctional, crystalline and porous materials with their evolution dating back to late 1990s[1]. These porous materials often referred to as 'coordination polymers', are formed through coordination of organic linker molecules with metal ions by their self-assembly[2,3]. They find their applications in a plethora of fields ranging from gas storage[4–7], gas separation[8], catalysis[9–12] to drug delivery, theranostics and sensing[13–17]. For example, Cu-based MOFs are often used as nanozymes like proteases, peroxidases and laccases[18–20]. The applications of these MOFs are supported by their commendable properties such as uniform and tunable pore sizes, large accessible surface area, high thermal and chemical stabilities[1]. Some MOFs have intrinsic properties like low toxicity, inherent stability and good biocompatibility such as Zr-based MOFs[21]. However, for expansion and enrichment of their properties, further, these MOFs are often decorated with functional species to form composite materials with synergistic or improved features[22–24]. For example, Wen et al. in their recent work improved the electron-transfer efficiency of ZIF-8 by conjugating it with graphene for fabrication of a pesticide biosensor matrix[25]. Similarly, in a work by Lai et al.[26], a porphyrin-based MOF was doped with Mn^{2+} ions to selectively detect glutathione. In another study by Kulandaivel et al.[27], copper-based MOF nanozymes after being doped with Cu^{2+} ions, were found to be catalytic with oxidoreductase activity which helped in enhanced colorimetric paper-based detection of Cr^{6+}. Apart from doping, the key to MOF's reticular design lies with binding of metal nodes to different linker molecules yielding MOF structures of varying pore sizes and morphology. There is liberty for precise control of preferred topology by change in the molecular building blocks[28]. The guest accessible voids can be exploited as per needs for the development of optical, electromechanical, electrochemical, chemicapacitor sensors, and sensor arrays. For sensing applications, the target moiety's counter molecule can be either encapsulated or adsorbed on the MOF surface making its physical characteristics of significant interest. In addition to these intrinsic properties of MOFs, they are also engineered for conjugation of various receptors to develop a sensing interface for molecular analysis[29–31].

With all its applications gaining eminence widely, its biosensing based-applications are currently trending in the research arena[32,33]. Biosensors of various types depending upon the type of inducers, ranging from optical[34,35], electrochemical[36,37], photo-electrochemical[38,39] and mechanical[40], have found their utility in this field. MOFs can either be directly used as biosensing platforms[41] or can be modified/functionalized with different ions[42], nanoparticles[43,44], polymers[45], composites[46], or as combinations of these[47] to be used for effective fabrication of ultrasensitive detection systems. The use of MOFs involving multiple metal ions is on rise due to the synergistic effect of such systems leading to better analytical abilities[47,48]. For instance, Du et al.[49] synthesized bimetallic CuCo-MOF (ingrown on Ni-foam), with adjustment of metal ions in a specific ratio to develop a non-enzymatic electrochemical glucose biosensor. The sensor was capable of detecting glucose within a limit of detection (LOD) of about 0.023 mM without the use of any enzymes along with an improved electron transfer capability due to metal ion synergies. These types of work would pave path towards the development of MOF-based biosensors having diverse functionalities in coming years.

Based on a scientific survey conducted by us on the online database "Scopus", we discovered that there were no recent review articles highlighting MOF-based detection of different categories of molecules of clinical importance, as shown in **Figure 1.1**. There are some recently published articles which are really informative but are stringent in their content with a limited scope of study[50–54]. There still remains a lacuna in holistic understanding of these coordination compounds from their synthesis methods to their applications in electrochemical and optical biosensors which we have tried to address through this article. The first segment of the article discusses about properties and various synthetic approaches that are usually adopted in MOF fabrication. Then, the further segments highlight about free radicals, ions, small molecules, macromolecules and *in vitro* detection assays that have been explored in the recent times using these materials as sensor probe. Illustrative schemes and tables have been incorporated in order to give maximal overview of the sensing mechanism, fabrication parameters, dynamic range, LOD and real sample considered in those studies. Future prospects and limitations have also been discussed to promote further research in this field.

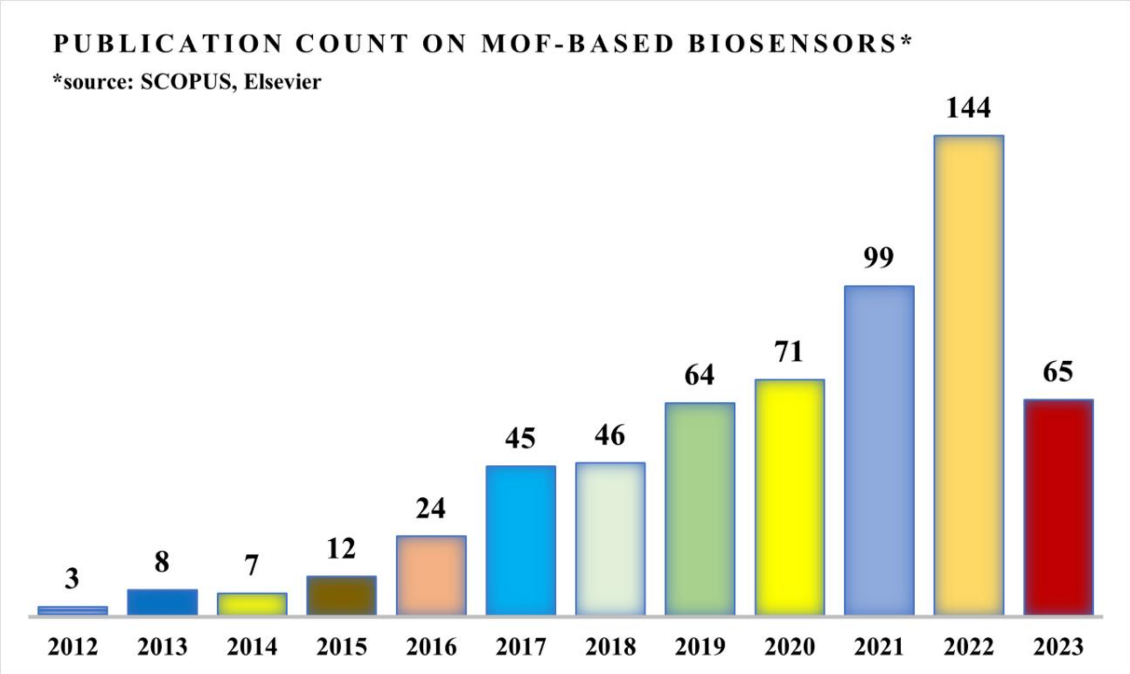

Figure 1.1. *A graphical demonstration giving an outlook of recently published research articles (in the last decade) on MOF-Based Biosensors, as per the online database ''Scopus'' using keywords "metal organic frameworks biosensors", till June 2023.*

2.1. Properties of MOFs

MOFs possess a plethora of advantageous properties (mechanical, catalytic, optical and electronic) owing to their porous structure and crystalline nature. Amongst the most common MOFs, zeolitic imidazolate frameworks (ZIFs) possess a distinct resemblance with zeolites with M-Im-M instead of the Si-O-Si angles present in the latter[55]. Some of the properties supporting role of MOFs in biosensing matrices have been discussed in the section below.

2.1.1. Mechanical properties

While discussing about the mechanical properties of ZIFs, the initial Diamond Anvil Cell diffraction experiments to understand the behaviour of ZIF-8 at high temperature and pressure was done by Cheetam et al.[56] They found that with an increase in solvent accessible volume, the hardness and elastic modulus of ZIF-4 increases. Coudert et al.[57] in their computational study highlighted the amorphous nature of ZIF-4 and ZIF-8 on compression can be explained by a "shear-mode softening mechanism". In another study by Ryder and Tan[58], the role of topology of MOFs with similar chemical components was investigated where it was found that the stability of MOFs is dependent over spatial orientation of its nodes and linker moieties. For example, ZIF-3 possesses an exceptionally low Young’s and shear modulus. Modification of the properties of linker molecules like electronic and stearic bulk can also act as an enhancer or diminisher of the MOFs mechanical properties as a whole[59]. The mechanical properties of MOFs have been reported to impart structural stability to biomaterials[60], however, such direct studies are still scarce in the field of biosensors but highlight their possible potential in the development of robust biosensors in forthcoming future.

Studies on phase diagrams of ZIFs (ZIF-62, ZIF-4) at high temperature and pressure revealed that liquid and glass MOF phases can be achieved at elevated hydrostatic pressure where the melting point of these MOFs can be lowered to a great extent. However, for conducting such studies, a slight change in test conditions like the choice of hydrostatic fluid can alter the results drastically. Other MOFs like MOF-5 and HKUST-1 have also been studied extensively. Both of these MOFs being cubic in nature, with the former being a prototypical carboxylate MOF, a rise in temperature from 25-100 °C can result into a steady drop in its hardness and Young’s modulus[61]. For MOF-5, a lot of studies have been done for calculating the change in its amorphization with application of pressure treatment, showing a pore collapse at pressure nearing 10.3 MPa[56].

2.1.2. Optical properties

The hybrid composition of MOFs encompasses it with a variety of optical properties being it fluorescence, phosphorescence or scintillation. They have shown to exhibit extraordinary emission characteristics ranging from metal-based emissions in lanthanides (more commonly known as ‘Ligand-to-metal charge transfer’) to exciplex-excimer emissions and ligand-based luminescence [62]. MOFs containing lanthanides are also known to exhibit "antenna effect" wherein they undergo indirect activation from adjoining ligands emitting distinctive luminescence. Eu^{3+} and Tb^{3+} ions are amongst the most reported MOFs in optical sensing applications due to their distinct visible luminescence properties due to evident Stokes shifts [63,64]. Apart from above discussed factors, it has also been found in studies that MOFs containing d^{10} transition elements devoid of any unpaired electrons exhibit linker-based luminescence with linker moiety instead of metals being the focal point of the luminescence [62,65]. MOFs tailored with materials with better properties and stability tend to minimize diffusion barriers and solve mass transfer issues leading to enhanced ion and energy transport[66,67]. In a recent article by Jamali et al.[68], MOF-5, with enhanced fluorescence properties and direct band gap, was subjected to metal-semiconductor-metal photodetectors to determine its optical properties when conjugated with zinc oxide (ZnO). The MOF acted as an electron acceptor molecule with an enhancement in its charge transfer characteristics by almost 6 folds.

2.1.3. Electronic Properties

Significant electrical conductivity is quite an uncommon trait in MOFs due to the presence of insulating organic linker moieties and a relatively poor π-π conjugation[69]. Previous reports have cited them as less conductive (conductivity between 10^{-8} and 10^{-10} S cm^{-1}) or insulating, limiting their applications in electrochemistry and fuel cells[70]. Hitherto they were being looked upon as highly non-conductive materials. However in recent times, use of MOFs has also been explored by tuning their electron density and band-gap through incorporation of semi-conductive materials such as $BiVO_4$[71]. The conductivity originates from ion or electron transport phenomenon occurring between host and guest species [72]. With advancements in material science in the last decade, newer conductive MOFs have been devised giving MOFs the role in sensory platforms[73].

Electrical conductivity in MOFs can either follow band-like or charge-transport mechanism involving redox-hopping. Along with it, the charge transfer characteristics of MOFs can be levied on the functional groups present on their surfaces. Narrowing of bandgap is possible in case of increase in the sp^2-hybridized carbon atoms. Also, in case of linker molecules like amine and nitro groups, the p-orbitals might interact with the aromatic carbon atoms facilitating band gap modulation[74]. For lesser discussed redox-hopping mechanisms in MOFs, a recent article by Li et al., discusses thoroughly on the redox conductivity of Zn-based MOFs grown on fluorine-doped tin oxide surface exhibiting exceptional conductivity and minimal electrical resistance[72]. Such approaches can be fascinating for future development of microporous conductors and reconfigurable electronics with applications in sensors.

2.1.4. Catalytic properties

Studies on MOFs have also highlighted their catalytic behaviour. In an article where Co-based MOF executed synthesis of multicomponent reactions had a Co metal centre linked with 4, 6-diamino-2-thiopyrimidine that imparted it with lewis acid properties[75]. Not only MOFs, but also their derivatives such as Ni/NiO/C composite have found to be excellent electrocatalysts for hydrogen evolution reactions[76]. MOFs with Cu^+ sites have found their applicability in CO_2 hydrogenation to alcohols due to their catalytic behaviour and unique coordination assembly at the room temperature[77]. Catalytic properties of MOFs, both photocatalysis or electrocatalysis, can be attributed to their enriched electron transfer capabilities from their metal centers to their respective ligand molecules[78,79].

2.2. General Methods of MOF Synthesis

MOFs have garnered tremendous interest recently, with efforts put up in modulation in its synthesis and post synthesis modifications. They have been synthesized through innumerable ways since its popularization by Yaghi et al. around 1995[80,81].The primary concept of MOF synthesis revolves around linking of the organic linker molecule with the metal center to develop a porous framework with the objective of not disrupting the integrity of the linker molecule during the synthesis procedure. Variation in the surface area and pore size of MOFs is highly subjective to the temperature changes and reaction conditions. A general schematic representation of the different synthetic routes for MOFs has been shown in **Figure 1.2**.

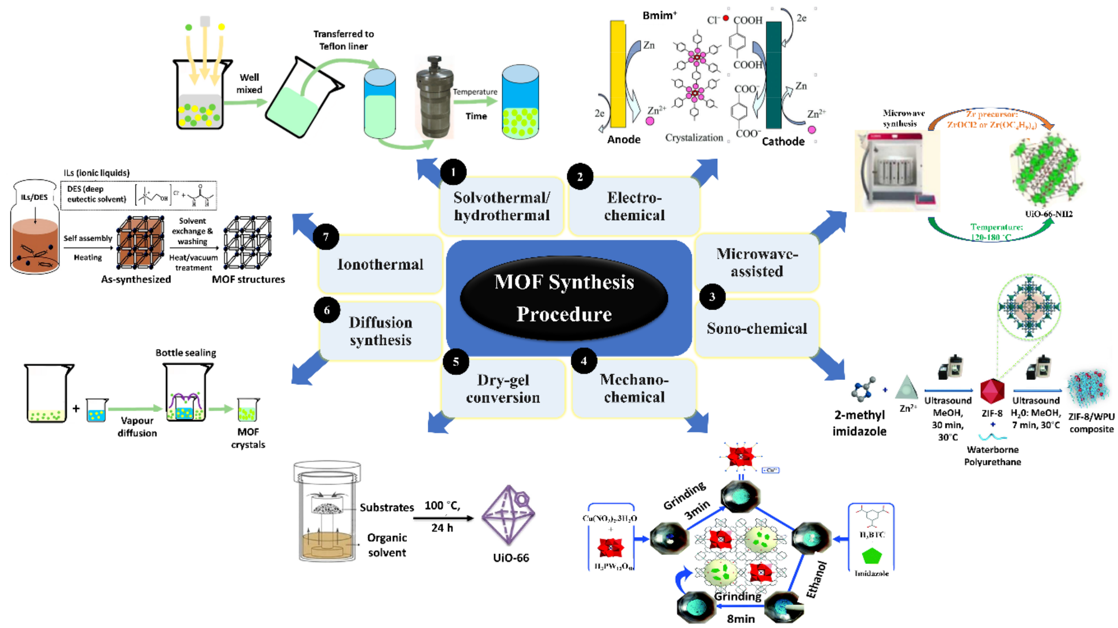

Figure 1.2. *A general schematic representation of the prime MOF synthesis routes. Reprinted with permission from Ref.*[82–88]*.* ***1)*** *Solvothermal/ hydrothermal synthesis, Copyright 2018, Bian et al.;* ***2)*** *Electrochemical synthesis, Copyright 2015, Yang et al.;* ***3)*** *Microwave-assisted synthesis and Sono-chemical synthesis, Copyright 2022, Solís et al.; Copyright 2022, Borse et al.;* ***4)*** *Mechano-chemical synthesis, Copyright 2021, Wang et al.;* ***5)*** *Dry-gel conversion, Copyright 2017, Lu et al.;* ***6)*** *Diffusion synthesis, Copyright 2018, Bian et al.;* ***7)*** *Ionothermal synthesis, Copyright 2016, Zhao et al.*

These synthetic routes used have been briefly discussed with recently published examples for better clarity in section below.

2.2.1. Solvothermal MOF synthesis

Reaction temperature is a key parameter for synthesis of MOFs. So, the method of MOF synthesis can be broadly categorized as solvothermal and non-solvothermal synthesis. According to Albrecht Rabenau[89], reactions taking place under autogenous pressure (above 1 bar) in closed vessel above the boiling point of the solvent are termed as solvothermal synthesis. Such synthesis can also be termed as hydrothermal synthesis in aqueous solvent system when temperature exceeds 100°C. A generalized scheme for solvothermal MOF synthesis has been shown in **Figure 1.2.1**. However, this process can be easily understood through examples discussed in the section ahead. For instance, in a recent article on S-doped CAU-17 based tetracycline removing system, different proportions of CH_4N_2S were added to a mixture of solution containing bismuth nitrate [$Bi(NO_3)_3 \cdot 5H_2O$] and benzene-1,3,5-tricarboxylic acid [H_3BTC]. They had been dissolved in methanol and dimethyl formamide (DMF) solvent systems respectively and the reaction mixture was stirred and heated at 120 °C for 2 h in a Teflon lined reactor, leading to MOF synthesis[90]. Similar case has also been reported for MIL-100(Fe) MOF which has been synthesized at 150 °C for 12 hours in an autoclave[91]. The major advantage of this method includes chemical and structural stability along with morphological symmetry[92] whereas the disadvantage lies in optimizing the temperature conditions for desirable morphological characteristics.

2.2.2. Electrochemical MOF synthesis

Electrochemical synthesis is a fast, clean and cost-effective method for nanoparticle fabrication including MOFs[93]. A general representation of electrochemical MOF synthesis has been shown in **Figure 1.2.2**. This method has been widely favoured due to its potential in growing MOFs in specific patterned thin films and versatile coatings. The pioneers of electrochemical MOF synthesis are believed to be researchers at Baden Aniline and Soda Factory (BASF) who proposed salt free continuous synthesis, advantageous for an industrial setup. The process typically involves supplying a metal building block (placed at the anode) to a synthetic solution containing organic linker and a conducting salt[94]. Other reports have similar claims for metal salt-free synthesis of

MOFs too[95,96]. The reaction conditions are carefully controlled for production of bulk MOF material. A well-known MOF structure [$Cu_3(BTC)_2$] was electrochemically formed on pure copper electrodes where Cu^{2+} ions were linked to a tridentate ligand H_3BTC[97]. On application of anodic voltage at the copper electrodes, the Cu^{2+} ions dissolute into the synthesis solution which contained a mixture of H_3BTC and methyltributylammoniummethyl sulfate (MTBS). It is relatively easier to obtain crystals of varying sizes (2-50 μm) with simple alterations in synthesis conditions. For example, a ten-fold rise in the applied anodic voltage increases the metal ion concentration near the surface facilitating thin films formation with smaller crystals. On contrary to this, larger crystals are obtained on addition of more water to the synthesis solution resulting from slowed nucleation. In a study on electrochemical synthesis of MOF-5, polished zinc was used as an anode and titanium sheet was taken as the cathode[84]. Terephthalic acid was dissolved in DMF in which zinc nitrate was added to serve as the conductive medium. Afterwards, an ionic liquid (1-butyl-3-methylimidazolium (Bmim) chloride) was added into this solution and agitated with a magnetic agitator. With passage of current, a white flocculent substance was obtained which is the desired MOF. The study stated that the MOF-5 synthesized by this method possessed higher thermal stability and better crystallinity which can be accredited to π–π stacking interactions, coordination bond and ionic bond prevalence. This method could be a choice for fabrication of films and layers of MOFs since the thickness can be controlled by alteration in applied voltage and current in mild synthesis conditions[98,99].

2.2.3. Microwave-assisted (MW) and ultra-sonochemical (US) MOF synthesis

MW involves usage of microwave irradiation as energy source for conducting solid-solid as well as solution-based syntheses. Both MW and US syntheses are considered inexpensive and unconventional irradiation systems on the basis of various parameters of concern like phase-selective crystallization, degree of acceleration and crystal size reduction. A general perspective of these processes can be gained through **Figure 1.2.3** but some recent examples would make things more lucid. For example, in MOFs like ZIF-8, the conventional methods rely on nitrate and acetates of zinc as precursors which are expensive. However, for ZnO precursors, the problem lies on poor conversion rate and relatively high reaction time. Yet, the ZnO-based synthesis possesses multiple benefits among which one is being sustainable leading to water as a by-product. In a latest study by Bazzi et al.[100], both the US and MW methods of ZIF-8 synthesis have been discussed where the former led to a better conversion rate while more particle dispersion and better material regeneration was seen in the latter. The group had tried synthesizing ZIF-8 in different types of solvents and demonstrated the product usage in phosphate adsorption study. MW-assisted MOF synthesis is often adopted for its shorter reaction time, superior phase purity, uniform particle morphology and simplicity of procedure[101]. However, a study on MW-assisted MOF synthesis stated its shortcomings highlighting about generation of hotspots in MW reactor due to complex distribution of MW field which results into localized overheating. This is unfavorable for growth and nucleation of MOFs' crystals. These hotspots are regulated by various operating parameters such as dielectric property of reactants, input power, stirring rate and shape/dimension of the cavities that are needed to be taken care of[102].

Alternatively, ultrasounds have been used for MOF synthesis mostly for its energy efficiency benefits accompanied with a reduced reaction time[103]. The frequency of ultrasonic waves can alter its application causing innumerable physical and chemical variations in a non-equilibrium state of reaction. In a zinc-based MOF synthesis, zinc nitrate hexahydrate along with adipic acid was added to DMF and the solution was transferred to a round bottom flask (RBF). Then, an ultrasonic probe (dia. 13 mm) was dipped into it and the synthesis was carried out at 65% power. The synthesized particles were found to be equally thermal stable with smaller crystallite size when compared to those synthesized by other methods[104]. In another study by Bui et al.[105] for Fe_3O_4 encapsulated ZIF-8 synthesis, sonochemical method was chosen over all other methods to increase the microporous loading efficiency and enhancement of reaction rate caused by confined high temperature and pressure-mediated cavitation of the MOF.

2.2.4. Mechanochemical MOF synthesis

This efficient yet simple method involves greener approach of solvent-free or extremely low-solvent synthesis using grinding of only powdered raw material. This solid-solid reaction is a convenient method over the conventional solvent intensive methods, which poses potential advantage for large scale production and eases handling by many folds. **Figure 1.2.4** shows a diagrammatic general representation of this process. Recently, ZIF-8 was mechanochemically synthesized by Imawaka et al.[106], wherein, they compared the relative crystallinity and convenience of synthesis with conventional methods involving usage of solvent systems. Their method used 50 yttria-stabilized zirconia (YTZ) ball-based milling of powdered ZnO and 2-methylimidazole in a ceramic pot. The synthesis was carried out at 150 rpm for one hour and was catalyzed by cobalt acetate or zinc acetate dihydrate in two different reaction conditions. This acetate-assisted mechanosynthesis procedure can be explained as reaction between cobalt acetate with 2-methyl imidazole yielding acetic acid which thereby dissolves ZnO. The mass transfer by *in situ* generated acetic acid and hydrated water encouraged formation of the complex between the ionized metal to the linker molecule. Both, the complex formation and dissolution of the complex by continuously forming acetic acid, led to agglomeration and growth of the macroporous structure. An alternative to this ball-milling process could be the single screw (SSE) and double screw (DSE) extrusion methods where a screw is employed with a gradually increasing root diameter covering large portion of a conveying section, and a kneading element in the final zone. However, in case of SSE, the work is applied through compressive forces which are generated by a reduction in screw channel depth upon movement from feeding to metering section. The barrel of the extruder is heated to a temperature which exceeds the melting point of the ligand. The extrusion process possesses better control on temperature in the barrel which is missing in the case of ball-milling where temperature cannot be standardized and is inevitable due to friction[107].

2.2.5. Dry-gel conversion (DGC) MOF synthesis

DGC is a rapid process which involves treating amorphous gel powder in minimal solvent conditions without the use of modulators to form crystalline compounds in small reactor volumes[87], as represented in **Figure 1.2.5**. It was described by Ploskonka et al.[99] for synthesis of UiO-66 and UiO-66-NH_2, where heating under a vacuum environment promoted the nucleation without any need for solvent exchange by virtue of acetone's low boiling point. Lu et al.[87] synthesized UiO-66 MOF through the DGC route without the use of any acid or salt. Earlier reports too claim for such benign synthesis route for zeolites and zeolitic membranes aided by vapors of water or volatile amines[108,109]. This method eliminates the usage of toxic solvents and release of hazardous by-products[87]. It is a relatively safer, economical and environment-friendly technique that avoids use of acid modulators which sometimes limits the yield of the reaction. This method is often used in conjugation with other techniques like ball-milling as seen in case of Cr-MIL-101 synthesis where the properties of both methods were envisaged to obtain MOF with a greater surface area and higher yield[110].

2.2.6. Diffusion-based MOF synthesis

The principle of diffusion-based MOF synthesis is absolutely contrary to the conventional solvothermal method. In this method, the reagents are separately placed within a sealed container in small glass vials. The method can be understood through the general schematic diagram in **Figure 1.2.6**. The container's atmosphere gradually fills with the surface evaporation of chemicals thereby diffusing into the reagent to complete the reaction and synthesize the target compound. In a typical MOF-70 synthesis method, lead nitrate [$Pb(NO_3)_2$] and 1,4-benzenedicarboxylic acid (BDC) were supplemented to the DMF solvent under stirring[111]. The solution was diluted with ethanol and hydrogen peroxide, later filtered and kept in glass vials within amber glass container along with a solution of trimethylamine and DMF. The lid was sealed with silicone oil with the standing solutions undisturbed for a period of 7 days to obtain the desired product. The method is feasible at room temperature and pressure making it highly sustainable yet time consuming. In another Cd-based MOF synthesis, similar method was employed where the aqueous solution of reagents was layered over metal solution in a crystal tube to obtain the desired MOF in 30 days[112].

2.2.7. Ionothermal MOF synthesis

This benchtop and time-efficient synthesis method is often regarded as an alternative to mechanochemical process. It tries to overcome the shortcomings of mechanochemical technique like use of specialized instruments (ball-mills and extruders) to evolve as a solvent-free, cost-effective and green synthesis approach. It also poses a control over MOF crystallization kinetics and induces chirality via inclusion of ionic liquids within the framework. However, the condition lies in usage of low-melting point salt which can serve the dual purpose of reaction solvent as well as that of a metal precursor.

The general schematic representation of ionothermal MOF synthesis can be seen in **Figure 1.2.7**. To understand it further, as per a recent study on synthesis of Ca-based MOFs, use of deep eutectic solvent was explored for creation of ionic environment[113]. This environment was favorable over other synthetic approaches for prevention of competing coordination by water. This is because the alkali metal's ability to bind with water molecules is higher over any other ligand due to its oxophilicity. The reaction involved terephthalic acid and calcium nitrate [$Ca(NO_3)_2$] addition to a vial containing choline chloride and eutectic urea deep eutectic solvent (e-urea DES). The mixture was heated to 140 °C for 10 days to obtain the desired MOF. In another study by Azbell et al.[114], a similar approach without the use of eutectic mixture was chalked out where low melting metal precursor salts were added to an autoclave containing equivalent molar concentration of linker and the temperature was maintained just above the melting point of the salt to facilitate MOF synthesis without the use of solvent. On extraction of solid product, washing was done via different approaches, Soxhlet extraction also being one of them. This method is largely untapped and is restricted to certain specific categories of MOFs like ZIFs and carboxylates. Stable azolate and salicylate MOFs are now being explored too but the area remains greatly unexplored.

For all above methods, each one has certain restricted usage e.g., methods like sonochemical, microwave-based and mechanosynthesis might involve high energy consumption within complex processes with an additional requirement for advanced machinery, lengthy reactions, introduction of undesirable anions and tough process regulations. Hence, the synthesis scheme can be modified and adopted as per one's choice of material and its implementation in various fields.

3. Application of Biosensors in Molecular Sensing and Disease Diagnosis

3.1. Detection of Clinically Significant Molecules Using MOF-based Sensors

3.1.1. Free Radicals and Metal Ions

3.1.1.1. MOF-based Electrochemical sensors for free radical and metal ion detection

Hydrogen peroxide (H_2O_2) is one of the crucial markers for clinical and physical conditions aiding to their early diagnosis[115,116]. It has often been linked with several other disorders too such as Parkinson's disease, Alzheimer's disease and myocardial infarction[117,118]. According to Huang et al.[119], ultrathin 2D MOF nanosheets can be used as nanozymes for electrochemical biosensing of H_2O_2. The 2D Cu-HHTP-NSs being ultrathin can facilitate better charge mobility along with exposed active sites for anchorage of functional molecules. The sheet surface was decorated with in-grown AuNPs for structural and electrical property enhancement. Peroxidase-like activity (POD) was explored for the composite in the presence of H_2O_2 to oxidise 3,3′,5,5′-tetramethylbenzidine (TMB) in the pH range of 3.2-4.8, exhibiting blue colour. Interfacial behaviour and electrocatalytic performance of the modified electrode was also confirmed using electrochemical impedance spectroscopy (EIS) and cyclic voltammetry (CV) measurements, respectively. Electrode sensitivity was measured through amperometry which showed a fast signal response in 50 nM to 2 mM H_2O_2 concentration within 3s. Electrochemical sensing was seen in wide linear dynamic range (LDR) of 50 nM-16.4 mM H_2O_2 with LOD of 5.6 nM. The group used colon cancer cells for analysis which when stimulated with N-formyl-methionyl-leucyl-phenylalanine initiate H_2O_2 generation[95]. Similarly, Xie et al.[120] in their study on electrochemical H_2O_2 detection in HeLa cells, electrodeposited gold-platinum NPs on Co-MOF modified glass carbon electrode (GCE). The 2D Co-MOF nanosheets exhibited electrocatalytic activity for the reduction of H_2O_2 in the meantime also acting as a supporting material. The catalytic current exhibited a linear trend with rise in concentration of H_2O_2 from 0.1 μM to 5 mM and 5mM to 60 mM, as measured by amperometry measurements, with an LOD of 0.02 μM (**Figure 1.3A**). In another study on H_2O_2 detection by Xiong et al.[121], a lower LOD of 2.32 nM was achieved through ZIF-67 MOF-derived Co_3O_4 NPs functioning as H_2O_2 nanozyme (**Figure 1.3B**). The study focussed on live detection of H_2O_2 in A549 (human lung cancer cell), 4T1 (mouse breast cancer cell) and HUVEC (human epithelial cells) cells by Co_3O_4@CNBs modified GCE at −0.22 V. A linear response was recorded, through CV and amperometry analysis, with H_2O_2 concentrations from 0.01 to 359 μM. Similar MOF/MOF-based composite's peroxidase-like activity have been exploited in past few years for sensitive H_2O_2 detection[122–128].

Apart from H_2O_2, efforts are underway on the development of highly sensitive detection probes for highly reactive oxygen species (hROS) like superoxide ($O_2^{\bullet-}$), peroxynitrite ($ONOO^-$), hydroxyl radical (•OH), singlet oxygen ($^1O_2$) and hypochlorite (ClO^-) which are modulators of redox homeostasis and cellular signalling in living systems[129,130]. Their overaccumulation can lead of oxidative stress which can thereby result into human pathologies like inflammation, carcinogenesis, neurological disorders and ischemia-reperfusion injury etc.[131–133]. Another recent study proposed a superoxide anion sensor ($O_2^{\bullet-}$) where Ag and 2-aminoterephthalate based MOF was used to derive a carbon-based nanomaterial for probe fabrication[134]. A GCE electrode surface was coated with the AgNPs-MC to fabricate the electrochemical sensor which exhibited excellent $O_2^{\bullet-}$ detection in living human glioma cells. Chronoamperometry analysis confirmed a LDR of the constructed sensor between 3.69×10^{-11} to 5.26×10^{-7} M and 1.68×10^{-6} to 3.06×10^{-4} M with an LOD of 12.3 pM.

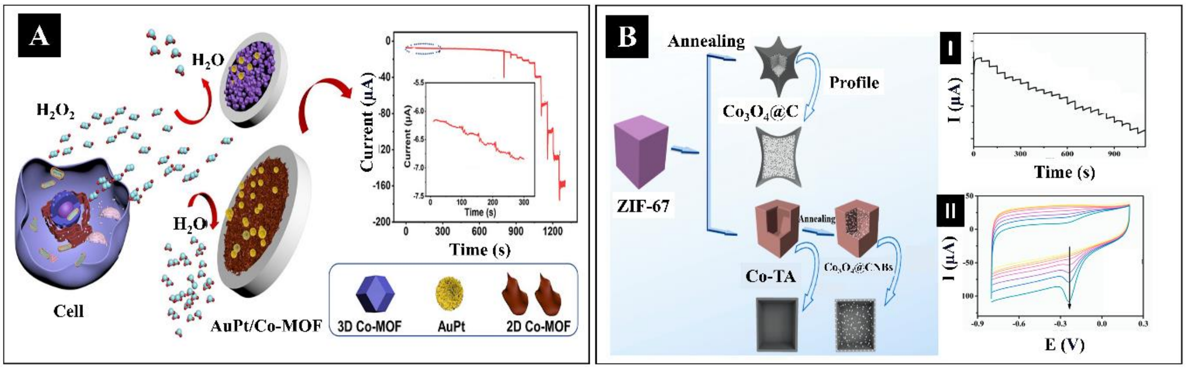

Figure 1.3. ***(A)*** *Schematic illustration showing H_2O_2 detection in HeLa cells, electrochemically. Adopted from Xie et al.[120], copyright 2022.* ***(B)*** *Illustration depicting ZIF-67 based nanozyme sensor for H_2O_2 detection.* ***I)*** *Amperometric response of the carbonized MOF fabricated on GCE surface against different concentrations of H_2O_2, when scanned at -0.22V in PBS solution.* ***II)*** *CV response of the MOF-based sensor in the presence of different H_2O_2 concentrations. Reprinted with permission from Xiong et al.[121], copyright 2022.*

3.1.1.2. MOF-based Optical sensors for free radical and metal ion detection

MOF-based optical sensors have also been devised in recent times for free radical and metal ion detection. In a latest work by Huang et al.[135], a redox-active luminescent MOF, Mg(DHT), was synthesized for encapsulation of hydroquinone moiety for sensitive detection of •OH and ClO^-. The MOF comprised of 2,5-dihydroxyterephthalic acid (H_2DHT), a bidentate ligand, which endowed it with large stokes shift and an ultrafast response due to enol transfer aided by enol-keto tautomerism. On the other hand, presence of Mg^{2+} as the metal centre enhanced the luminescence efficiency due to reduced non-radiative decay. The hydroquinone underwent a reversible transformation by •OH and ClO^- to become quinone because of its reducing capability. The MOF displayed a strong fluorescence at 556 nm which got quenched upto 76% and 90% in the presence of •OH and ClO^- species, respectively (**Figure 1.4A**). The same results were conferred with UV-vis data where oxidation of hydroquinone led to appearance of a new absorption peak at 285 nm. The probe was also used for endogenous detection of the ROS species in MCF-7 cells, which were pre-treated with lipopolysaccharide (LPS) and phorbol 12-myristate 13-acetate (PMA) to simulate oxidative stress induction. The results proved applicability of the biosensor for imaging and monitoring of ROS in live cells within a detection range of 2.5-50 μM and an LOD of 0.22 μM and 0.18 μM for •OH and ClO^-, respectively. Similar sensors for superoxide anions have also been fabricated with a different principle where MOFs have been used as electrocatalysts for *in situ* real time detection of cellular O_2•$^-$. Zhang and group[136] used Mn-MOF in three different forms (NPs, nanorods and nanolollipops) to detect the target ROS species in MCF-7, H9c2 and HepG2 cells. The concentration of O_2•$^-$ was initially determined through spectrophotometry where the reduction of ferricytochrome c was investigated. For electrochemical measurements, Mn-MOF was then coated on the GCE surface to record the oxidation of O_2•$^-$ at 0.69 V in an LSV curve. For comparison of all three forms of MOF, half-wave potential and peak current values were considered for evaluation of individual electrochemical performance. Amperometric technique was employed for sensitive detection of O_2•$^-$ which revealed the biosensor to be highly sensitive in an LDR of 3.0-1350 nM with an LOD of 1.0 nM. The highest sensing performance was observed for Mn-MOF nanolollipops modified electrode due to heavily exposed active sites and faster charge transfer kinetics benefitted from its unique spatial structure aiding to ultrasensitive sensing.

Mercury ions (Hg^{2+}) are one of the heavy metal pollutants which are environmental contaminants posing global health hazard by contributing to biomagnification. They cause neurological and cardiovascular disorders along with impairment at molecular level including genetic mutations and mitosis defects[137,138]. In an article by Uttam et al.[139], calixarene was conjugated with ZIF-8 MOF to enable sensing as well as adsorption capabilities for the metal ions (**Figure 1.4B**). The adsorption of metal ions on DanC4A (dansyl appended calix[4]arene) was investigated in THF solvent system. DanC4A showed an excitation peak at 345 nm and a strong emission at 510 nm. When subjected to Hg^{2+}, it showed a reduction in its absorbance band at 345 nm and simultaneously increment at 285 nm. The limit of detection was found to be 0.56 μM. Confocal microscopy was also done for sensing of the target metal ion by DanC4A in HeLa cells. The green fluorescence which was seen upon treatment of cells with DanC4A, gradually faded with its intensity decreasing to ∼60% indicative of Hg^{2+}-receptor interaction.

Precious metals like Pd^{2+} and Au^{3+} are known for their unique physical and chemical properties like catalytic activity, high electrical conductivity and corrosion resistance. They find their enormous industrial applications in the form of computer hard drives, wires and switches, etc.[140] with a global surge in their demands each year. With their growing demands but limited supply, there is a dire need for recovery of these precious metals from e-wastes and for environmental remediation purposes along with minimization occupational health hazards linked to recycling[141,142]. In a study by Alharbi et al.[143], an azo-HNTA-MIL-101(Al) sensor was fabricated for fluorescent, ultrasensitive detection of Pd^{2+} and Au^{3+} ions. The group initially synthesized an azo dye and then used it as a linker for preparing the Al-MOF using solvothermal method. This approach enabled coupling of all amino groups of 2-aminoterephthalic acid with 2-naphthol even before the MOF synthesis. An increase in chemosensor sensitivity was found to be proportional to the increased functionalized amino groups on the MOF surface thereby increased adsorbed target metal ions. The absorbance of the sensor increased with an increase in Pd^{2+} and Au^{3+} ions whereas its fluorescence emission decreases significantly. This could be possibly because of the selective reactivity of Pd^{2+} with the carboxylic group and Au^{3+} with the phenolic group of 2-naphthol leading to the change in sensor spectra. The LOD for Pd^{2+} was reported as 6.79 ppb and that for Au^{3+} was 3.57 ppb with an LDR of 0 ppm- 0.3 ppm and 0 ppm- 0.1 ppm, respectively. The applicability of developed biosensor was tested against extraction of these metal ions from phone-grounded motherboards and was found to be efficient and cost-effective.

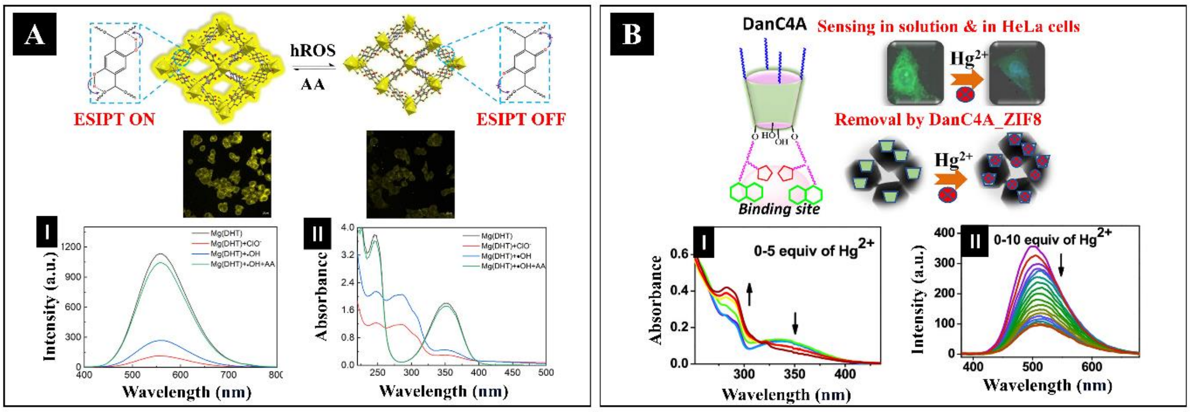

Figure 1.4. ***(A)*** *Schematic representation of MOF incorporating hydroquinone moiety for detection of highly reactive oxygen species (hROS) through ESIPT by linker.* ***I)*** *Fluorescence and* ***II)*** *UV-vis absorption spectra of MOF with different ROS species. Reused with permission from Huang et al.[135], copyright 2022.* ***(B)*** *Diagrammatic illustration of DanC4A MOF-based sensor for sensitive detection of Hg^{2+} ions.* ***I)*** *Absorption and* ***II)*** *Fluorescence spectrum of different concentrations of Hg^{2+} ions in Tetra hydrofuran (THF) solution, when titrated with DanC4A. Reprinted with permission from Uttam et al.[139], copyright 2022.*

Recently reported MOF-based biosensors for detection of free radicals and metal ions have been comprehensively discussed in **Table 1.1** below with their respective target analytes, detection techniques, fabrication strategies, real samples considerations and detection efficiency parameters (LDR and LOD).

Table 1.1. *Detailed list of latest MOF-based biosensors for sensing of free radicals and metal ions (N.R.: Not Reported)*

S.No.	Target Analyte	Detection Mechanism	Sensor Composite	Fabrication strategy	Mechanistic Role of MOF	Real Sample	LDR	LOD	Reference
1.	H_2O_2	CV, EIS, CA	SWNT-MOF(Cu)	Gold wire was dip-coated with catalytic ink which facilitated nanotube growth. Then it was modified with SWNTs deposited through CVD. Finally, the surface was electrodeposited with *in situ* synthesized Cu MOF.	Increase in electroactive surface area	Live cells (RAW 264.7), Raw milk	1 to 2000 µM	0.21 µM	Nandhini et al.[144]
	H_2O_2	DPV	BSA-AuNPs-MFOF	BSA-capped AuNPs were synthesized through sonication which were further embedded in MFOF.	Increase in electroactive surface area	Human whole blood, Egg yolk, Butter, Milk, Goat meat, Cheese, Yogurt and ice cream, Beer and apple juice, live cells (RAW 264.7 cells)	100 nM to 10 mM	18.4 nM	Arul et al.[145]
	H_2O_2	CV, CA	Ce-UiO-66-BPDC	Ce-UiO-66-BPDC flakes were covered entirely with Au-Pt NPs through electrodeposition.	Increase in electroactive surface area	A549 cancer cells	0.15 to 64.8 and 114.8 to 1164.8 µM	89 nM	Yang et al.[146]
	H_2O_2	Colorimetry	IrNCs@Ti-MOF	IrNCs@Ti-MOF, TMB and various concentrations of H_2O_2 were added into sodium acetate–acetic acid buffer to record chromogenic reaction.	Ideal support matrix with high porosity, robustness	Rabbit serum	0 to 900 µM	14.12 µM	Mu et al.[147]
	H_2O_2	Colorimetry	M-PCN-222 where, M = Mn, Fe, Co, and Ni	Microwave-assisted hydrothermal synthesis of MOFs was done that exhibited improved peroxidase-mimicking activity. Presence of Fe-PCN-222, H_2O_2, and TMB, resulted into oxidation of TMB into blue ox-TMB.	Contains porphyrin active sites exhibiting potential biomimetic catalytic activities	Milk, Orange juice, Grape juice, human tears	Fe-PCN-222: 1 to 100 mM	Fe-PCN-222: 0.3 µM Mn-PCN-222: 0.9 µM Co-PCN-222: 1.0mM Ni-PCN-222: 9.6 µM	Shu et al.[148]
	H_2O_2	Fluorescence, Colorimetry	Cyclodextrin MOF (CD-MOF)	The CD MOF exhibited peroxidase (POD) and oxidase (OXD)-like property. POD-like activity using TMB as POD substrate with ˙OH release readout using visible colour change. OXD-like activity was determined using L-ascorbic acid assay and TMB colorimetry.	Peroxidase and oxidase-like activity, hydrolytic stability	HepG2 cells	0.11 to 0.95 mM	0.06 mM	Tan et al.[127]
2.	Hg^{2+}	ECL, CV, EIS	Ag-MOF	Capture strand DNA (c-DNA) with a terminal modification was attached to Au-electrode. Then, mercury-ion aptamer was adhered to electrode by being paired with c-DNA. ECL signal reduction was done using streptavidin aided by biotin as linker molecule.	High specific surface area and large pore diameter	Tap water, Lake water	300 fM to 1 µM	66 fM	Liu et al.[149]

3.	Cr^{3+}	PEC, EIS	Cu-MOF	Tetra-ammine cobalt phthalocyanine-based COF was grown over a Cu-MOF substrate via covalent bonds. This acted as an efficient platform for immobilization of DNA strand which binds to Cr^{3+} ions, thereby detecting it.	High porosity and rich functionality tightly anchored the DNA strands	River water, Tap water	0.1 pM to 100 nM	PEC: 14.5 fM EC: 22.9 fM	Zhang et al.[150]
4.	OH^-, Al^{3+}, Fe^{3+}	Fluorescence	Zn-DHNDC MOF	Zn^{2+} and 4,8-dihydroxynaphthalene based MOF was functionalized with OH^-. When MOF was subjected to OH^- ions, ESIPT suppression turned on bluish fluorescence. When MOF was subjected to Al^{3+} ions, a CHEF-mediated green luminescence was observed. When MOF was subjected to Fe^{3+} ions, a CHEQ-mediated fluorescence quenching was observed.	Participates in excited state intramolecular proton transfer	N.R.	N.R.	OH^-: 48 nM Al^{3+}:95 nM Fe^{3+}:33 nM	Bhowal and Ghosh[151]
5.	Al^{3+} and Ga^{3+}	Photoluminescence	Eu-MOFs (JXUST-11)	Eu-based MOF acted as a photoluminescent sensor for detection of Al^{3+} and Ga^{3+} by fluorescence enrichment visualized through naked eye. The 'N' and 'S' atoms of H_2BTDB ligand's thiadiazole ring acted as the site for metal coordination.	Exhibits excellent luminescence	MCF-7 cells	N.R.	Al^{3+}: 2.9 ppm Ga^{3+}:10.2 ppm	Li et al.[152]
6.	F^- and $Cr_2O_7^{2-}$	Fluorescence	UiO-66-NH_2 @EY	Ratiometric fluorescent probe was constructed by utilizing Zr-MOF cavity to encapsulate eosin Y molecule. F^- detection was through effect of hydrogen bond whereas, for $Cr_2O_7^{2-}$, it was based upon energy competition transfer mechanism.	Provides cavities for eosin Y encapsulation	Sweat latent fingerprint, human serum, HepG2 cells	N.R.	F^- 34.7 nM $Cr_2O_7^{2-}$ 22.3 nM	Zhang et al.[153]
7.	Cu^{2+}	Fluorescence	Fe-MIL-88NH_2@RhB	Ratiometric fluorescent probe was fabricated with the aid of encapsulated RhB into porous framework of Fe-MIL-88NH_2. The MOF composite was mixed with different concentrations of target ion solutions to get optical measurements due to binding of ion with -NH_2 group of the MOF.	Provides cavities for eosin Y encapsulation	A549 cells, human serum, river water, reed leaves	N.R.	4.23×10^{-6} M	Zhang et al.[153]
8.	Cu^{2+} and Fe^{2+}	Fluorescence	Tb-TATB MOF	MOF was synthesized through solvothermal route. When Tb^{3+} was excited at 349 nm, it gave characteristic transitions at 490, 544, 582 and 620 nm. The fluorescent intensity gradually decreased with an increase in ion concentration at 544 nm	Abundant luminescence sites, visible color, and sharp characteristic emission peak	N.R.	N.R.	Cu^{2+}: 2.92 µM Fe^{2+}: 4.84 µM	Zhang et al.[154]
9.	ClO^-	Fluorescence	UiO-66-NH_2	The MOF was developed which on excitation at 400 nm exhibited new emission at 533 nm on reaction with ClO, which otherwise emits at 432 nm.	Excellent thermal stability, water tolerance, and permanent porosity	Water, L02, Hela and RAW 264.7 cells	0.1 to 150 µM	63.8 nM	Yu et al.[155]

Abbreviations: *CV: Cyclic Voltammetry, EIS: Electrochemical Impedance Spectroscopy, CA: Chrono Amperometry; SWNTS: Single Walled Nanotubes; CVD: Chemical Vapour Deposition; DPV: Differential Pulse Voltammetry; BSA: Bovine Serum Albumin, AuNPs: Gold Nanoparticles; MFOF: Metal free organic framework; Pt: Platinum; TMB: 3,3',5,5'-Tetramethylbenzidine; RhB: Rhodamine B dye; ECL: Electro-chemi Luminescence; DNA: Deoxy-ribonucleic Acid; PEC: Photoelectrochemical Luminescence; COF: Covalent Organic Framework; ESIPT: Excited State Intramolecular Proton Transfer; CHEF: Chelation Enhanced Fluorescence; CHEQ: Chelation Enhanced Quenching*

3.1.2. Small Molecules

Small molecules' detection gains its importance due to their easy penetration and involvement in human metabolic pathways[156,157].

3.1.2.1. MOF-based Electrochemical sensors for small molecule detection

Pesticides and herbicides are current environmental menace due to severe toxicity even at mild concentrations. Some of the organophosphorus pesticides like methylparathions, chlorpyrifos are known to cause acetylcholinesterase (AChE) inhibition leading to serious nervous disorders, human poisoning and even death[158,159]. These potent threats have urged for development of sensitive detection tools against these hazardous chemicals. In a work by Wen et al.[25], ZIF-8 has been used as a substratum for immobilization of AChE enzyme on its periphery for the sensitive detection of isocarbophos (ICP) (**Figure 1.5A**). GCE electrode surface was drop-casted with AChE-CS/Gr/ZIF-8 where graphene (Gr) was used to enhance conductivity of the system. CV, EIS and DPV tests were done at -0.2 to 0.6 V, 0.23 V and 0.3 to 0.9 V, respectively. AChE catalysed acetylthiocholine to generate acetate and thiocholine (TCI) on hydrolysis. This TCI got oxidized further at a specific voltage to generate oxidative current corresponding to its concentration. Cabbage leachate and tap water samples were used for analysis by spiking it with different concentrations of ICP. The LDR for the sensor was found to be in the range 0.5 to 100 ng/mL with an LOD of 0.18 ng/mL.

Another study by Niu et al.[160] on electrochemical detection of paraquat herbicide, a fast sterilant and lethal herbicide to humans, uses the same ZIF-8 skeleton (**Figure 1.5B**). ZIF-8 and para-sulfonylcalix[4]arene (pSC4) coated with AuNPs on GCE electrode were found to be excellent sensing platform for the herbicide with an LDR of 0 pM to 10 nM and a detection limit of 0.49 pM. EIS measurements were done within a frequency range of 0.1 Hz to 100 kHz with $[Fe(CN)_6]^{3-/4-}$ as the electronic mediator. The activity of the sensor was confirmed against real tap water samples spiked with the target herbicide. Paraoxon, another organophosphorus pesticide, has been detected through 2D cMOFs with Cu and Ni metal centers coupled with organic ligands namely hexahydroxytriphenylene (HHTP), and tetrahydroxy-1,4-quinone (THQ)[161]. The $Cu_3(THQ)_2$-based biosensor used AChE for electrocatalysis of acetylthiocholine chlorine (ATCh) and thereby its oxidative conversion to oxTCH was aided by the MOF substrate. This conversion was recorded at a remarkable lower potential of 0.3 V due to electroactivity of thiocholine (a product of the reaction cascade) in presence of the MOF substrate ($Cu_3(THQ)_2$ when compared to $Cu_3(HHTP)_2$ and $Ni_3(HHTP)_2$. The biosensor worked efficiently with an LDR of 1 to 1000 ng mL^{-1} and LOD of 0.37 ng mL^{-1}. The sensor's applicability was also checked by testing on real samples such as soil, water, vegetables and fruits.

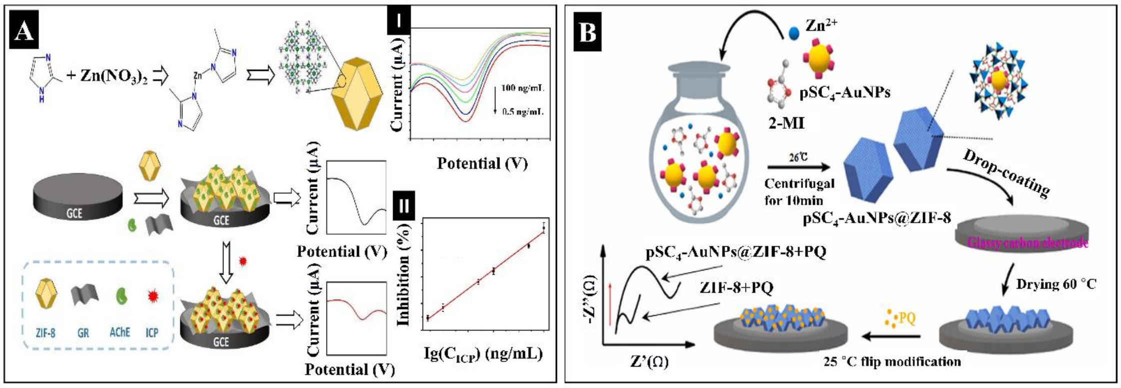

Figure 1.5. ***A)*** *Schematic representation depicting applicability of acetylcholinesterase enzyme immobilized-MOF for electrochemical detection of organophosphorus pesticides.* ***I)*** *DPV response curve, and* ***II)*** *Calibration curve showing enzymatic inhibition rate vs logarithmic pesticide (ICP) concentration. Adopted with permission from Wen et al. [25], copyright 2022.* ***B)*** *A graphical illustration depicting electrochemical sensing of paraquat herbicide using ZIF-8 nanocomposite. Reused with permission from Niu et al. [160], copyright 2022.*

3.1.2.2. MOF-based Optical sensors for small molecule detection

Apart from electrochemical biosensors, MOFs have found their application in sensing small molecules through optical means too. Another potent carcinogen and human health threat, 2,4-Dichloropheoxyacetic acid (2,4-D) is a prominent herbicide with auxin-like properties that is widely used in agriculture[162]. Its high-water solubility and non-biodegradability[163,164] enables it to easily enter human food chain and act as an endocrine disruptor. According to the International Agency for Research on Cancer (IARC), it has been recognized as a potent human carcinogen which makes its environmental surveillance important for public health concerns[165,166]. In a recent article on its colorimetric detection, use of Co-hemin MOF was demonstrated where Co-hemin oxidized TMB into ox-TMB. The detection of 2,4-D did not involve addition of H_2O_2, depicting the composite's oxidase-like activity, with a wide LDR from 0.1 μg mL^{-1} to 240 μg mL^{-1} and LOD of 33 ng mL^{-1} [167]. The biosensor had its applicability tested for real samples like rice and apple too.

Glucose is a crucial energy provider in living organisms for cellular activity and homeostasis[168,169]. A poorly balanced blood glucose level may lead to diabetes and related diseases such as renal failure, blindness and cardiovascular diseases[170,171]. With a rise in diabetes cases worldwide, the demand for ultrasensitive glucose-based biosensors has become crucial. With conventional methods like high performance liquid chromatography[172], gas chromatography[173], capillary electrophoresis[174], spectrometry[175], electrochemistry[176,177], electroluminescence[178], etc. still prevalent in field of glucose diagnostics, the urge for its rapid, accurate and cost-effective quantification still remains a field of research. According to the guidelines by the American Diabetes Association (ADA), a person is termed diabetic if its blood glucose level exceeds 6.1 mM[179]. In a recent article by Wu et al.[180], Ag conjugated MIL-101 (Fe) was used for colorimetric sensing of blood glucose. The conjugate behaved as a peroxidase mimic nanozyme which in presence of H_2O_2 (released from glucose oxidation by glucose-oxidase (GOx)) caused oxidation of TMB into ox-TMB to yield colorimetric response at 652 nm (**Figure 1.6A**). The LDR of the detection platform to glucose levels was found to be 0.5 to 50 μM with an LOD of 0.23 μM. The response was verified and reliability was checked using actual human serum samples. Apart from MOF composites acting as enzyme, MOFs have also been used as enzyme immobilization units for sensitive glucose detection. In a study, defected ZIF-8 based biohybrid hydrogel containing GOx was used to release H_2O_2 from glucose oxidation. This release further cascaded into another process where peroxidase enzyme labelled with rhodamine-B fluorophore converted ABTS into $ABTS^+$ which was analysed using a mobile application. This diagnosis met the quantitative range of 0.05-4 mM glucose level[181]. Label-free colorimetric sensing of glucose by exploring peroxidase-like behaviour of MOFs like Cu-MOF@Pt and IrNCs@Ti-MOF has also been done recently where the LODs were 0.42 mM and 20.0 μM, respectively[147,182].Adenosine diphosphate (ADP) and Adenosine triphosphate (ATP) are two cellular metabolites whose ratio indicates cellular energy status and regulates various cell signalling activities. Their concentration determination can be quite informative for early diagnosis of diseases including cancers[183]. Recently, Wang et al.[118] proposed an ultrasensitive quantification system for simultaneous sensing of ADP and ATP (**Figure 1.6B**). They fabricated a system comprising of clustered regularly interspaced short palindromic repeats (CRISPR) and associated proteins (Cas)12a integrated to ZIF-90 MOF nanocomposite encapsulating oleic acid capped Ag_3AuS_2@Fe_3O_4. The ADP aptamer binding with the MOF composite was facilitated by amidation between amino group of the former with the latter's carboxyl group. In presence of ADP nucleotide target, it bound to the aptamer forming an ADP/aptamer complex, releasing and activating the Cas12a. It was followed by binding of the Cas12a/crRNA and thereafter cleavage of the ssDNA reporter, exhibiting a strong fluorescence emission signal at 520 nm within an LDR of 0.03 to 5 nM with an LOD of 0.022 nM. On the other hand, the ATP competed with Zn^{2+} to cause ZIF-90 splitting and release of the encapsulated composite from its cavity. These composite-constituents led to quenching of fluorescence intensity which was caused by polyethyleneimine-modified carbon dots. Linear relationship was established between the fluorescence intensity at 450 nm and ATP concentration with an LDR of 0.1 to 5 nM with an LOD of 0.079 nM. The biosensor applicability was tested in diluted serum samples spiked with different concentrations of ADP and ATP to compare with commercially available detection kits. This shows the fruitfulness of these robust materials in the sensitive recognition of small molecules from different domains.

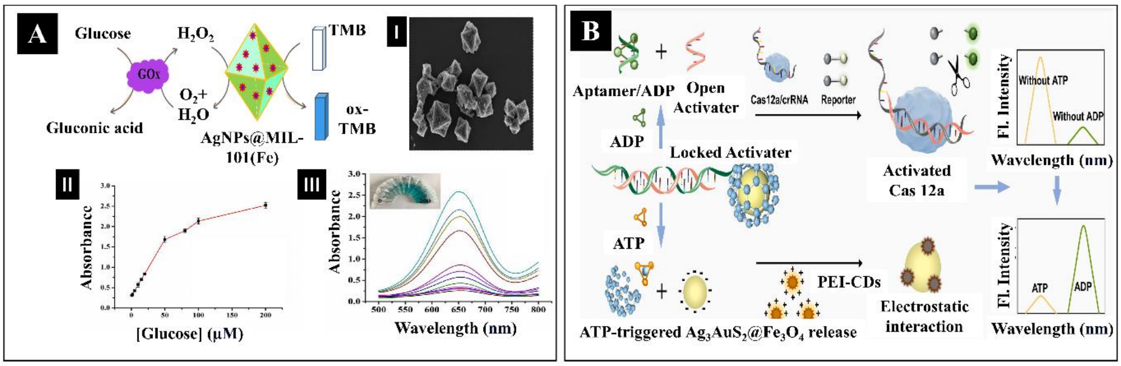

Figure 1.6. ***A)*** *Diagrammatic representation of MOF encapsulated with silver nanoparticles for glucose sensing through colorimetry* ***I)*** *SEM image of AgNPs@MOF hybrid.* ***II)*** *Calibration curve of absorbance vs glucose concentrations.* ***III)*** *Absorption spectra of ox-TMB (at 652 nm) for different glucose concentrations. Reprinted with permission from Wu et al. [180], copyright 2022.* ***B)*** *Pictorial illustration for simultaneous quantification of ATP and ADP using a ZIF-90 composite. Reprinted with permission from Wang et al. [118], copyright 2022.*

Recently reported MOF-based biosensors for detection of small molecules have been comprehensively discussed in **Table 1.2** below with their respective target analytes, detection techniques, fabrication strategies, real samples considerations and detection efficiency parameters (LDR and LOD).

Table 1.2. *Detailed list of latest MOF-based biosensors for sensing of small molecules. (N.R.: Not Reported)*

S.No.	Target Analyte	Detection Mechanism	Sensor Composite	Fabrication strategy	Mechanistic Role of MOF	Real Sample	LDR	LOD	Reference
1.	Glucose	CA, EIS	SWNT-MOF(Cu)	Nanotube catalytic ink was prepared to further dip coat a gold wire. It was followed by nanotube synthesis using CVD and electrodeposition.	Increase in electroactive surface area	Whole blood and milk	1 to 3000 µM	0.16 µM	C. Nandhini et al.[184]
	Glucose	CV, EIS, CA	NiCo-MOFs	NiCo-BTC nanosheets were synthesized through solvothermal method. The sensor system was synthesized through magnetron aided sputtering of concentric circular pattern on a PET matrix.	Excellent electrical conductivity and faster ion mobility	Sweat	10 to 200 µM	10 µM	Zha et al.[185]
	Glucose	EIS, CV	ZIF-8	PET substrate was modified by bonding it to hydrogel. The PET surface was functionalized with Aam, BIS, APS, TEMED, SA, GS NPs as monomers, cross-linker, initiator, accelerator, crosslinking agent and crosslinking metal ions source, respectively.	Encapsulate protein into the matrix	Honey	0.75 to 4 mg/mL	N.R.	Wang et al.[186]
	Glucose	CA	Cu-MOF (HKUST-1-MWCNTs)	Au electrode was pre-treated with H_2O_2 and H_2SO_4 mixture. Then, it was electrodeposited with Pt and DA+HKUST-1-MWCNTs+GOxr the oxidation of DA was triggered by H_2O_2. EP tube was used to avoid water evaporation.	Offers high porosity to improve the active specific surface area of enzyme	Human serum	0.005 to 7.05 mM	0.12 µM	Chen et al.[31]
	Glucose	CA	ZIF-8@ZIF-67	Polyimide film was used as substrate for flexible electrode fabrication. PI film was transformed into graphene using universal CO_2 pulsed laser (LIG) followed by spray coating H-NPC solution. Temperature/pH, glucose and lactate sensors were fabricated by different functionalization.	Source of nanoporous carbon (NPC) materials	Human sweat	0.3 µM to 1.5 mM	0.025 µM	Asaduzzaman et al.[187]

	Glucose	Colorimetry	M-PCN-222 where, M = Mn, Fe, Co, and Ni	Microwave-assisted hydrothermal synthesis of MOFs was done which then exhibited improved peroxidase-mimicking activity. Presence of Fe-PCN-222, H_2O_2, and TMB, resulted into oxidation of TMB into blue colored ox-TMB. GOx was introduced in the system for glucose sensing.	Contains porphyrin active sites exhibiting potential biomimetic catalytic activities	Milk, Orange juice, Grape juice, human tears	Fe-PCN-222:1 to 80 µM	Fe-PCN-222: 0.4 µM	Shu et al.[29]
	Glucose	Colorimetry	IrNCs@Ti-MOF	IrNCs@Ti-MOF, TMB and varying concentrations of H_2O_2 were added into sodium acetate-acetic acid buffer to record chromogenic reaction.	Provides ideal support with high porosity, robustness	Rabbit serum	0 to 600 µM	20.0 µM	Mu et al.[147]
	Glucose	SPR	M-BDC (where, M = Cu, Mn, Ni, and Zr)	The synthesized M-BDC MOFs were hybridized with the Au surface embedded on the SPR chip sensor.	Capturing and co-localizing enzymes and receptors with the target biomolecule	Human serum	Bare Au:5 to 20 mmol/L Cu-BDC:1 to 20 mmol/L Mn-BDC:1 to 20 mmol/L Ni-BDC:1 to 20 mmol/L Zr-BDC: 0.1 to 20 mmol/L	Bare Au: 14.763 mmol/L Cu-BDC: 10.383 mmol/L Mn-BDC: 4.790 mmol/L Ni-BDC: 4.945 mmol/L Zr-BDC: 0.97702 mmol/L	Gumilar et al.[188]
2.	Cholesterol	DPV	BSA-AuNPs-MFOF	BSA-capped AuNPs were synthesized through sonication which were further embedded in MFOF	High S.area, Support matrix	Human whole blood, Egg yolk, Butter, Milk, Goat meat, Cheese, Yogurt and icecream, Beer and apple juice, live cells (RAW 264.7 cells)	250 nM to 3.0 mM	53.2 nM	Arul et al.[189]
3.	L-cysteine	Colorimetry	IrNCs@Ti-MOF	IrNCs@Ti-MOF, TMB and varying concentrations of H_2O_2 were added to a sodium acetate–acetic acid	Peroxidase-mimic activity	Rabbit serum	0 to 50 µM	3.41 µM	Mu et al.[147]

				buffer solution to record chromogenic reaction.					
4.	Glutathione	Colorimetry	Pi@Ce-doped Zr-based MOF	MOF composite was synthesized by the hydrothermal route and then combined with phosphate to enhance its oxidase-like activity.	Possesses strongly positive surface which combine with phosphate to enhances the composite's oxidase-like activity	Human serum	0.8 to 15 μM	0.24 μM	Wang et al.[190]
5.	Dopamine	CA, CV,	MIL-53 (Fe) on carbonized seaweed	Dried seaweed was carbonized through pyrolysis onto which a ZnO nanomembrane was deposited through ALD through multiple cycles. *In situ* synthesis of MIL(Fe) was done on these substrates through solvothermal synthesis.	Outstanding electrochemical performance	Urine, Juice	1.0 to 200 μM	0.73 μM	Ke et al.[191]
	Dopamine	Co-reactant ECL, CV	Zn-tpMOF	Zn-tpMOF was synthesized through one-pot synthesis. The Zn-tpMOF acted as a luminophore in ECL reactions. It exhibited a strong blue-green luminescence with AIE characteristics. ECL emissions were enhanced using DABCO as the co-reactant.	ECL emitter with AIE property	Serum samples	10 nM to 1 mM	8.2 nM	Fu et al.[192]
6.	Sialic Acid	CA	Co/Fe MOF	The sensor was constructed on an Au-SPE through the immobilization of Co/Fe MOF followed by functionalization with N-acetylneuraminic acid aldolase enzyme. The MOF was synthesized through solvothermal route.	Biorecognition element	GD3 ganglioside, HeLa cell lines	0.20 to 1.00 mM	0.026 mM	Kıyıkçı et al.[193]
	Sialic acid	PEC, Colorimetry, EIS	Au@PCN-224	Au@PCN-224 was synthesized and used along with Bi_2S_3 (Au NPs@Bi_2S_3) to form a sandwich like-arrangement on the electrode surface to detect SA aided by two pairs of cis-diol groups.	Inert electroconductivity and nanozyme activity	Human serum samples	5 to 1000 μmol/L	1.44 μmol/L	Cheng et al.[194]
7.	5-fluorouracil	ECL- RET, CV, EIS	Zn-MOF	Ultrasonication based Zn-MOF (energy donor) synthesis was followed with decorated by 5-FU on its surface. CoOOH nanosheets	Organic luminophore with low trigger potential	Human serum	0.001 to 1000 ng/mL	0.52 pg/mL	Peng et al.[195]

				(energy acceptor) were decorated with 5-FU antibody.					
8.	Uric acid	CV, DPV, EIS	Co(II) MOF	GCE electrode surface was modified with Co(II)MOF along with an ink made from carbon black and ethanol.	Monolithic peroxidase mimic	Serum	20 to 350 µmol/L	0.2 µmol/L	Wang et al.[196]
9.	Bisphenol A	ECL, CV, EIS	CD-COF	CD-COF and Pt NPs were mixed then coated on the GCE surface mediated by chitosan followed by dropwise addition Fc-ssDNA onto surface of modified electrode.	Improving the ECL response	Water	1.0×10^{-14} mol/L to 1.0×10^{-5} mol/L	2.21 fM	Ma, et al.[197]
	Bisphenol A	CV, DPV	2D Cu-TCPP	2D Cu-TCPP was fabricated with Tyr assembled within it layer by layer. GCE was polished and drop-casted with the above Tyr@Cu-TCPP composite for electrochemical measurement.	Preserve biological functions of the assembled biomacromolecules	Milk, Plastic mineral water bottle samples	3.5 nM to 18.9 µM	1.2 nM	Ma et al.[198]
10.	Trenbolone	ECL, CV	Eu-BDPO MOF	Au deposition on GCE electrode surface was followed by drop casting TB antibody solution. Then, TB standard substances followed by antigen@Eu-BDPO were dropped on electrode to complete the ECL biosensor assembly.	ECL luminophore	River water	10 fg/mLto 100 ng/mL in all three pH conditions.	pH 5.0: 3.95 fg/mL pH 7.4: 2.36 fg/mL pH 8.5: 5.48 fg/mL	Zhao et al.[199]
11.	Hypoxanthine	LSV, CA	Al-TCPP(Zn) MOF	Al-TCPP(Zn) was spread over ITO surface followed by casting xanthine oxidase on its surface.	Photoactive material	N.R.	1 to 100 µM	0.1 µM	Wang et al.[200]
12.	Ochratoxin A (OTA) Mycotoxin	EIS, CV, DPV	Co-MOFs	AuNPs were conjugated with Co-MOFs. Streptavidin was modified on composite surface followed labelling with DNA2. The GCE electrode was modified with Au NPs@Ti_3C_2MXene. Then, the above synthesized complex was dropped over the surface to complete electrode fabrication.	Electrochemical signal tag and internal reference probe	Red wine	1 to 50 ng/mL	0.31 fg/mL	Guan et al.[201]
	OTA	Chemiluminescence	UiO-66-NH_2	Fe_3O_4@SiO_2@UiO-66-NH_2 was used as the working solution. The sensor was a kind of an optical fibre-mediated homogeneous chemiluminescent immunosensor	Pre-enrichment of OTA in food matrices by OTA adsorption	Crushed wheat, corn, bread mixture	0.1 to 100 ng/mL	0.28 ng/mL	Wei et al. [202]

				which could estimate the adsorption kinetics and isotherms.					
13.	Kanamycin	EIS, ECL	Dy-MOF	Dy-MOF was used as a reaction accelerator, with Gd(III) complex GdPc(acac) as an ECL emitter, all assembled on a GCE electrode.	Co-reaction accelerator	Milk	0.001 pg/mL to 1000 ng/mL	0.3 fg/mL	Duan et al.[203]
	Kanamycin	PEC	Cu-MOF	ITO electrode was coated with Cu-MOF through drop-casting. Then, HP1 DNA was coated over it later being blocked with mercaptohexanol. Different concentrations of cDNA was added dropwise finally functionalizing with SP DNA@ZIS/ZnS QDs@Au–Ag NPs.	Good PEC material showing cathodic photocurrent	Human serum, Milk	1 pM to 1 μM	0.34 pM	Du et al.[204]
14.	Lactate	CA	ZIF-8@ZIF-67	Polyimide film was used as substrate for flexible electrode fabrication. PI film was transformed into graphene using universal CO_2 pulsed laser (LIG) followed by spray coating H-NPC solution. Temperature/pH, glucose and lactate sensors were fabricated by different functionalizations.	Source of nanoporous carbon materials	Human sweat	0 to 56 mM	4 μM	Asaduzzaman et al.[187]
15.	H_2S	Fluorescence	RhB/UiO-66-N_3 MOF	RhB/UiO-66-N_3 MOF acted as a reaction-based ratiometric fluorescent nanosensor. The MOF acts as a platform for accommodation of guest molecule (H_2S) triggering reduction of -N_3 to -NH_2 emitting blue fluorescence which enhances with increasing concentration of H_2S.	Inherent photophysical property and porosity with respect to the guest-encapsulating ability	HepG2 cells	0.05 to 5 mM	29.9 μM	Gao et al.[205]

Abbreviations: *PET: Polyethylene Terephthalate; AAm: Acrylamide; APS: Ammonium persulphate; TEMED: N,N,N',N'-tetramethylethylenediamine; SA: Sodium Alginate; SPE: Screen Printed Electrode; GS NPs: GOx@ZIF-8 NPs; ALD: Atomic Layer Deposition; AIE: Aggregation-induced Emission; MWCNTs: Multiwalled Carbon Nanotubes; DA: Dopamine; SPR: Surface Plasmon Resonance; 5-FU: 5-Fluoro Uracil; ITO: Indium Tin Oxide; LSV: Linear Sweep Voltammetry*

3.1.3. Macromolecules

Macromolecules are high molecular mass compounds comprising of small repetitive monomeric units. The most common biological molecules of this class are proteins, RNA or DNA. However, being a polymer is not a mandatory criterion for these to be called 'macro' molecules since many heterocyclic compounds such as lipids also fall under them. They play a crucial role as biomarkers, hormones or enzymes in the living system[206]. The below segment describes a few of such macromolecules which have been detected using MOF-based electrochemical and optical transducing systems in recent times.

3.1.3.1. MOF-based Electrochemical sensors for macromolecules detection

p53 gene, a transcription factor which plays crucial role in activation and expression of numerous genes and microRNA, is also a tumour suppressor[207]. Its mutation causes a loss in its physiological function leading to promotion of tumour metabolism. Therefore, it can be found in almost half of cancerous tumours in tissues of breast, lung and colon[208]. Various biosensing approaches have already been adopted for its detection in recent times[209,210] but either have complicated operation or suffer with a narrow LDR. In a recent article by Lv et al.[211] on MOF based electrochemical biosensor development for p53 detection, Cr-doped MIL-101-NH_2 MOF was fabricated to act as a hybrid sensor with target responsive releasing and self-catalytic properties (**Figure 1.7A**). The MOF encapsulated methylene blue (MB), a signal probe, which was sealed within MOF cavity by a hairpin (HP) DNA acting as a gatekeeper, covalently immobilized on it. On encountering the aptamer, it hybridized to form dsDNA which had a site for cleavage of HP by the nicking endonuclease, to open the pore thereby releasing MB. The rich G-sequences in the cleaved HP formed a Hemin/G-quadruplex DNAzymes which would combine with MOF to catalyse MB in a redox reaction to observe a signal amplification. The electrochemical detection used DPV in a voltage range from -0.5V to 0V. The current signals generated from released MB corresponded to p53 concentration in a range of 1×10^{-14} to 1×10^{-7} M with an LOD of 1.4×10^{-15} M. This technique can also be adopted for sensitive detection of diverse DNA sequences with specific recognition sites as well.

Insulin, being one of the most important peptide hormones of the body, caters the need for glucose metabolism which thereby regulates normal blood glucose level[212,213]. Detection of insulin levels can be a holy grail for timely detection of diabetes. However, the prominent detection methods rely on expensive machinery and suffer from poor sensitivity and LOD[214,215]. Therefore, electrochemical detection methods using aptasensors have now been into major limelight for its ultrasensitive and cost-effective detection. In a recent article by Sakthivel et al.[216], two MOFs (ZIF-L and Cu-BTC) were synthesized and made into composites to modify Au electrodes for insulin detection upto 0.027 pM within LDR of 0.1 pM to 5 μM (**Figure 1.7B**). Briefly, the electrode was fabricated by dropcast method where the MOF composite was dropped on to disposable Au electrode surface followed by further surface modification using insulin aptamer. 6-mercapto-1-hexanol solution was utilized for blockage of remaining active sites. Insulin solution with varying concentrations was prepared and dropped over modified electrode surface to record the corresponding aptamer mediated reaction using DPV.

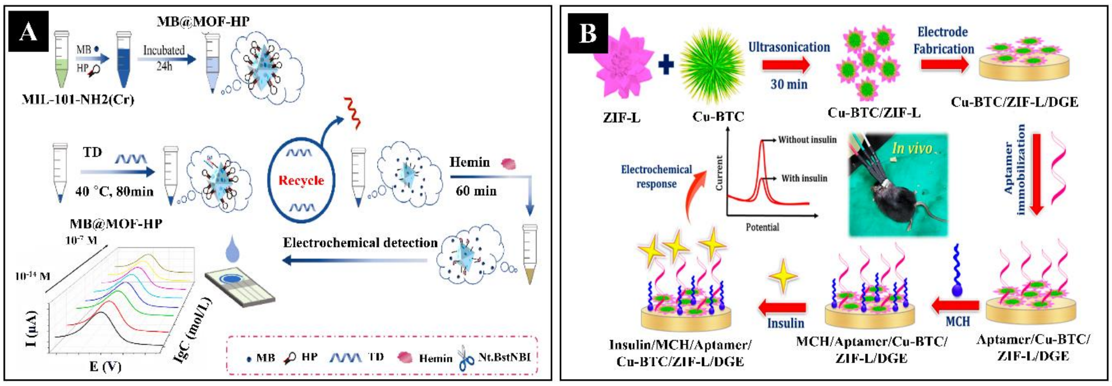

Figure 1.7. ***A)*** *Diagrammatic representation of MIL-101-NH$_2$ synthesis followed by electrochemical sensing of p53 of varying concentrations in PBS buffer solution. Adopted with from Lv et al. [211], copyright 2022.* ***B)*** *Schematic representation of 2D leaf-like ZIF-aptamer sensor for detection of insulin. The DPV response was recorded at several insulin concentrations followed by real time insulin monitoring. Reprinted with permission from Sakthivel et al. [216], copyright 2022.*

3.1.3.2. MOF-based Optical sensors for macromolecules detection

microRNAs are small, non-coding RNAs with a dimension of about 22 nucleotides, that act as gene expression mediators, modulating cellular signalling pathways through mRNA degradation and translational inhibitions[217,218]. The expression levels of these miRNAs play a pivotal role in prognosis and diagnosis of different diseases with its mis-regulation also relating to cancers[219,220]. In a latest study on detection of microRNA in prostate cancer cell lines, an assembly of carbofluorescein FAM-Probe21 with NMOF-FA was made to facilitate fluorescence sensing[221]. Briefly, UiO-66-NH_2 MOF was conjugated to folic acid, followed by mixing it with FAM-Probe21. The expression level of miRNA was determined for different prostate cancer cells like DU145, PC3 and LNCaP of which PC3 is well known for its high expression of folic acid receptors. Fluorescence studies revealed that the target miRNA released the dye-labelled oligonucleotide (Probe21) from the NMOF causing an increase in the fluorescent intensity which was quenched previously due to MOF encapsulation. Therefore, an increase in the miRNA concentration was found proportionate to the fluorescence intensity at 520 nm. The sensor probe was found to be sensitive towards miRNA detection within an LDR of 0 to 1000nM and an LOD of 10 pM.

Apart from RNA molecules, (circulating tumor DNA) ctDNA is also of clinical importance which is a primary triple-negative breast cancer biomarker at an early stage. Its quantitative detection is of significant prognostic and postoperative importance. In a recent work by Zha et al., an ultrasensitive sensing platform for ctDNA was developed using Nd-MOFs (**Figure 1.8A**)[222]. The MOF nanosheet was functionalized with ionic liquid along with AuNPs. This MOF-AuNP combination facilitated higher photocurrent response along with a rise in overall surface area thereby increasing the probe active sites. The GCE/NdMOF@AuNP was functionalized with CP which resulted into generation of an "off signal" for ctDNA in visible light conditions. Post encountering the ctDNA, ferrocene-labelled signalling probes were allowed to attach on the sensing probe which thereby generated a rise in current signals, observable through square-wave voltammetry, termed as a "signal-on". The model system was found capable of detecting ctDNA in a concentration range of 1.0 fmol L^{-1} to 10 nmol L^{-1} as well as 1.0 fmol L^{-1} to 1.0 nmol L^{-1} for PEC and EC model systems, respectively. Two LODs were estimated for the two systems that were 0.63 fmol $L^{-1}$and 0.3 fmol L^{-1}.

Ulinastatin (UTI) is a glycoprotein-based protease inhibitor found in human urine[223]. Its role is in the enhancement of microcirculation by prevention of multiple protease generation[128]. Its imbalance can lead to serious health risks which makes its ultrasensitive detection a clinical necessity. Electrochemiluminescence (ECL) can be an important technique for the purpose, using lanthanide-based MOFs (L-MOFs) as the ECL emitter. In another study by Li et al.[124], europium-based L-MOF has been synthesized via one-pot synthesis method and then, Eu-TATAB has been used as a chromophore for UTI detection and $K_2S_2O_8$ was taken as a co-reactant. The electrode fabrication process involved drop-casting of Eu-TATAB on a polished GCE surface followed by modification with 1-methylimidazole solution for activation of carboxyl group. Then, the surface was modified with antibody Ab_1 attachment followed by immersion of the modified electrode into UTI solutions of varying concentrations. The electrode was finally wrapped with Ab_2/CCB/MNPs subjecting it to ECL detection in $K_2S_2O_8$. Characterization of the ECL sensor was done through EIS which showed a sharp decline in transfer resistance of the modified electrode when compared to bare GCE. The sensor detected UTI within LDR of 0.1 ng mL^{-1} to 10^5 ng mL^{-1} with an LOD of 9.7 pg mL^{-1}. The feasibility of the sensor was demonstrated in spiked real serum samples.

Amongst the clinically importance proteins, one of them is the C-reactive proteins (CRP) which is produced in the liver as a response to inflammation[224–226]. Its synthesis is regulated by the action of IL-6 on gene accountable for its transcription at the site of wound or affliction[227]. This pentameric protein rises in different pathological conditions ranging from edema, cardiac ailment, autoimmune disorders to even the severe acute respiratory syndrome coronavirus 2 (SARS-CoV-2)[228,229]. Therefore, its detection method development is on rise in recent times due to surging cases of CRP increase worldwide. In an article by Ali and Omer[230], they fabricated an ultrasensitive optical biosensor comprising of an aptamer-functionalized Cu-MOF fluorescent nanozyme which detected CRP (**Figure 1.8B**). The biosensor can be operated on dual mode and could detect CRP with an LOD of 40 pg mL^{-1} in fluorescence mode and 240 pg mL^{-1} in the colorimetric mode. The POD activity of the Cu-MOF was exploited to oxidize TMB into ox-TMB generating blue color whereas, on addition of RNA to the MOF restricted its POD like-activity thereby diminishing the signal. An addition of CRP to the MOF/RNA composite caused a release of RNA from the MOF surface leading to consequential restoration of POD-like activity. The fluorescence-based method was found to be more sensitive towards CRP levels. COVID-19 patient serum samples spiked with the CRP protein with varying concentrations was used as the real sample for CRP detection.

Human Epidermal Growth Factor, a 185 kDa transmembrane glycoprotein complex, is overexpressed in most of the primary invasive breast cancers (BC) causing uncontrolled tumor growth and metastasis[231,232]. A rise in its concentration in cancer patients to 15-75 ng mL^{-1} is observed, which is highly elevated to its normal concentration of about 2-15 ng mL^{-1} [233]. So, development of detection methods for its (or its receptor's human epidermal growth factor receptor 2 (HER-2)) ultrasensitive quantification is of great clinical significance. Recently, a group of scientists have worked on fabrication of an

ECL biosensor towards its detection using a novel ECL system comprising of ZMB/$S_2O_8^{2}$ [234]. They have used AuNPs decorated graphite-like carbon nitride (g-C_3N_4@Au) as the sensing matrix that could function in a potential range of −1.2 V to 0 V to generate an ECL signal in presence of peroxydisulfate ($S_2O_8^{2-}$) co-reactant. Amino-modified capture probes (CP) were immobilized on this complex via the Au-N bonds. Additionally, a Zr-based MOF modified with boron carbon oxynitride (ZMB) was also synthesized which exhibited ECL intensity in the potential range of −2.0 V to 0 V with 0.8 mM $S_2O_8^{2-}$. For the fabrication of the ECL biosensor, a pre-treated GCE electrode surface was coated with g-C_3N_4@Au. Then on drying, it was incubated with CP solution followed by treatment with BSA to block the redundant non-specific binding sites. The surface was topped with dropping the tracer label to form the modified electrode for HER-2 detection. ECL experiments were performed in 0.1 M PBS (pH 7.0) containing 0.8 mM $K_2S_2O_8$. An ECL intensity which was initially hindered on addition of CP and BSA was greatly enhanced, in form of cathode ECL emission, on introduction of the tracer label. On addition of HER-2 solutions of varying concentration, the tracer label detached from the electrode surface rooting a decline in ECL emissions again. The biosensor worked well in an LDR of 0 fg mL^{-1} to 100 ng mL^{-1} with an LOD of 0.2 fg mL^{-1}. The applicability of the sensor was verified on real diluted human serum samples spiked with HER-2 solutions, exhibiting a good recovery of almost 95%. Hence, the discussion proves utility of MOFs in sensing matrices for ultrasensitive detection of macromolecules ranging from biomarkers to hormones and many more.

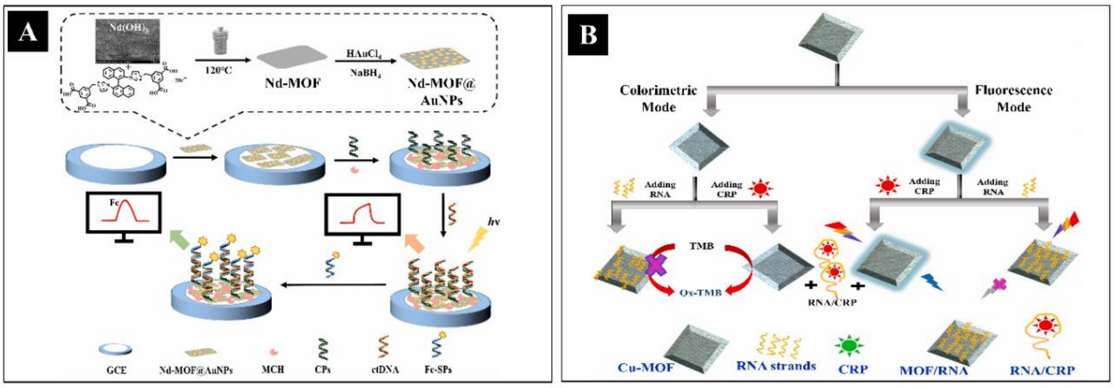

Figure 1.8. ***A)*** *A schematic representation of Nd-MOF-based nanosheets capable of detecting ctDNA facilitated by gold nanoparticles and ionic liquid. Reprinted with permission from Zha et al.*[222]*, copyright 2023.* ***B)*** *Graphical illustration of Cu-MOF functionalized with aptamer for ultrasensitive detection of C-reactive protein. Reused with permission from Ali and Omer [230], copyright 2022.*

Recently reported MOF-based biosensors for detection of macromolecules have been comprehensively discussed in **Table 1.3** below with their respective target analytes, detection techniques, fabrication strategies, real samples considerations and detection efficiency parameters (LDR and LOD).

Table 1.3. *Detailed list of latest MOF-based biosensors for sensing of macromolecules. (N.R.: Not Reported)*

S.No.	Target Analyte	Detection Mechanism	Sensor Composite	Fabrication strategy	MechanisticRole of MOF	Real Sample	LDR	LOD	Reference
1.	Lincomycin	PEC	Heterostructured NiS@Ni_3S_2/CdS photoactive composite derived from a Ni-ZIF MOF	Sulfofication of Ni-Zr MOF was done to synthesize a photoactive composite which was modified further to form an aptamer-based (APT) sensing electrode based on a coupling reaction.	High S.Area, Superior photocurrent response	Milk	0.0001 to 1.25 nM	0.067 pM	Zhang et al.[235]
2.	G-triplex mediated DNA of Mycoplasma bovine pneumonia	CV, EIS, DPV	NH_2-MIL-53(Al)	GCE surface was electrodeposited with AuNPs which were further immersed into PEG and MOF composite solution. The electrode surface was then drop casted with G3 DNA probe. Methylene blue and phenothiazine were used as electrochemical indicator	Adsorption matrix	10% goat serum	10^{-10} to 10^{-6} M	1.00 pM	You et al.[236]
3.	Glutathione S-transferase	Colorimetry	Pi@Ce-doped Zr-based MOF	The MOF composite was synthesized by the hydrothermal method and then was combined with phosphate to enhance its oxidase-like activity.	Oxidase-like activity	Human serum	0.0002 to 0.006 U/L	0.19 mU/L	Wang et al.[190]
4.	Alpha-fetoprotein (AFP)	ECL, CV, EIS	NiZn MOF	NiZn as catalysts were synthesized through partial pyrolysis and then the surface was decorated with AuNPs followed by functionalization with anti-AFP proteins on its surface for selective detection of AFP.	Energy-sorption for catalysis	Human serum	5×10^{-5} to 10^{2} ng/mL	0.98 fg/mL	Zhao et al.[237]
5.	I27L gene	ECL	Eu-MOFs	A one-step room temperature synthesis approach was adopted for the Eu-MOF growth. It was then immobilized on a GCE electrode surface successively with AuNPs. Finally, H1(target DNA strand) was drop-casted on it for selective cleavage and detection of the target protein.	ECL emitter	Human serum	1 fM to 10 nM	447 aM	Dai et al.[238]

6.	Exosomal piR-823	Ratiometric Fluorescence	AuNCs/UiO-66-NH_2	UiO-66-NH_2 MOF composite was synthesized by hydrothermal route and was subsequently conjugated with AuNCs through Au-N bond.	Support matrix	Human serum	0.04 to 4 pM	10.2 fM	Tong et al.[239]
7.	Thrombin	Photoluminescence, ECL, CV, EIS	Ru@$Ni_3(HITP)_2$	Ru@$Ni_3(HITP)_2$ was adorned on the GCE, followed by dripping the surface with AuNPs. It was then followed by immobilization of TB aptamer on it. Thereafter, the ferrocene-labelled single-stranded DNA (Fc-S1) was added to conjugate with the TB aptamer to cause ECL signal quenching.	ECl-conductivity enhancer	Human serum	1 fM to 1 nM	0.62 fM	Zhang et al.[240]
8.	Neuron-specific enolase (NSE)	ECL-RET, EIS	FeMOFs-sCuO	FeMOFs were prepared through hydrothermal synthesis. They were applied to load sCuO to obtain FeMOFs-sCuO nanocomposite which was used as a quenching probe for P-C_3N_4-CoPdNPs towards sensitive analysis of NSE.	ECL-RET dual quencher	Human serum	0.00005 to 100 ng/mL	20.4 fg/mL	Hu et al.[241]
9.	CRISPR/Cas14a-based *Burkholderia pseudomallei* specific DNA sequences detection	DPV, EIS, CV	PtPd@PCN-224	Solvothermal synthesis of PCN-224 was followed by *in situ* generation of PtPdNPs to facilitate its binding with P-ssDNA	Signal-amplification tag	Human serum	100 aM to 10 nM	12.8 aM	Li et al.[242]
10.	Nanoscale exosomes	ECL, CV	TCPP/UiO-66-NH_2	TCPP/UiO-66-NH_2 synthesis was carried out through a one-pot solvothermal reaction followed by post-synthetic metalation with Zn^{2+}ions. Fluorine-doped tin oxide (FTO) electrodes were coated with positively charged chitosan followed dipping the electrode in negatively charged AuNP solution. Thiol-modified CD63-binding peptide was drop casted on electrode surface.	ECL emitter	HepG2 cells derived exosomes added in exosome depleted fetal bovine serum (FBS)	1.00×10^4 to 3.16×10^6 particles/µL	9.08×10^3 particles/µL	Wang et. al.[243]
11.	Glial Fibrillary Acidic Protein	CV, EIS	Au@ZIF-8@rGO	One-pot solvothermal synthesis of ZIF-8 was done. *In situ* AuNPs were synthesized in GO, ZIF-8	High S. area	Urine	50.0 to 10 000.0 fg/mL	50.0 fg/mL	Mehmandoust et al.[244]

				solution mixture to form the composite.				
12.	MicroRNA	DPV	Co-MOFs	Co-MOFs were synthesized by solvothermal route and then functionalized with Streptavidin. In another set of experiments, the walker DNA (WD)/blocker DNA (BD) complex, with which miRNA-141 would react, were decorated on the HP1-functionalized Magnetic Beads' surface to complete probe fabrication.	Signal probe	Human serum	1 fM to 10 nM	0.46 fM	Guan et al.[245]
13.	α-Glucooxidase, Alkaline phosphatase, and AAO	Colorimetry	AuNPs/UiO-66	UiO-66 MOF was prepared through solvothermal synthesis followed by composite formation involving MOF and AuNPs for the colorimetric analysis.	Enhanced peroxidase-like activity	Human serum	α-Glucooxidase:0.005 to 1.9 U/mL Alkaline phosphatase: 1.25 to 37.5 mU/mL AAO: 0.5 to 10 mU/mL	α-Glucooxidase: 0.002 U/mL Alkaline phosphatase: 0.14 mU/mL AAO: 0.34 mU/mL	Liu et al.[246]
14.	Acetylcholinesterase (AChE)	Colorimetry	Cu-CAT NSs (Copper chatecholate Nanosheets)	2D MOF was synthesized based upon Cu-CAT using dextran-assisted ultrasound exfoliation of the bulk Cu-CAT. The synthesized Cu-CAT nanosheets exhibited peroxidase like activity leading to AChE sensing.	Peroxidase-like activity	HA tablets	0.01 to 4.0 mU/mL	0.01 mU/mL	Wang et al.[247]
15.	miRNA-10b	CV, EIS	NMOF@Cu^{2+}	NMOF coordinated with Cu^{2+} was coupled with a 3D DNA walker. The carboxyl group in the organic ligand of NMOF assembled complementary DNA strand for biorecognition reaction.	DNA strand assembly, Catalysis	Human serum	0.8 pM to 250 pM	0.5 pM	Tang et al.[248]
16.	miRNA-21	CV, LSV, DPV	ZIF8	Fluorine-doped tin oxide electrode was primarily electrodeposited with AuNPs with subsequent modification by GDH/NAD^+ followed by controlled etching and TA addition.	Encapsulation of moieties	Spiked healthy human serum, human normal liver cells (L-02	0.01 to 1000 fM	2 aM	Yan et al.[249]

						cells), human liver cancer cells (HepG2 cells), and human BC cells (MCF-7 cells)			
17.	Amyloid β 42	Aggregation-induced ECL resonance energy transfer (AIECL-RET), CV	Au@UiO-66-NH_2	GCE electrode was drop-casted with Ag@ZnPTC/BSA/Ab_1. Aβ42 antigen solution of varying concentrations was added to the modified electrode surface. Then, finally Au@UiO-66-NH_2/BSA/Ab_2 was dropped on its surface to complete the sandwich biosensor.	ECL emission acceptor and donor	Spiked human serum	10 fg/mL to 100 ng/mL	2.4 fg/mL	Yang et al.[250]
18.	HBV DNA	ECL, CV	Al-MOF	Polished GCE surface was drop-casted successively with Al-MOF (synthesized through solvothermal method) and AuNPs. Then, it was dripped with S1 followed by DA-S2. Afterwards, various concentrations of HBV and Exo III were added to its surface successively. Post washing with PBS, the fabricated electrode was tested in HEPES buffer.	ECL activity	Human serum	100 aM to 10 pM	62.1 aM	Chen et al.[251]
19.	Exosomal miRNA-155	Surface Plasmon Resonance	Zr-MOF	Aptamer-engineered RBCs were labelled with PKH26 and exosomes with PKH67. The fluorescence-labelled engineered RBCs and exosome suspensions were visualized through microscope.	Complexation and strengthening of SPR response	Human plasma	1 fM to 1×10^6 fM	2.03 fM	Fan et al.[252]
20.	SARS-CoV-2 spike antigen	Fluorescence	MOF-5/$CoNi_2S_4$	MOF-5 was adorned with $CoNi_2S_4$.followed with H_2TMP for the antigen detection.		Recombinant SARS-CoV-2 spike antigen	NR	5 nM	Rabiee et al.[253]
21.	VEGF165	PEC, EIS	Nd-MOF	Nd-MOF/GCE electrode surface was introduced with dsDNA and	High S.Area	Human serum	0.01 to 100 ng/mL	3.51 pg/mL	Zhong et al.[254]

				ALP. Aptamer-antigen reaction led to aptamer shedding from electrode surface leading to decline in the charge-transfer resistance. Thereafter, ascorbic acid was yielded by the catalysis of l-ascorbic acid 2-phosphate which subsequently reduced $HAuCl_4$ to produce AuNPs leading to localized SPR and VEGF165 sensing.					
22.	CEA	PEC	Cu-MOF	ITO electrode was coated with Cu-MOF through drop-casting. Then, HP1 DNA was coated over it later being blocked with mercaptohexanol. Varying concentrations of cDNA were added dropwise finally functionalizing with SP DNA@ZIS/ZnS QDs@Au–Ag NPs.	PEC material for cathodic photocurrent generation	Human serum, Milk	0.1 fg/mL to 0.1 ng/mL	0.045 fg/mL	Du et al.[204]

Abbreviations: *S.Area: Surface Area; AuNcs: Gold Nanoclusters; TB:Thrombin; GO: Graphene Oxide; HA: huperzine A; GDH: Glucose Dehydrogenase, NADH: nicotinamide adenine dinucleotide; BC: Breast Cancer; TA:Tannic acid; RBCs: Red Blood Cells, CEA: Carcinoembryonic Antigen*

3.1.4. In vitro cell detection

3.1.4.1. Prokaryotic cell detection

Bacillus anthracis is a dangerous pathogen known to cause severe pulmonary anthrax in mammals with a fatality of about 90%. Electrochemical and luminescence-based approaches have been readily adopted for recognition of bacterial markers such as 2,6-pyridine dicarboxylic acid (DPA) over other methods due to simpler operation and low cost. In a recent research by Liu et al.[255], NH_2 functionalized Eu-based MOF was used for fluorescent-sensing of DPA molecules (**Figure 1.9A**). The MOF exhibited no luminescence in ethanol (MOF dispersive medium) but with addition of DPA, luminescence of both Eu^{3+} and amino ligand NH_2-BDC got recovered due to stable complexation of Eu^{3+} with DPA. Fluorescence intensity of amino ligand at 460 nm was found proportionate to DPA concentrations whereas that of Eu^{3+} at 705 nm shifted to 624 nm, with an LDR of 0-100 μM. Two LODs as 0.36 μM and 0.8 μM were reported for two different solvent systems water and ethanol, respectively. The values were much lower than infectious bacterial spore load for humans.

Another pathogenic bacterium, *Burkholderia pseudomallei* known for its high fatality infection in humans, is nowadays being detected sensitively using MOFs. In a recent article by Wang et al.[256], this pathogenic species was detected using Co-doped MOF adorned with AuNPs and N-(4-aminobutyl)-N-(ethylisoluminol) exhibiting improved ECL activity as compared to previously reported biosensors. This was aided by its zero-distance catalytic properties. The LOD was found to be 60.3 aM with a detection capability as low as 9.0 CFU mL^{-1}. Briefly, the biosensor was prepared on GCE electrode with immobilization of Au@Co-MOF@ABEI on its surface followed by aptamer DNA strands which bound to dopamine and thereby quenched the ECL. Then another DNA strand attachment turned the signal "on". The characterization of electrode was done using techniques such as EIS and CV at every step of electrode modification. LDR was found in the range of 10^2 to 10^8 aM. On verification of biosensing platform in serum samples containing the pathogen, it had a good applicability for detecting *B. pseudomallei* within a range of 1.5×10^1 to 1.5×10^5 CFU mL^{-1}.

Various microbial species are currently of public health concern including *Staphylococcus aureus* which is known to cause life-threatening illness including sepsis, acute renal failure, meningitis and gastrointestinal reaction[257]. It is often detected through techniques like qPCR and ELISA which are rapid but have high cost and low stability. Therefore, these shortcomings have been resolved through latest works by Chen et al.[258]. According to the study group, development of MOF-based aptasensor with colorimetry and electrochemical modes of detection was proposed. Cu-MOF conjugated with gold nanoparticles served the dual purpose of catalysis (in chromogenic reaction) and electrochemical response genesis by virtue of its Cu^{2+} dopant (**Figure 1.9B**). Screen-printed carbon electrode was modified with MB aptamer/ssDNA-Au/CuMOF and scanned in the potential range of 0.2-0.6 V with pulse amplitude of 50mV and pulse width of 0.05s for DPV response measurement. The peroxidase-mimicking activity was also explored taking TMB-H_2O_2 reaction system as a typical model system which has a distinct oxidation peak of 450 nm in presence of Au/Cu-MOF. The aptasensor indicated a good electrochemical response in a range of 10 to 10^8 CFU mL^{-1} with an LOD of 5 CFU mL^{-1}[258].

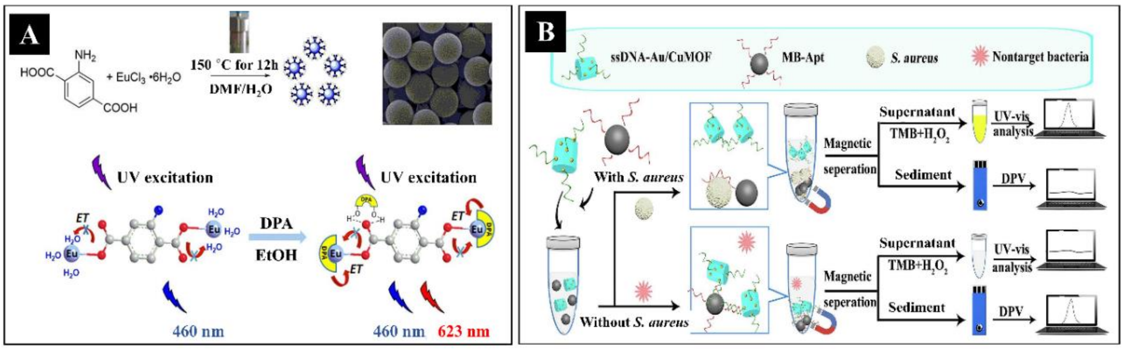

Figure 1.9. ***A)*** *Graphical representation of Eu-MOF for detection of anthrax biomarker (DPA). Inset image corresponds to SEM result for NH_2-BDC-Eu-MOF composite. Reused with permission from Liu et al. [255], copyright 2022.* ***B)*** *Pictorial representation of multifunctional MOF-based dual mode (colorimetric and electrochemical) aptasensor for S. aureus detection. Reported with permission from Chen et al. [258], copyright 2023.*

3.1.4.2. Eukaryotic cell detection

Breast cancer (BC) being one of the most common cancers affecting women globally, if diagnosed at an early stage is usually non-aggressive in nature. However, the aggressiveness of BC is attributed to over expressivity of multiple cell markers including HER-2[259–262]. Therefore, identification of aggressive BC cells' phenotype can help in therapy and its timely prognosis. Addressing the problem, Wang et al.[263] in their recent study have developed an electrochemical biosensor using a MOF-based probe AuNPs@HRP@ZIF-8 (**Figure 1.10A**). They synthesized HRP-encapsulated ZIF-8 which was further modified using AuNPs. HER-2 protein is a transmembrane tyrosine kinase receptor belonging to the family of epidermal growth factor receptors (EGFR or ErbB). It is overexpressed in different cancer types such as ovarian, gastric, breast and oral[264,265]. The ZIF-8 surface used in the study catered attachment of peptides specific to target protein HER-2 and MMP-2 due to presence of numerous active sites. Then this recognition sequence was immobilized on indium tin oxide (ITO) electrode as well. On encountering BC cells, the AuNPs@HRP@ZIF-8 was cleaved off leading to target protein detection. The sensing performance was studied using CV and EIS measurements. DPV was also performed from 0.5 V to -0.1 V and i-t curve was recorded at -0.1 V. The results revealed detection range for HER-2 and MMP-2 from 50 fg mL^{-1} to 50 ng mL^{-1} and 10 fg mL^{-1} to 10 ng mL^{-1} with an LOD of 16.8 fg mL^{-1} and 5.33 fg mL^{-1}, respectively. The results were verified on real samples to detect the phenotype of four different types of BC cells to quantify these markers. SK-BR-3 and BT-474 cells were found to be more aggressive on the level of HER-2 expression when compared to MCF-7 and MDA-MB-231 triple-negative BC cells. In another study on electrochemical fluorescence-based CDs@ZrHf-MOF, CDs were embedded in the MOF cavity[266]. The sensor possessed a very low detection limit of 19 fg mL^{-1} for HER-2 protein and 23 cell mL^{-1} for MCF-7 cells, with their respective detection ranges of 0.001-10 ng mL^{-1} and 1×10^{2} to 1×10^{5} cell mL^{-1}. The aptasensor fabrication involved drop-casting of CDs@ZrHf-MOF suspension on pre-treated Au surface succeeded by incubation with HER-2 aptamer solution to embed the aptamer on its surface. EIS, CV and DPV measurements were carried out to validate sensor assembly at each step. On interaction of HER-2 with the aptamer, complex formation took place which resulted to an increase in the R_{ct} value from 0.261 kΩ to 0.480 kΩ. Apart from BC, cancer cases in general are on rise with colorectal cancers (CRC) contributing a major part of gastrointestinal malignancies globally[267,268]. Electrochemical method when compared to other diagnosis approaches is highly time efficient, low cost and fluorescent-label free with aptamer-based ones gaining more attention[269,270]. In a study by Duan and group[271], CT26 cells present in CRC were selectively detected using Cr-MOF/CoPc hybrid immobilizing cell-targeted aptamer. Au electrode was drop-casted with Cr-MOF@CoPc-2 followed by immersion into aptamer solution. Finally, the modified electrode was dipped into CT26 cell suspension. EIS and DPV studies showed LOD values for the cells to be 36 and 8 cells mL^{-1} which was further verified through real sample analysis using human serum samples spiked with CT26 cells of varying concentrations.

Circulating tumor cells (CTCs) are easy and less painful source of cancer detection when compared to conventional tissue biopsy[272]. However, the challenge lies in their rare abundance in blood circulation with only 1-10 circulating cells mL^{-1} on an average amid a lot of significant interferents surrounding them[273]. Recently, Zhang et al.[274] have proposed a dual-mode aptamer based electrochemical and fluorescent sensor detecting MCF-7, HepG2, MB-468, HeLa, and MCF-10A cell types (**Figure 1.10B**). The Mapt-EF sensor, fabricated on ITO electrode used Co-Fe bimetallic MOF which was capable of catalysing the disintegration of H_2O_2 to release oxygen. An aptamer chain was designed with a dual purpose of capturing three cancer biomarkers namely, PTK7, EpCAM and MUC1 along with inhibiting the catalase like-activity of the MOF. The ITO electrode was negatively biased to adsorb positively charged compound, MB and TMB molecules imparting high fluorescence and electrochemical signal intensity. CV-based sensor characterization was done followed with checking its applicability in real blood sample. The sensor was found capable of detecting upto a single cell in the medium with an LOD of 11, 9, 10, 10, 11 cells mL^{-1} for HepG2, HeLa, MCF7, MDA-MB-468 and MCF-10 BC cells, respectively. Colorimetry-based CTCs detection has also been demonstrated by another group using CuFe-NH_2-MIL-101 MOFs[275]. The MOF possessing peroxidase-mimicking activity derived its fluorescence ability in the excitation wavelength range of 280-410 nm from Cu present in the MOF composite. EpCAM receptors on the HCT116 cells were used as the transmembrane cell surface glycoprotein which were targeted using specific antibodies to capture the cells. The fluorescence intensity was governed by binding of CuFe-NH_2-MIL-101 with EpCAM antibody. Moreover, the colorimetric response increased with increase in the cell concentrations contrary to the fluorescence readout which decreased over time. The sensor was capable enough to detect cells in the range of 10^2 to 2×10^6 cells mL^{-1} with the LOD being 12 cells mL^{-1}.

Therefore, as per the detailed discussion in the above section it can emphasized that these MOFs have been a material of choice in recent times for biosensor probe fabrication for detection of all kinds of cells. They can be an optimal sensing matrix when conjugated with cell specific antibodies for ultrasensitive cell detection.

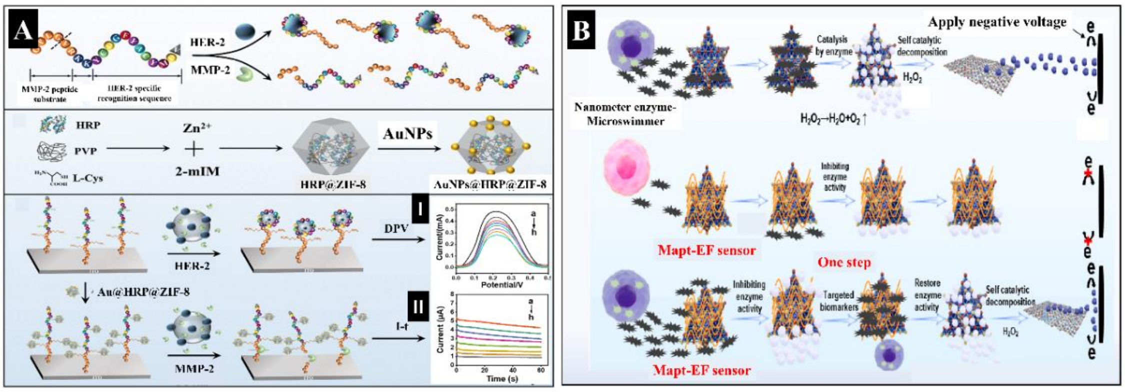

Figure 1.10. ***A)*** *Diagrammatic illustration depicting MOF-based biosensor for identification of aggressive BC cells using overexpressed HER-2.* ***I)*** *DPV curve for analysis of HER-2 at varying concentrations.* ***II)*** *Amperometric response for varying concentrations of MMP-2. Adopted from Wang et al. [263], copyright 2023.* ***B)*** *Diagrammatic representation of Co-Fe-MOF for simultaneous detection of multiple cancer markers for CTC capturing, identification and counting. Reprinted with permission from Zhang et al. [274], copyright 2023.*

Recently reported MOF-based biosensors for detection of prokaryotic as well as eukaryotic cells have been comprehensively discussed in **Table 1.4** below with their respective target analytes, detection techniques, fabrication strategies, real samples considerations and detection efficiency parameters (LDR and LOD).

Table 1.4. *Detailed list of latest MOF-based biosensors for sensing of cells (prokaryotic and eukaryotic). (N.R.: Not Reported)*

S.No.	Target Analyte	Detection Mechanism	Sensor Composite	Fabrication strategy	MechanisticRole of MOF	Real Sample	LDR	LOD	Reference
1.	*Salmonella typhimurium*	Colorimetry	MIL-88@Pd/Pt	MIL-88@Pd/Pt composite was synthesized by *in situ* growth of Pd, Pt NPs over the surface of MIL-88 MOF. The complex acted as a peroxidase mimic which along with MNBs caused specific separation and labelling of target pathogen.	Peroxidase mimic and high S.Area	Chicken meat supernatant	4×10^1 to 4×10^5 CFU/mL	32 CFU/mL	Yuan et al.[276]
	Salmonella	Colorimetry	NH_2-MIL-101(Fe)	Modified magnetic nanobeads MNB-*Salmonella*-MOF sandwich complexes were made which were used to catalyse o-phenylenediamine to generate colorimetric response.	High S.Area	Spiked chicken meats	1.5×10^1 to 1.5×10^7 CFU/mL	14 CFU/mL	Qi et al.[277]
	Salmonella	Colorimetry	ZrPr-MOF	Zirconium praseodymium MOF acted as nanozyme to detect the pathogen by converting TMB to ox-TMB, liberating colorimetric response.	Peroxidase-mimic activity	Water, Milk	10^2 to10^8 CFU/mL	37 CFU/mL	Mirsadoughi et al.[278]
2.	*Escherichia coli (E. coli)*	PEC, CV, EIS	In_2O_3/CeO_2@mNC	PolyMOF(Ce) were hydrothermally synthesized to adsorb trace indium ions (In^{3+}). Further the complex was calcined at high temperature forming In_2O_3/CeO_2@mNC hybrids.	High S. area, large pore size, multiple functionalities for PEC	Raw milk, Bread	10^{-1} to 10^7 CFU/mL	1.12 CFU/mL	Wang et al.[279]
	E. coli	Photoluminescence	NH_2-MIL-53(Fe) MOF	NH_2-MIL-53(Fe) MOF-metal composite was synthesized and conjugated with galactose and mannose sugars.	Luminescent property and high S. area	Bacteria culture cells	19 to 10×10^6 CFU/mL	8 CFU/mL	Bhatt et al.[280]
	E. coli	Fluorescence	Zr-UiO-66-$B(OH)_2$	The MOF was functionalized with boric acid to adhere bacterial cells. Ab_1-MNP-target bacteria-Zr-UiO-66-$B(OH)_2$ complex was created and dispersed in H_2O_2 solution for quantitative estimation of bacteria.	Photocatalytic inactivation of bacteria, fluorescence properties	Drinking water, Milk	5.0 to 2.5×10^4 CFU/mL	1.0 CFU/mL	Zuo et al.[281]
3.	*Staphylococcus aureus* (*S. aureus*)	EIS, DPV	ML-Cu_2O@Cu-MOF	A suspension of ML-Cu_2O@Cu-MOF was dropcasted on a pre-treated Au electrode surface which was later incubated with a targeting aptamer.	Anchoring ability to aptamer, conductivity	Milk, honey, and biscuit	0 to 1×10^8 CFU/mL	1.6 CFU/mL	Tian et al.[282]

4.	*P. aeruginosa*	Photoluminescence	NH_2-MIL-53(Fe) MOF	NH_2-MIL-53(Fe) MOF was synthesized and conjugated with galactose and mannose sugars	Luminescent property and high S. area	Bacteria culture cells	170 to 33×10^7 CFU/mL	202 CFU/mL	Bhatt et al.[280]
5.	SARS-CoV-2	Colorimetry	MIL-101(CuFe)	CD147-modified MIL-101(CuFe) was prepared which oxidized TMB, yielding ox-TMB in the presence of H_2O_2, to generate a colorimetric response.	Peroxidase-like activity	SARS-CoV-2 pseudovirus in human serum and real virus sample	SARS-CoV-2 pseudovirus in human serum: 0.003 to 48.9 µg/mL; real virus sample:10 to 10^4 PFU/mL	SARS-CoV-2 pseudovirus in human serum: 0.09 ng/mL; real virus sample: 3 PFU/mL	Zhao et al.[283]
6.	Cauliflower mosaic virus 35S promoter (CaMV 35S)	PET, FRET	Fe-MIL-88	The FAM-ssDNA probe was fabricated complementary to the targeted CAMV 35S. In its absence, the FAM ssDNA got adsorbed on surface of the Fe-MIL-88 MOF causing a fluorescence quenching event.	High S. area, greater quenching and DNA binding abilities	Transgenic plant genomic DNA	5 pM to 50 nM	0.184 pM	Liu et al.[284]
7.	Breast cancer cells (HER-2, MMP-2)	EIS, CV	AuNPs@HRP@ZIF-8	ZIF-8 based probe was modified with AuNPs for binding with the target peptide (Au-S, Au-N bonding) and HRP.	High S. area	BC cells	HER-2:50 fg to 50 ng/mL MMP-2:10 fg to 10 ng/Ml	HER-2:16.8 fg/mL MMP-2:5.33 fg/mL	Wang et al.[263]

Abbreviations: *S.Area: Surface Area; MNBs: Magnetic Nanobeads; PET: Photoinduced electron transfer; FRET: Fluorescence resonance energy transfer; HRP: Horse Radish Peroxidase; BC: Breast Cancer*

3.2. Electrochemical MOF-based Biosensing matrices for Disease Diagnosis

In recent times, the convergence of nanotechnology, materials science, and bioengineering has led to revolutionary progress in the advancement of biosensors, heralding a new age of accurate diagnosis and personalized healthcare [285,286]. The increasing worldwide prevalence of infectious and fatal diseases, including those that can be transmitted and others that cannot, highlights the dire need for diagnostic methods that are simple, fast, accurate, and affordable [287]. Conventional laboratory diagnostic methods do not meet these requirements, thereby requiring novel technologies which are capable of tackling the difficulties such as early diagnosis, continuous monitoring, and point-of-care testing [288,289]. Electrochemical biosensors have emerged as plausible solutions overcoming previous methodological setbacks incorporating a plethora of nanomaterials[290].

Among the several materials investigated for the development of sensors, MOFs have emerged as an extremely promising category of materials with distinct features that make them well-suited for use in electrochemical sensing applications [291]. MOFs, distinguished by their elevated surface area, flexible porosity, and effortless functionalization have improved performance and specificity of sensors to many folds [292]. One of the key characteristics of MOFs is their modular structure, consisting of metal nodes and organic linkers, which enables the customization of their properties for the development of sensors that can detect a wide array of proteins and other molecules linked to different diseases [293,294]. The combination of the diverse attributes of MOFs and the responsiveness of electrochemical methods has facilitated the advancement of sensors that have improved analytical capabilities, establishing them as preferred materials in the field of healthcare [295]. One fundamental aspect of electrochemical sensors based on MOFs is their application in different sensing methods, such as amperometry [296], voltammetry [297], and impedance spectroscopy [298]. Such integration enables the identification of biomarkers at extremely low levels, hence allowing for the timely detection of diseases such as diabetes, cancer, cardiovascular, pulmonary, neurological disorders and infectious conditions [299].

Due to their ease in production and ability to work well with small electronic devices, MOF-based electrochemical sensors have great potential in the advancement of portable and user-friendly diagnostic systems. Commercial availability of MOFs such as ZIF-8, MIL-53(Al), HKUST-1, Fe-BTC and others is an imperative of MOF-enabled product demands in real world [300]. Point-of-care testing (POCT) devices have recently been engineered with MOFs to simplify testing and improve analytical performance supplementing devices to overcome the challenges associated with antibody-associated POCTs [301]. The possibility of incorporating MOF-based sensors with smartphones and wearable technology enhances the versatility of these sensors for the detection of multiple biomarkers by virtue of organic functioning, extended shelf-life and thermal stability [302].

The global burden due to infectious and fatal diseases is increasing and millions of mortalities are occurring from diabetes, viral infections, cardiovascular, pulmonary, and many others [303]. Various studies on MOF-based electrochemical sensors for the detection of different disease-specific biomarkers have recently highlighted MOF-mediated POCT research progression. Li et. al described the MOF based electrochemical sensors solely for the detection of glucose [304], similarly Wang et. al in their study discussed about MOFs used for electrochemical sensing of viruses [305], hence limiting their study to a particular disease. Another study by Li et. al discussed about MOF based sensors for small, macromolecules and cells but their study mainly revolved around the synthesis and fabrication of MOF with a limited discussion on targeting biomolecules [306]. Hitherto such studies evidently suggest the rising interest of researchers towards these molecules, our Scopus based analysis also backs the same. The studies that were limited to only a handful of reports on MOF-based electrochemical sensors in 2013 have risen to >200 annual articles. All such reports have emphasized on the role of MOFs in sensor matrices through molecular perspective while a study encompassing their crucial role through perspective of a range of diseases and their relevant biomarkers is still lacking. This review focusses on the recent advances in different kinds of MOFs, their functionalization strategies, and applications in the realm of electrochemical sensors for disease diagnosis. We have thoroughly studied the role of MOFs as a matrix component in conjugation with different nanomaterials for their application in healthcare and human wellbeing. Additionally, we have discussed various globally developed MOF-based sensor matrices for disease diagnosis in tabulated form describing their target analyte, detection technique, sensor composite, fabrication strategy, mechanistic role of MOF, real sample, linear dynamic range (LDR) and limit of detection (LOD). Also, the challenges and future prospects of MOF-based electrochemical sensors have been discussed which allows the readers to ponder and eventually work towards innovative technological translations from the laboratory to the clinical settings. In addition to improvement of analytical performance, the incorporation of MOFs into electrochemical sensing platforms brings in a new era in point-of-care diagnostics. We hope that our critical analysis will add to the expanding amount of information highlighting the revolutionary potential of MOF-based electrochemical sensors for more accurate diagnosis and enhanced medical outcomes.

Selective and sensitive detection of disease biomarker in a complex biological sample is of utmost importance for early disease diagnosis and prognosis. Electrochemical signal sampling plays a key role in POCT devices where the use of miniaturized electrochemical sensors to detect a range of electrolytes is done by observing a change in current, potential or impedance caused by the redox properties of the analyte species [301]. Such changes in signals within the MOF-based POCT devices are brought up by MOFs' electronic and catalytic properties levied by the functional groups such as amine and nitro which are often associated with their linker components [75]. Not only this, Co, Ni and Cu centred

MOFs have been found to be highly electrocatalytic in nature which is attributed to their enriched electron transfer capabilities from their metal centers to their respective ligands [76,77]. With advancement in technology, MOFs have gained importance in biomarker detection due to enormous surface tailoring possibilities they offer, bestowing them with catalytic potential, functionalization sites, porosity and huge surface area facilitating molecular adhesions (Shubhangi et al., 2024).

Researchers globally have understood the importance of these porous structures in the field of fluorescence and electrochemical sensing matrices for disease diagnosis. Some of the major disease detection sensing probes with electrochemical MOF-based nanocomposites' constituents have been elaborated in the upcoming sections.

3.2.1. MOF-based electrochemical sensors for Diabetes

Diabetes accounts to almost 4.2 million deaths worldwide with a whopping number of patients aged between 20-79 years, contributing to 11.3% of global deaths [308]. The World Health Organization in 2014 projected about >422 million world adult population to be suffering from diabetes mellitus with its prevalence on rise continuously [309]. The current impact of this disease is maximal in low and middle-income nations which necessitates its prevention and early diagnosis on an urgent basis. Its consequential impact can be seen on different vital organs; however, its major impact can be governed through its primary marker being elevated blood glucose levels [310]. MOF-based glucose detection systems can be an enticing approach serving two major roles, either as signal transduction systems or, as a substrate for embedding enzymes and nanoparticles [311]. MOF-based glucose sensors can be pristine or modified MOFs which can be used as a part of electrochemical sensing matrices.

In a recent study by Xu et al., catalytic potential of MOF in basic medium was illuminated [312]. A MOF/α-cyclodextrin-reduced graphene oxide (MOF/α-CD-rGO) hybrid was synthesized on a titanium mesh where the Ni-based MOF acted as an electrocatalyst whereas, the rGO enriched the composite's electrochemical performance **(Figure 1.11A)**. The Ni(II)/Ni(III) redox couple assisted by the OH^- in the electrolytic solution oxidized glucose to form gluconolactone, thereby generating amperometric oxidation peak current responses at +0.55 V. Two LDRs from 0.65 μM-4.828 mM and 4.828-9.178 mM with a LOD of 0.3 μM was obtained with a rapid response time of 1.9s. Fetal bovine serum sample was used for evaluation of sensor practicability exhibiting high recoveries. Similar enzymatic potential was seen for a non-toxic Fe(II)-MOF in acidic epidermal sweat environment [313]. The 3D printed device had a MOF-based Fe-centered nanozyme immobilized on its working electrode (WE) surface which oxidized glucose to gluconolactone generating a defined anodic peak response at -1.2 V. An interesting observation in this case would be a shift in the analytical peak potential from +0.55 V to -1.2 V, from the former discussed sensor, with change in the pH of the electrolyte solution from basic to acidic. The carbon black-polylactic acid (PLA) filament used as a WE which was drop-casted with a solvothermally synthesized Fe(II)-MOF, entrapped using a Nafion film (**Figure 1.11B**). The Fe(II) component of the MOF underwent a cascadic reduction [Fe(0)] and thereafter oxidation [Fe(III)] by sweeping the potential between -1.4V to +2.0V. At the oxidized state, the Fe(III) enabled an oxidative conversion of glucose, thereby bringing back the oxidation state of Fe to its original. The sensor had an optimum LDR of 0-600 μmol L^{-1} and a LOD of 17.6 μmol L^{-1}. It is interesting to note that such MOF-based sweat glucose sensors have been focussed upon recently for wearable electrochemical glucose monitoring devices as well. In a study by Xia et al., multiwalled carbon nanotubes/Polydimethylsiloxane (PDMS) based film electrode surface, stamped with CNTs, was functionalized with enzyme mimicking Ni-Co bimetallic MOF to fabricate a wearable glucose sensor [314]. In this case, the redox reaction occurred between the bimetallic centres Ni and Co in an alkaline medium where Ni(III) and Co(IV) species were converted to Ni(II) and Co(III) states respectively, thereby aiding the oxidation of glucose to gluconolactone at +0.5 V **(Figure 1.11C)**. The highly electrocatalytic coating endowed the sensor with a LDR of 20 μM-1.1 mM and a LOD of 6.78 μM. The non-invasive MOF-based sensors not only have been explored to estimate sweat glucose but also salivary glucose levels. In a recent work on conductive carbon paper layered with Ni-MOF, the probe was configured with extended gate field effect transistor for sensing glucose in a LDR of 20 μM-47 mM, working in physiological pH range at a potential of +0.7 V [315]. Such MOF-mediated analytical systems can be integrated with smart phone-enabled portable devices too to simplify and introduce the sensor application into public domain and better reachability [316].

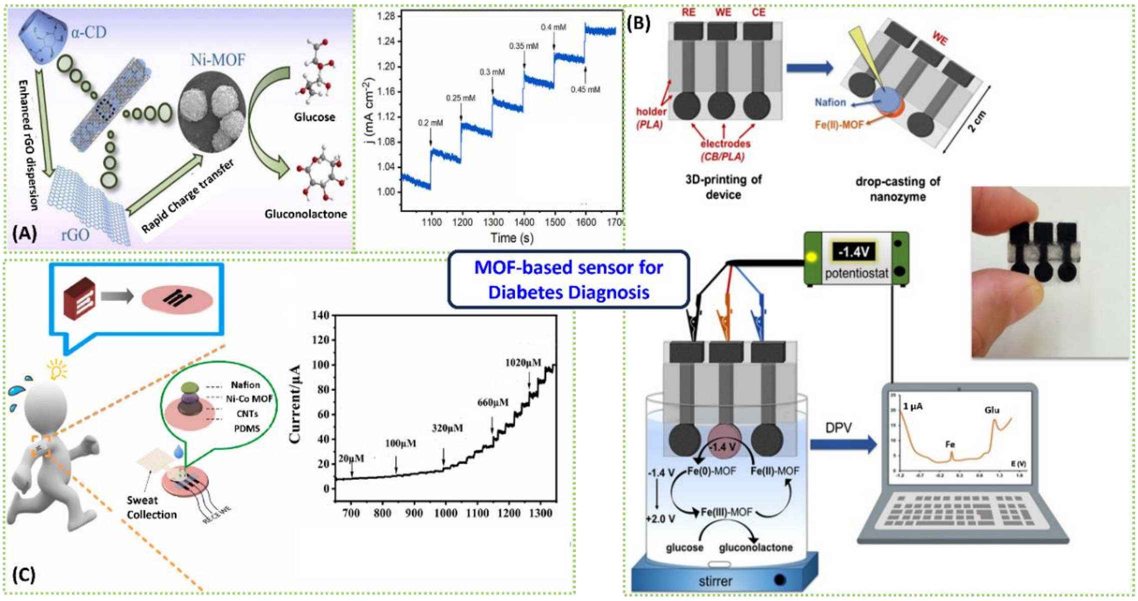

Figure 1.11. *A) Schematic representation of Ni-MOF α-CD-rGO hybrid based electrochemical sensor for catalytic conversion of glucose to gluconolactone generating amperometric response (adopted from Xu et al., copyright 2022). B) Fe(II)-MOF based biocompatible nanozyme sweat glucose sensor fabrication strategy, reprinted with permission from Koukouviti et al., copyright 2023. C) Incorporation of Ni-Co bimetallic MOFs, as enzyme mimics, in glucose sweat sensor (adopted from Xia et al., copyright 2023).*

In addition to these few representative examples there are several reports MOF-based biosensors for diagnosis of diabetes which have been comprehensively discussed in **Table 1.5** with their respective target analytes, detection techniques, sensor composite, fabrication strategies, mechanistic role of MOF, real samples considerations and detection efficiency parameters (LDR and LOD).

Table 1.5. *Detailed list of latest MOF-based electrochemical biosensors for diagnosis of diabetes*

S.No.	Target Analyte	Detection Technique	Sensor Composite	Fabrication Strategy	Mechanistic Role of MOF	Real Sample	LDR	LOD	Reference
1.	Glucose	Amperometry, CV	NF/$NiCo_2O_4$NWs@Co_3O_4NPs	NF was topped with $NiCo_2O_4$ NWs which acted as a substrate for growth of NPs derived from Co_3O_4 MOF to complete the electrode fabrication.	Good structural stability and high conductivity	Mouse serum	0.001-1.7 mmol/L	0.5 µM	317
2.	Glucose	Amperometry	Ni/Mn-LDH-MOF	GCE electrode was used as WE by simply drop-casting the Ni/Mn MOF-74 suspension solution dispersed in Nafion.	Electrocatalytic activity	Human serum	4.9 µM-2.2 mM	0.87 µM	318
3.	Glucose	Amperometry, CV, DPV	Ni/Co MOF	Nitric acid treated CC was used as a substrate for growing Ni/Co(HHTP)MOF through the process of electrodeposition.	Large surface area, effective active sites, electrocatalytic activity	Human serum, tea, orange juice	0.3 µM-2.312 mM	100 nM	319
4.	Glucose	CV, Amperometry, EIS	Ni/Co-BTC MOF	Polished GCE was potential cycled in the presence of 0.1 M NaOH for 10 consecutive cycles. Then, the electrode was immersed in a solution containing $Co(NO_3)_2{\cdot}6H_2O$, $Ni(NO_3)_2{\cdot}6H_2O$, and KNO_3 for a period of 200s followed by dipping into a solution of ethanolic H_3BTC to synthesize Ni/Co-BTC MOF on its surface.	Electrocatalytic activity	Human serum	0.001-1.78mM; 1.78-5.03mM	0.187 µM	320
5.	Glucose	CV	Ni/Co MOF	The electrode fabrication started with gold layer deposition over a hydrophilic PDMS surface followed by drop-casting Ni/Co MOF nanosheets.	Electrocatalytic activity	Human sweat	20-790 µM	4.25 µM	321
6.	Glucose	Amperometry	Ni/Co-BTC MOF	Screen printed PET substrate was modified with CC and Ni/Co-BTC MOF by pasting it to the electrode surface with the aid of a conducting resin followed by covering with KOH-PVA gel.	High conductivity and metal synergy leading to improved catalytic activity	Human sweat	5-205 µM	0.09µM	322
7.	Glucose	CV, Amperometry	Ni/Co MOF	rGO/PU fiber was coated with Ag glue on the electrode surface. Then, Ni/Co MOF with 1% Nafion was drop-casted on the modified electrode to obtain the final Ni/Co MOF/Ag/rGO/PU surface.	Large specific surface area and high catalytic activity	Human sweat	10µM-0.66mM	3.28µM	323
8.	Glucose	CV, Amperometry	2D M-BDC MOFs where M= Cu, Mn, Ni, Zr	The MOF powder was mixed with isopropanol and Nafion, and drop-casted on to the surface of polished GCE to obtain the desired probe.	Electrocatalytic potential	N.R.	Ni-BDC MOF: 0.01-0.8 mM	6.68 µM	324

9.	Glucose	CV, Amperometry	Ni-MOF	Polished GCE electrode was modified by drop-casting Ni-MOF on its surface to obtain the desired electrode.	High specific surface area and abundant active catalytic sites	Human serum	0.001-2.0 mM, and 2.0-3.4 mM	0.7 μM	325
10.	Glucose	CV, Amperometry	Cu-MOF	Cu-MOF/C composite dispersed in DMF was drop-casted onto the GCE. Then, the surface was electrodeposited with NiNPs to obtain NiNP/Cu-MOF-C/GCE.	Electrocatalytic synergy between Cu and Ni metals.	Human saliva	0.3-1150 μM	0.090 μM	326
11.	Glucose	Amperometry	Ni/Co MOF	CCFs were cleaned and pretreated to be used as substrate for MOF growth. Co and Ni salts along with the ligand were dissolved in DMF and the CCF was soaked into this solution followed by hydrothermal synthesis in autoclave. The obtained MOF decorated on the CCF surface was used as the sensor probe.	Electrocatalytic potential	Human blood serum, Saliva	0.04-3.13 mM and 3.63-8.28 mM	0.348 μM	327

Abbreviations: *NF: Nickel Foam; NW: Nanowires; NPs: Nanoparticles; GCE: Glassy Carbon Electrode; WE: Working Electrode; CV: Cyclic Voltammetry; DPV: Differential Pulse Voltammetry; EIS: Electrochemical Impedance Spectroscopy; CC: Carbon cloth; HHTP: Triphenylene-2,3,6,7,10,11-hexaol; PDMS: Polydimethylsiloxane; PET: Polyethylene terephthalate; BTC: Trimesic acid; PVA: Polyvinyl Alcohol; rGO: Reduced Graphene oxide; PU: Polyurethane; NiNPs: Nickel Nanoparticles; CCF: Commercial Cotton Fabrics; DMF: Dimethyl Formamide; NR: Not Reported*

3.2.2. MOF-based electrochemical sensors for Virus and bacteria-borne infectious Diseases

3.2.2.1. Viral diseases

Infectious diseases originating from viral pathogens can aggravate and result into pandemics as evident from our recent past [328]. These can overturn economies and can lead to human survival challenges. The world has encountered various viruses in recent times ranging from single stranded RNA viruses like Corona virus (COVID-19) [329,330], Middle east respiratory syndrome (MERS), severe acute respiratory syndrome (SARS), and influenza viruses [331]. Where these viruses usually affect the pulmonary pathway of humans, viruses like Zika [332], Hepatitis [333,334] and Human immuno-deficiency virus (HIV) [335] can affect specific organs and thereby lead to multiple organ failures, due to compromised immune system and opportunistic infections by other pathogens. Some vector-transmitted viruses like Chikangunya [336] and dengue [337] can cause febrile illness leading to an annual mortality of more than 20,000 in tropical and sub-tropical regions of the world. Recently, some viruses like human papillomavirus, herpes simplexvirus [338] and Epstein-barr viruses have been known to cause cancers with their unique route of transmission which in cases can even transfer from mother to child [339].

With the advent of these viral-borne diseases worldwide, there have been tremendous diagnostic advancements in the field [331,340,341]. Viruses are mostly diagnosed using detection techniques like real-time PCR, quantitative PCR or high-throughput sequencing techniques which are usually high cost and sophisticated ones [342,343]. MOF-based virus biosensors have recently gained limelight due to their positively charged metal centres flanked with abundant functional groups within linker entities which endow them with good charge transfer characteristics aided with hydrogen bonding, electrostatic and, π-π stacking interactions [342]. In a study by Lin et al., a Cu-MOF based biosensor was projected to be efficient in detecting hepatitis B (HBV) viral DNA [344]. The Cu-MOF was adopted as a signal probe and was coupled with electrochemically reduced graphene oxide (ErGO), through π-π stacking interactions, as a signal amplification matrix. The MOF possessed a 3D honey-comb like structure with Cu(II) metal centres linked with H_2btca (5-carboxybenzotriazole) as the bridging ligand, giving a penta-clustered arrangement facilitating electron transfer along the b-axis of the MOF **(Figure 1.12A)**. The Cu component was also postulated to interact with amino functional groups of the probe DNA molecule leading to their strong binding affinity. With attachment of the target DNA to the sensor probe the redox signal intensity was weakened at -0.050 V signifying the conversion of $Cu^{2+} \rightarrow Cu^0$ and further at 0.268 V corresponding to $Cu^0 \rightarrow Cu^{2+}$. The sensor worked within an LDR of 50.0 fM-10.0 nM and LOD of 5.2 fM with a DNA hybridization efficiency of 89.9%.

There are only a handful of reports of MOFs as electrochemical sensing matrix component for macromolecular detection including viral proteins and its nucleotide. A noticeable hurdle could be imparting selectivity to these molecules through suitable functionalization, which can be addressed through application of supramolecular chemistry principles. A recent study highlighting one such approach explains the fabrication of sandwich type-DNA sensor for hepatitis B virus (HBV) determination [345]. In the probe fabrication strategy, WE was functionalized with rGO sheet adorned with pillar[5]arene (WP-5) stabilized Pd NPs. This modified surface was immobilized with methylene labelled DNA (MB-DNA) by virtue of interaction between MB-DNA with WP5. In a separate setup, ZIF-67 MOF was modified to functionalize hydroxylatopillar[5]arene-AuNPs conjugate possessing superior electrocatalytic properties assisting in signal amplification. The proposed model used the former setup to attach the target antigen DNA sandwiched by the later setup at the top, as per depicted in

Figure 1.12B. The developed probe worked in an LDR of 1×10^{-15} mol/L-1×10^{-9} mol/L with a LOD of 0.32 fmol/L. Such probes can be promising prospects for DNA sensor development using MOFs as matrix components.

3.2.2.2. Bacterial Sepsis

With a rise in global viral diseases like COVID-19, the world experienced an advent rise in opportunistic bacterial infections like those caused by *Staphylococcus aureus (S. aureus).* There has also been a dramatic rise in multidrug resistant gram-negative bacterial infections such as rifampin-resistant tuberculosis, caused due to the abrupt and disproportionate usage of antibiotics [74]. Drug-resistant bacterial infections in bloodstream have led to worldwide disease burden with priority concerns against Enterobacteriaceae and Staphylococcaceae bacterial families, as per WHO [346], contributing to almost 2,50,000 annual deaths in America and Europe alone [347]. Neonatal sepsis within the first 3 days of child birth still remains the leading cause for morbidity and mortality, particularly in Asian countries primarily caused by staphylococcus species [348,349] So, this global scenario brings us to the urgency of detecting bacterial pathogens from diverse domains through simpler and rapid detection techniques like electrochemistry.

In a recent study on pathogenic strain *S. aureus*, a ratiometric electrochemical sensor was developed based on a ZIF/AuNP composite [350]. The electrode fabrication comprised of a polished GCE functionalized with a layer of ZIF-MOF, sealed with a film of Nafion. The use of Nafion film was strategically done to adsorb the positively charged AuNPs, followed by incubation in 2-mercaptothylamine for an hour. The electrode was further treated with H1 DNA probe, followed by immersion in trigger DNA solution and thereafter in H2-methylene blue (H2-MB), to facilitate the recycling of the latter. To understand the generation of trigger DNA, **Figure 1.12C** sums up the steps involved in the process which has been briefed as follows. The aptameric probe corresponding to the

S. aureus DNA was initially bound to helper DNA (HP) which dissociated on attachment of the target sequence. This detached HP then, got involved in a different set of process where a padlock DNA was ligated to it through a T4 DNA ligase. This ligation triggered a DNA polymerization reaction resulting into generation of two DNA fragments, viz., trigger DNA and ssDNA, aided by BbvCI nicking endonuclease. This trigger DNA, subsequently combined with H1 probe followed by H2-MB probe, generating an electrochemical response. The ratiometric response was a function of ferrocene (Fc) and MB current ratio, with respect to the trigger DNA. With an increase in *S. aureus* concentration, the Fc signal response at 0.43 V was reduced whereas, the oxidation of MB was elevated at the same time at -0.087 V, attributing to a reversal in current change tendency, as depicted through DPV curves in **Figure 1.12C**. The probe exhibited a sensing ability for *S. aureus* within a LDR of 5-10^8 CFU/mL, with a LOD of 1 CFU/mL. The sensor applicability was also tested in real samples such as milk and orange juice. With all the discussions revolving around the probe performance so far, the vital role of MOF grabbed the attention of readers towards the multi-fold enhancement of probe surface area due to its incorporation in the matrix. Similar role of MOF-borne surface area enhancement was attempted in a recent study by Ye et al. [351] where they constructed a dual-channel biosensor which could simultaneously detect two deadly foodborne pathogens *Salmonella typhimurium* (*S. typhimurium*) and *Listeria monocytogenes (L. monocytogenes).* The sensor comprised of MOF-based nanotags functionalized with gold nanoparticles (Au@CuMOF and Au@PbMOF) with each containing specific target DNA sequences corresponding to these bacterial species. The nanotags were hybridized onto the surface of electrode and achieved sensitive detection through DPV. The dual channel sensor detected the bacterial genes invA and invlA efficiently within a LDR of 1 x 10^{-14}-1 x 10^{-8} M and 1 x 10^{-13}-1 x 10^{-8} M, respectively. As far as the detection of the bacteria directly was concerned, *S. typhimurium* was detected within a LDR of 5-1.0×10^4 CFU mL^{-1} (LOD of 2.33 CFU mL^{-1}), and *L. monocytogenes* within LDR of 10-1.0×10^4 CFU mL^{-1} (LOD of 6.61 CFU mL^{-1}). Such studies are suggestive for guest molecule holding capabilities of MOFs, thereby easing electrochemical probe assembly fabrication.

Apart from their role as support matrices, MOFs have also been used as nanozymes in sensors for detection of pathogenic bacterial strains. Peroxidase mimicking activity of MOFs have been explored in recent times (Shubhangi, et al., 2023). One such was explored in a case where bacteria captured through GCE functionalized with vancomycin was detected through a separate AuNP-MOF decorated with Rabbit anti-*S. aureus* rosenbach tropina antibody (Ab_2) [353]. This whole system was eventually generating cathodic current response by virtue of MOF exhibiting peroxidase activity and catalysing o-phenylenediamine in presence of hydrogen peroxide. The generated signal was proportional to the concentrations of *S. aureus*. The 2D Fe-based MOF was found capable of detecting *S. aureus* in a concentration range of 10-7.5 x 10^7 CFU/mL with a LOD of 6 CFU/mL.

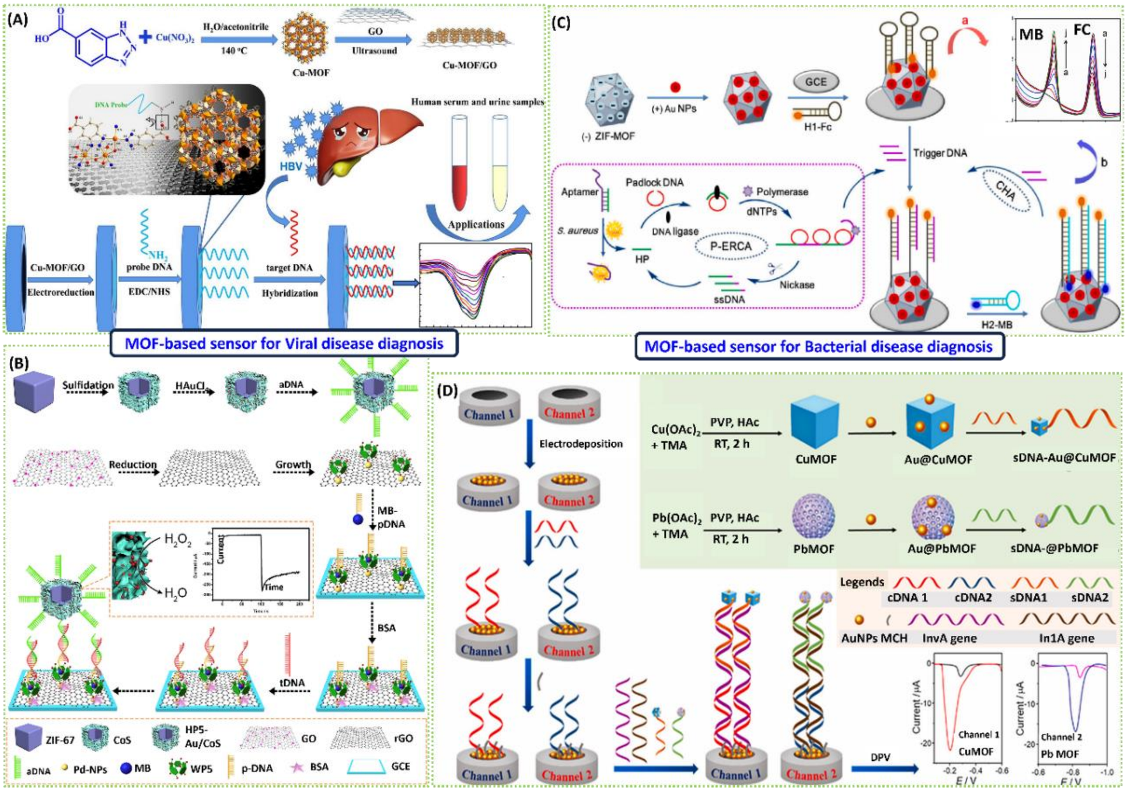

Figure 1.12. *A) and B) schematically demonstrate strategies for fabrication of MOF-based viral disease biomarker, viz., HBV viral DNA (adopted and reprinted with permission from Lin et al. 2020; Qian et al., 2020). C) and D) correspond to studies on bacterial disease diagnosis through electrochemical tools deploying ZIF, Cu and Pb MOFs targeting specific bacterial DNA (reprinted with permission from Shan et al., 2023; Ye et al., 2023).*

The above discussions can be more vividly established through elaborately stated recent reports on MOF-based biosensors for diagnosis of viral and bacterial infectious diseases, as per **Table 1.6** with their respective target analytes, detection techniques, sensor composite, fabrication strategies, mechanistic role of MOF, real samples considerations and detection efficiency parameters (LDR and LOD).

Table 1.6. *Detailed list of latest MOF-based electrochemical biosensors for viral and bacterial disease diagnosis*

S.No.	Target Analyte	Detection Technique	Sensor Composite	Fabrication Strategy	Mechanistic Role of MOF	Real Sample	LDR	LOD	Reference
				Viral Infection diagnosis					
1.	a) Recombinant SARS-CoV-2 spike glycoprotein b) SARS-CoV-2 pseudovirus	EIS	CoFeBDCNH$_2$-CoFe$_2$O$_4$ MOF-nanohybrids	The MOF-nanohybrid was coated on a gold chip was used as a substrate. Further, the electrode surface was modified by conjugating it with the virus specific antibody using 11-MUA as the linker entity through SAM.	Conductive synergy between CoFeBDCNH$_2$-MOF and CoFe$_2$O$_4$ nanomaterials.	Serum	a) 10 ng/mL- 100 fg/mL b) 10 ng/mL-10 fg/mL	a) 6.68 fg/mL b) 6.20 fg/mL	354
2.	HIV-1 DNA	EIS	Ni/Co-MOF	The Ni/Co-MOF was transformed into NiCo$_2$O$_4$/CoO@CNTs. This composite was then immobilized with HIV-1 probe DNA for its detection.	Carrier for probe DNA, biocompatibility, electrochemical conductivity	Human serum	0.1 pM-20 nM	16.7 fM	355
3.	SARS-CoV-2	EIS	Ni$_3$(BTC)$_2$ MOF	Ni$_3$(BTC)$_2$ MOF was coated on SPCE surface which was further modified with SARS-CoV-2 S protein specific aptamer followed by dopamine deposition through electro polymerization.	High surface area substrate for covalent immobilization of aptamer	Serum from sick and healthy individuals with SARS-CoV-2 virus	10-10^8 PFU/mL	3.3 ± 0.04 PFU/mL	356
4.	HCV-RNA	CV, EIS	Ni-MOF	The working electrode was fabricated using a GCE electrode coated with the Ni-MOF. The MOF surface was then functionalized with polyaniline followed by a DNA probe and BSA.	Highly porous matrix for loading target DNA probe	Serum	1 fM-100 nM	0.75 fM	357
5.	Hantavirus	DPV	Cu-MOF	GCE surface was electrodeposited with AuNPs-rGO composite and further immobilized with cDNA aided by Au-S bonding. Subsequent attachment of t-DNA was followed by its coupling with Cu-MOF-sDNA composite completing the sensing platform.	As a signal tag	Real virus samples	10^{-15}-10^{-9} M	0.74 fM	358

6.	HCV-RNA	DPV	Ag/Zn MOF	GCE electrode surface was modified with the Ag/Zn bimetallic MOF and was further modified with the capture probe (nucleic acid-based) for HCV detection.	Immobilization matrix for DNA probe	Human serum	1 fM-100 nM	0.64 fM	[359]
7.	Foot and mouth disease virus (FMDV)	SWV	TB@MOFs	GCE surface was drop-casted with TB@MOF which was followed by coating with AuNPs. The electrode was then coated with Ab and then treated with BSA for redundant site blockage.	Large surface area for TB encapsulation	Pig serum	0.1 pg/mL-10 ng/mL	0.008pg/mL	[360]
8.	FMDV	DPV	CdS@Zn-MOF	Pretreated GCE surface was coated with solution of MWCNTs. The modified electrode was then functionalized with Ab_1 followed by incubation and BSA treatment. The electrode was then treated with different concentrations of antigen followed by Ab_2 to complete sandwich probe fabrication and initiate immunoreaction. Zn-BTC MOF was used as a label which was stained with CdS for FMDV detection.	As encapsulation matrix for CdS	Human serum	0.5 fg/mL- 5 ng/mL	0.05 fg/mL	[361]
9.	HBV DNA	DPV	Cu-MOF	Non-enzymatic sensor was developed by functionalizing GCE surface with Cu-MOF as electroactive sensor probe. It was further coated with GO, which was electrochemically reduced to ErGO, for signal amplification. Cu-MOF due to its high affinity with DNA, acts a functional platform for its immobilization which can thereby determine concentrations of the target DNA.	As a signal probe and multisite matrix	Human serum, urine	50.0 fM-10.0 nM	5.2 fM	[344]
10.	HBV DNA	Amperometry	ZIF-67	Polished GCE surface was drop-casted with WP5-Pd/rGO and dried at room temperature. Then, MB-DNA was functionalized onto the	As nanobox anchor for adhering probe components	Serum	1 fM-1nM	0.32 fM	[345]

				modified electrode surface followed by treatment with BSA to block redundant sites. It was followed by addition of different concentrations of target DNA at RT to develop the sandwich type DNA sensor.					
Bacterial Infection diagnosis									
11.	*Pseudomonas aeruginosa (P. aeruginosa)*	DPV	Zr-MOF	Cu doped Zr-MOF was used for conjugating the aptamer/DNA/Super P signal probe on the surface of a gold electrode.	Large surface area for Cu-doping	Urine	10-10^6 CFU/mL	2 CFU/mL	[362]
12.	*Escherichia coli (E. coli) O157:H7*	DPV	CdS@ZIF-8	ZIF-8 MOFs were encapsulated with CdS QDs which was further functionalized with polyethyleneimine followed by attachment of bacteria specific antibody. The CdS particles act as signal tags on releasing through HCl leaching event, releasing Cd^{2+} from MOF cavity and consequently detecting E. coli.	CdS encapsulation matrix	Milk	10^{-8} CFU/mL	3 CFU/mL	[363]
13.	a) *E. coli O157:H7* b) *Staphylococcus aureus (S. aureus)* c) *Salmonella enterica*	DPV	Poly Mn-MOF	The poly Mn-MOF was synthesized using polyH_2BDC units linked to 4,4′-bipyridine, $MnCl_2$ and polyvinyl pyrrolidone. The developed MOF was conjugated with the bacterium specific aptamer for their respective sensing.	Aptamer adherence, backbone stability and release of metal ions in aqueous system	Milk, Frozen shrimp (Samples were spiked with pathogen)	10-10^8 CFU/mL	a) 1.5 CFU/mL b) 3.5 CFU/mL c) 2.6, CFU/mL	[364]
14.	*Mycobacterium bovis (MB)*	SWV	TB@MOFs	GCE surface was drop-casted with TB@MOF which was followed by coating with AuNPs. The electrode was then coated with Ab and then treated with BSA for redundant site blockage.	Large surface area for TB encapsulation	Pig serum	0.1pg/mL-10µg/mL	0.002 pg/mL	[360]
15.	Mycobacterium tuberculosis	DPV	Fe-MOF	Fe-MOF was functionalized with PEI to form P-MOF which was later drop-casted on electrode surface. A thin film comprising of Au@Pt was	Electrochemical conductivity, absorption of Au/Pt nanoparticles	Human serum of healthy and	1 fg/mL- 1 ng/mL	0.33 fg/mL	[365]

	antigen (MPT64)			deposited on the surface of this MOF-coated electrode. On another setup, C_{60}NPs-N-CNTs/GO was doped AuNPs which was further functionalized with MAA II to form a tracer label. This tracer label and the former modified electrode bonded to the MPT64 antigen selectively leading to its detection.		infected individuals			
16.	*S. aureus*	DPV	Cu-MOF	GCE surface treated with BSA was attached to vancomycin via EDC/NHS chemistry and then incubated with varying concentrations of bacteria. Following it, Ab_2/AuNPs/MOFs was added to the modified electrode surface sealed with Nafion.	Peroxidase-mimic nanozyme	N.R.	10-7.5 × 10^7 CFU/mL	6 CFU/mL	[366]
17.	*S. aureus*	DPV	ZIF	GCE surface was modified by coating its surface with ZIF-MOF. It was then functionalized with AuNPs aided by ethanolic Nafion. Further treatment with mercaptoethylamine was done for the adhesion of H1(helper DNA) probe. Then, the target DNA was attached to it surface followed by attachment of H2-MB probe.	Electron transport promoter, provides surface area for absorption	Orange juice, Milk	5- 10^8 CFU/mL	1 CFU/mL	[350]
18.	*E. coli*	EIS	Cu-MOF	Initially PANI was mixed with the linker molecule H_3BTC followed by mixing with the MOF precursor salt to form $Cu_3(BTC)_2$-PANI. The prepared MOF composite was drop-casted on the surface of ITO followed by annealing the electrode surface at 100 °C. Then, Ab was incubated using EDC-NHS on modified surface for an hour and un-specific binding sites were blocked through treatment with Tween-20.	Bio-interface for attachment of anti-*E. coli* antibodies	Water	2.0- 2.0 × 10^8 CFU/mL	2 CFU/mL	[367]

19.	Methicillin-resistant *S. aureus*	DPV	UiO-66-NH_2	GCE surface was drop-casted with a dispersed alcoholic mixture of N-doped porous carbon material, dried in oven. Two electroactive dyes, methylene blue and epirubicin were encapsulated within the MOF and treated with different concentrations of target DNA to obtain results.	Nano-carrier	Tap water, Milk samples	5×10^{-15}- 1×10^{-10} M	Bacterial genes: mecA gene: 3.7 fM nuc gene: 1.6 fM	[368]
20.	*S. aureus*	EIS, DPV	Zn-Glu@PTBD-COF	The aptameric sensor was fabricated through functionalization with L-glutamic acid, 1,10-phenanthroline-2,9-dicarbaldehyde and benzene-1,4-diamine linker molecules. Aptamer adhesion on composite surface was aided by abundant active sites on the MOF-COF surfaces facilitating specific recognition of SA.	MOF defects provide anchoring sites for aptamers	Milk, Honey	10- 10^8 CFU/mL	EIS: 2.0 CFU/mL DPV:1.0 CFU/mL	[369]

Abbreviations: *EIS: Electrochemical Impedance Spectroscopy.; DPV: Differential Pulse Voltammetry; SWV: Square Wave Voltammetry; SAM: Self assembled monolayers; HIV: human immunodeficiency virus; HCV: Hepatitis C virus; HBV: Hepatitis B virus; CNT: Carbon nanotubes; BTC: Trimesic acid; TB: Toluidine blue; BSA: Bovine Serum Albumin; rGO: Reduced graphene oxide ;MB: Methylene Blue*

3.2.3. MOF-based electrochemical sensors for Neurological disorders

Neurological disorders are referred to diseases which target the nervous system and include nerves, spine and the brain. They are the leading cause of severe-long term disabilities and second largest cause of deaths in the world [370]. More than 600 diseases have been reported in this category and their symptoms largely aggravate with age and are modulated by risk factors. Some of them include dementia, stroke, parkinson's disease, alzheimer's, epilepsy etc. [371]. The etiologic aspects of such diseases still remain poorly understood therefore their timely detection remains crucial. Various neurological diseases including some of the neurodegenerative disorders have shown involvement of certain neurotransmitters and peptides which can be target analytes for their timely diagnosis [372]. MOFs-based electrochemical biosensing platforms can serve as point-of-care diagnostic tools for the timely, sensitive and low-cost detection of these disorders.

Dopamine (DA), a catecholamine neurotransmitter is essentially utilized by cells for conversion of chemical signals into impulses [373].It is responsible for modulation of the central nervous system and cognitive functioning of organisms [374]. Its abnormal levels may affect the human nervous system triggering neurological dysfunctions [375]. There have been recent developments on the sensitive detection of DA however, have faced challenges like complicated operations, complex sample handling and overlapping signals. Electrochemical DA sensing could be plausible solution to such challenges. If the recent developments of MOF-based sensors are looked upon, two different approaches could be visualised. The first one focusses on detection of DA directly through exploitation of its redox behaviour while the second approach relies on catalysing it to further constituents. In a recent study by Zhou et al., CoNi MOF was ultrasonically mixed with GO to develop a sensor probe where the components were coated electrochemically on polished electrode surface to form the final sensor probe, as shown in **Figure 1.13A**

[376]. The MOF structure exhibits an enhanced conductivity while also offers abundant sites for DA absorption exhibiting sensitivity towards it in a wide LDR of 0.1–400 μM with a LOD of 0.086 μM, when tested in DPV premises. Bimetallic MOF like this tends to impart synergistic effect to the sensing matrices. In another study on DA detection using a Co-based ZIF-67 MOF discussed about calcination of the ZIF followed by its hydrothermal treatment in a solution of cerium nitrate hexahydrate [377]. This different strategy not only exposed the pre-existing active sites on the MOF but also prevented the agglomeration of the constituted dopant CeO_2 **(Figure 1.13B)**. Again, in this case the electrocatalytic response was a result of Co and Ce metal centre synergies. The GCE/CeO_2 /Co_3O_4 exhibited an LOD of 0.13 μM with a LDR of 0.13 μM-60 μM using the DPV method. This catalytic sensor was capable of converting DA into DA-Q even in human urine samples but dealt with a small dynamic range of detection. For clinically relevant sensors a wide detection range is favoured which most of the MOF-based sensors lack for [374]. To overcome this issue, researchers have tried microenvironment modulation in ZIFs where MOFs have been incorporated with composite materials to improve their electrocatalytic behaviour (Shubhangi et al., 2023; Sun et al., 2024). Apart from the examples discussed in the text, there have been many recent advancements on MOF-based DA sensors which have been comprehensively discussed in **Table 1.7**. Apart from DA, there lies a deep lacuna in the field of development of MOF-based electrochemical sensors for this category of disease due to limitations in accessible biomarkers. 5-hydroxytryptamine(5-HT), commonly known as serotonin, is also one of the neurotransmitters which is less explored but plays role in regulating mood and related functions [378]. Its specific concentration in serum, urine and CSF is important and if altered can cause depression, Alzheimer's disease and irritable bowel syndrome [379,380]. In a recent study on its electrochemical MOF-based detection, a group utilized Nickel bis

(dithiophen-dibenzoic acid) ligand to construct a nickel zinc bis(dithiolene) MOF with good catalytic potential [379]. The MOF was ultrasonically dispersed with acidified MWCNTs (Ni Zn-MOF/MWCNTs) and dripped onto the electrode surface to develop the final probe (**Figure 1.13C**). DPV-based oxidative detection of 5-HT was carried out in Tris-HCl solution with a LDR of 0.5-115 μM and LOD of 0.03 μM. Human urine was considered as the real sample matrix to understand the sensor's utility which yielded commendable recovery of 99.94 % to 102.02 %. The current studies though being quite limited but hold tremendous scope for MOF based electrochemical sensing solutions for amyloid disease biomarkers such as amyloid β peptides [381]. Therefore, MOFs could be more emerging sensor matrix components in coming times for neurological disorders.

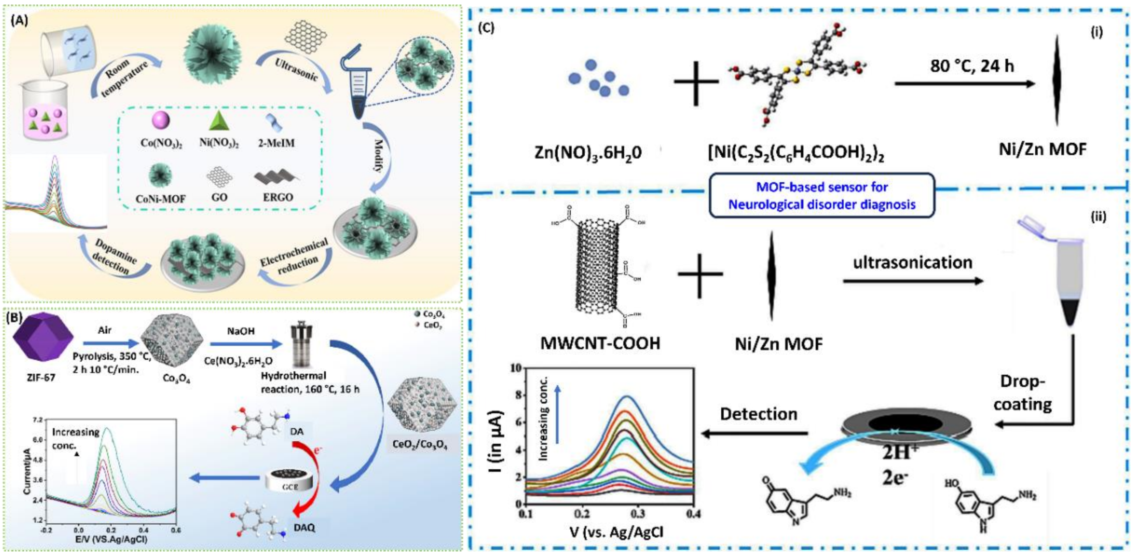

Figure 1.13. *A) Illustration on step-wise fabrication of CoNi bimetallic MOF as an efficient platform for dopamine detection, adopted with permission from Zhou et al., copyright 2023. B) Synthesis strategy for electrocatalytic conversion of DA to DAQ through modified ZIF-67 and thereby generation of DPV signal response, reprinted with permission from Ding et al., copyright 2023. C)* ***Upper panel:*** *Hydrothermal synthesis of bimetallic Ni Zn MOF;* ***Lower panel:*** *Fabrication of MWCNT functionalized Ni Zn MOF for oxidative detection of 5-HT, adopted with permission from Chen et al., copyright 2023.*

Table 1.7. *Detailed list of latest MOF-based electrochemical biosensors for neurodegenerative disease diagnosis*

S.No.	Target Analyte	Detection Technique	Sensor Composite	Fabrication Strategy	Mechanistic Role of MOF	Real Sample	LDR	LOD	Reference
1.	Dopamine	CV, DPV	Polyoxometalate-γ-cyclodextrin MOF	POM-γCD MOF was drop-casted on the laser-scribed graphene electrode (LSGE) and dried at ambient conditions to get POM-γCD MOF/LSGE.	It acts as an electrocatalyst and provide selective detection	Serum samples and *SH-SY5Y neuroblastoma* cells	50 nM-1.0 mM	10 nM	[382]
2.	Dopamine	DPV	Ni-MOF	A polished GCE electrode surface was coated with Ni-MOF dispersed within ethanol. On drying, the electrode surface was layered with 1% Nafion solution to complete the fabrication process.	Enhances electrocatalytic activity of sensor	Commercial DA hydrochloride injection	0.2-100 µM	60 nM	[383]
3.	Dopamine	DPV	Fe-MOF	2D Fe-MOF was synthesized at room temperature through a wet chemistry approach followed by its pyrolysis at 900 °C forming Fe/CNS. It was then soaked into conc. 1.0 M H_2SO_4 solution forming 2D CNS. This solution was then dispersed in ultrapure water and dropped on clean GCE to obtain the final probe.	Increases surface area and electrical conductivity	Human serum	0.05-80 µM	0.01 µM	[384]
4.	Dopamine	DPV	Ce (III, IV)-MOF	A polished GCE surface was coated with a layer of CB/Ce (MV)-MOFs dispersed in 0.5 % alcoholic Nafion solution. The modified electrode was then dried at 60 °C, 5 minutes to obtain the final probe.	Provides high surface area, chemical stability	DA injections, Urine	0.3-252.0 µM	0.0955 µM	[385]
5.	Dopamine	CV, DPV	β-CD/Ni–MOF	A clean polished GCE surface was coated with β-CD/Ni–MOF suspension and dried under red lamp.	Increases catalytic sites which enhances redox reaction	DA hydrochloride injection, human serum	0.7-310.2 µM	0.227 µM	[386]
6.	Serotonin	DPV	ZnO-Cu MOF/NF	Uniform-sized Ni foam strip was cut and rinsed with conc. HCl to remove any surface oxides. Then, it was pretreated with ethanol, acetone and DI water and later dried to obtain in the desired form. ZnOCu MOF was ultrasonically prepared and dispersed in water using sonication. 100 μl of this suspension was drop casted onto the Ni-foam and dried at 70 °C for 1 h to obtain the final sensing probe.	Higher surface area and improved electrocatalytic activity	Simulated blood serum	1ng/mL-1 mg/mL	0.49 nM	[387]
7.	Beta-site secretase (BACE1)	LSSV	ph-AgNPs@Zr-MOF	Cytosine (C) rich sequence-templated AgNPs/Zr-based metal–organic framework (*MOF*) composite is modified by phenol groups, and then the prepared tag (ph-AgNPs@MOF) is captured in microplate surface	Large surface area and water stability	Serum	1-200 pM	0.8 pM	[388]

				by the conjugation reaction of phenolic groups between tyrosine and tag.					
8.	β-amyloid (Aβ) oligomer	DPV	AuNPs/Cu-MOF	By using an aptamer-tethered gold nanoflower (AuNF) modified electrode for target capture and aptamer-tagged gold nanoparticles/Cu-MOF (AuNPs/Cu-MOF) conjugates, an effective sandwich sensor was obtained.	Provides both increased surface area and conductivity	Human Aβ oligomer (82E1-specific) ELISA kit	1 nM-2 μM	0.45 nM	[389]
9.	Dopamine	CV, DPV	Cu-Co(2-Meim)MOF@CNF	A CNF mat was fabricated using electrospinning method. The mat was then hybridized with Cu-Co(2-MeIm)MOFs through solvothermal method. Post hybridization the composite was washed with ethanol/water mixture and dried at 70 ◦C.	Enhances catalytic activity and sensitivity of sensor towards analyte	DA: cheese Tyramine: banana	5-800 μM	DA: 44.2 nM Tyramine: 52.7 nM	[390]
10.	Dopamine	CV, DPV	DUT-67/$ZnCo_2O_4$-MWCNTs	A polished GCE surface was dried under N_2 flow. DUT-67/$ZnCo_2O_4$ and activated MWCNTs were dispersed in DMF solution and dropcoated onto the surface followed by drying under IR lamp.	Composite provide specificity towards dopamine	DA injection	1.0-180 μM	12 nM	[391]

Abbreviations: *EIS: Electrochemical Impedance Spectroscopy; DPV: Differential Pulse Voltammetry; CV: Cyclic Voltammetry; LSSV: linear sweep stripping voltammetry; DMF: Dimethyl Formamide; IR: Infra red ; MeIM: 2-methyl imidazole.*

3.2.4. MOF-based electrochemical sensors for Cardio-vascular diseases

Claimed to be one of the most common non-communicable diseases worldwide, cardiovascular diseases are the leading cause deaths which are estimated to rise to a figure of 22.2 million deaths by 2030. As per WHO, 31% of global deaths were cardio-vascular disease-related with heart attacks and strokes being the highest contributors in the statistics [392]. Acute myocardial infarction (AMI) or heart attack is usually diagnosed through various approaches commonly being electrocardiography, radioimmunoassay and enzyme-linked immunosorbent assay [393]. However, biosensors involving MOFs could be better choice for point-of-care rapid diagnostic solutions for better management of this disease [394].

A crucial cardiac biomarker is Antigen galectin-3 (GL-3) which belongs to the family of β-galactoside proteins which poses its significance in detection of cardiac fibrosis [395]. A study aiming its detection fabricated an amperometric sensor based upon AuNPs functionalized on graphitic carbon nitride nanosheet (g-C_3N_4@AuNPs) surface with Ti-MOF@COF covalent composite as the signal amplification component. A GCE electrode surface was initially modified with g-C_3N_4@Au NPs through a dispersive coating followed by immobilization with anti-GL-3-Ab_1 assisted by amino-gold binding affinity. Thereafter, a parallel preparation of Ti-MOF@COF composite was functionalized with anti-GL-3-Ab_2 which was sandwiched upon the former setup to develop the final immunosensor probe. The amperometric measurements were performed in H_2O_2 solution which acted as a mediator for GL-3 detection **(Figure 1.14A)**. The sensor was found to be capable of detecting GL-3 in a wide LDR of 0.0001-20.0 ng mL^{-1} with a LOD of 25.0 fg mL^{-1}.In another case on detection of a blood-based AMI biomarker detection strategy by Gupta et al., screen-printed electrodes were drop casted and annealed twice at 90 °C for 4 h with ethanolic solutions of $Cu_3(BTC)_2$/PANI MOF composite to obtain uniform sensor matrix [393]. The electrodes were then incubated in carbodiimide (EDC) and N-hydroxysuccinimide (NHS) solution to facilitate attachment of cardiac troponin I antibody (anti-cTnI) followed by blocking non-specific binding sites through 0.01% Tween 20. The impedimetric immunosensor was found to be detecting the cardiac troponin I (cTnI) antigen in a clinically significant LDR of 1- 400 ng mL^{-1} with a LOD of 0.8 ng mL^{-1}. The significance of the sensor was also deduced by testing its practicability in mice serum samples with satisfactory recoveries. The unique properties of MOFs have created their impact on development of such label-free electrochemical sensing approaches. A similar approach involving Cu-MOF for cTnI was attempted by Ling et al. where they fabricated Cu-MOF-74 as a bifunctional material which not only acted as antibody immobilization matrix but also attributed to signal generation [396]. Briefly, the immunosensor was developed on a GCE surface which was initially electrochemically pretreated with 2.5% $K_2Cr_2O_7$ and 10% HNO_3 solutions to obtain -COOH groups on its surface. Subsequently, the electrode was activated with EDC/NHS and NH_2-rGO pitching a ground for electrodeposition of Cu-MOF. The MOF was electrodeposited in two step process with an initial Cu-salt deposition at -0.4V followed by electrochemical scanning in PBS solution containing H_4dhtp to produce Cu-MOF-74/NH_2-rGO/GCE. Finally, the surface was adorned with anti-cTnI antibodies aided by -NH_2 condensation reaction between the antibody and EDC-NHS moieties (as shown in **Figure 1.14B**). The DPV-based immunosensor could efficiently detect the target analyte with a LDR of 0.01 pg mL^{-1}-1.0 ng mL^{-1} and LOD of 4.5 fg mL^{-1}. The standard-addition method-based serum sample analysis projected a commendable recovery of the spiked samples vouching the reliability of the sensor. Similar label-free approaches using MOFs against cTnI have also been adopted by others in recent times [397,398]. It is worthy to mention that MOF-based sensors against the exploration of several other cardiac biomarkers like myoglobin, creatine kinase isoenzyme remains the need of the hour with current global health scenario.

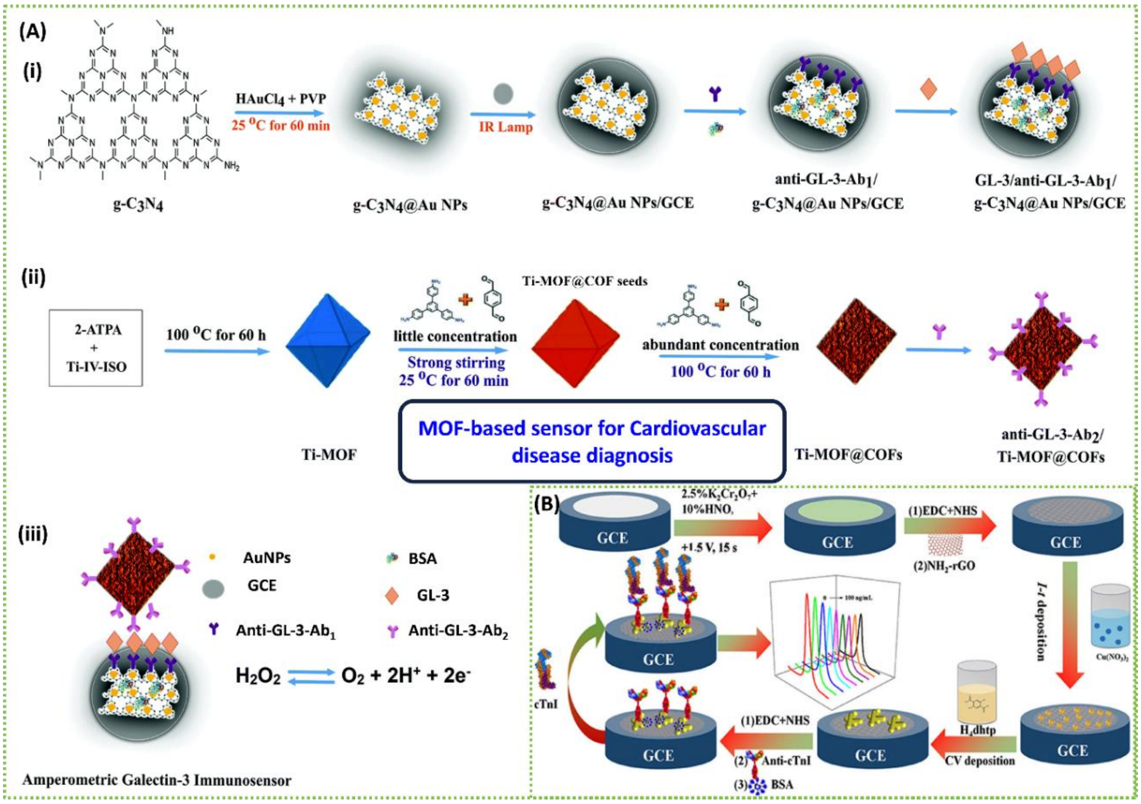

Figure 1.14. *A) An elaborated overview on the fabrication of sandwich-type MOF-based sensing and detection principle for GL-3 biomarker. i) The panel describes about functionalization of graphitic carbon nitride sheet with AuNPs followed by attachment of anti-GL3 Ab_1. ii) demonstrates the synthesis of Ti-MOF followed by hydrothermal synthesis of TiMOF@COF composite with attachment of anti-GL3 Ab_2. iii) Assembly of setup i) and ii) to form sandwich type sensor generating signal by virtue of H_2O_2 as redox mediator (reprinted with permission from Yola & Atar, copyright 2020. B) Depicts the schematic step-wise probe fabrication involving functionalization of GCE with Cu-MOF-74/NH_2-rGO/GCE anti-body based electrochemical detection of cTnI (reprinted with permission from Ling et al., copyright 2022).*

Apart from the examples elaborated in the section above, there have been some noteworthy contributions recently in the field of MOF-based biosensors for diagnosis of cardiovascular diseases using their specific biomarkers which have been highlighted in **Table 1.8** stating their respective target analytes, detection techniques, sensor composite, fabrication strategies, mechanistic role of MOF, real samples considerations and detection efficiency parameters (LDR and LOD).

Table 1.8. *Detailed list of latest MOF-based electrochemical biosensors for cardiac and pulmonary disease diagnosis*

S.No.	Target Analyte	Detection Technique	Sensor Composite	Fabrication Strategy	Mechanistic Role of MOF	Real Sample	LDR	LOD	Reference
1	C-reactive protein (CRP)	DPV	Zn-MOF	Carbon paste electrode was used and further modified with ZnO/MPC and Ionic liquid composite.	Increase surface area and conductivity and helps in antibody immobilization	Human serum	0.01-1000 ng/mL	5 pg/mL	399
2	CRP	DPV	Cu-MOF	Toluidine blue loaded Cu-MOF was used with AuNPs and drop-casted on GCE surface. Then anti-CRP was deposited after that BSA was used for blocking non-specific sites. Further Au-MOFs-Ab2-CRP was used for specific detection of CRP.	The 3-D structure provide higher surface area which carries antibody	Serum	0.5-200 ng/mL	0.167 ng/mL	400
3.	CRP	DPV	Pt-COF	Pt-COF (PtNPs Modified Covalent Organic Frameworks) deposited on electrode surface and then anti-CRP was used. After blocking the nonspecific surface with BSA, MOFs anti-CRP was used for detection.	Increases electrical conductivity	Serum	1-400 ng/mL	0.2 ng/mL	401
4.	cTnI	EIS	Cu-MOF	$Cu_3(BTC)_2$/PANI composite were synthesized using solvothermal method. Then, the composite was drop-casted on the surface of SPEs followed by immobilization of anti-cTnI antibodies.	Composite MOF provide higher conductivity and sensitivity	Mice serum	1-400 ng/mL	0.8 ng/mL	402
5.	cTnI	DPV	Zn-MOF	Fe_3O_4–COOH was used as a electrocatalyst and Thi used as redox specie and were separately introduced into Zn-MOF. The developed Zn-MOF/Fe_3O_4–COOH/Thi nanocomposite was used further and anti-cTnI monoclonal antibody was immobilized.	It helps in carrying large number of electrocatalyst and redox specie	N.A.	0.04-50 ng/mL	0.9 pg/mL	403
6.	cTnI	DPV	Cu-MOF-74	The pretreated electrode was covalently modified with NH2-rGO. Further Cu-MOF-74 was electrodeposited over modified surface and then anti-cTnI was immobilized to form final sensing surface.	It provides both surface for immobilization of antibodies and signal enhancement	Serum	0.01 pg/mL-1.0 ng/mL	4.5 fg/mL	396
7.	cTnI	EIS	FeCo-MOF	FeCo bimetallic MOF was grown on Ni foam forming NH2-MIL-88B(Fe2Co)-MOF/NF surface. Further anti-cTnI antibody was immobilized for specific detection of cTnI.	Modified MOF provide ample active sites for carrying antibody	Serum	10 ng/mL-0.1 fg/mL	13 fg/mL	404

Abbreviations: *[BMIM]BF4 - 1-butyl-3-methylimidazolium tetrafluoroborate ; PAMAM- poly(amidoamine)*

3.2.5. MOF-based electrochemical sensors for Cancer

Cancer is a global health burden with its whopping cases standing tall at 18.1 million with 9.6 million mortalities reported in 2018, as per a recent report by WHO (WHO report, 2020). These figures are expected to double by 2040 however, its global response is believed to be uneven and inequitable with almost two-third cases in middle income countries. The spectrum of cancer control interventions comprises of prevention followed by timely and accurate screening and diagnosis. The challenge of cancer diagnosis lies on specificity of sensor towards cancer cells through lesser invasive testing and better detection index [226]. Its early detection is only possible through a powerful sensing of relevant biomarkers such as micro-RNA 21, carcinoembryonic antigen, human telomeric DNA and many others[406].

Of all diagnostic tools currently available, electrochemical methods are one of the most reliable ones due to their rational design, ease of fabrication, low cost and high-end sensitivity towards biomolecules. Cancer biomarkers not just comprise of macromolecules but also ROS like H_2O_2 [407] and superoxide which are now being explored for its early diagnosis. Huang et al. in their recent study have highlighted the significance of detecting H_2O_2 in a range of colon cancer cells (SW-48, NCM-460, and HCT-116) [408]. For the purpose of microelectrode fabrication, reduced graphene fiber was activated (AGF) through 30% H_2O_2 solution which was further placed in polytetrafluoroethylene (PTFE) autoclaves along with ZnO precursor solution at 90°C for 12 hours. The obtained product was further treated at 400°C to obtain ZnO/AGF and then incubated into 2-methylimidazole to obtain ZIF-8@ZnO/AGF. It was soaked in 0.5 M $Cu(NO_3)_2$ solution to finally obtain $Cu_2(OH)_3NO_3$@ZnO/AGF **(Figure 1.15A)**. The probe was electrochemically reducing H_2O_2 at -0.8 V which was further calibrated using choronoamperometry. The sensor was capable of detecting the radical in the range of

1 µM–17.4 mM with a LOD of 1 µM. MOFs not only find their purpose as sensor matrix support but also as catalytic metal center providers like in case of a recent study on sensing superoxide anions (Weizhou, Fan, 2021). In this case, an Ag-based MOF was pyrolyzed to form an AgNPs@C nanocomposite which was deposited onto the surface of a pre-treated GCE electrode to detect $O_2{\cdot}^-$ released from HeLa cells with an LDR of 3.032×10^{-13}-5.719×10^{-5} M and LOD of 1.011×10^{-13} M.

Apart from their role in single analyte detection, they have also been explored for detection of multiple cancer biomarkers through a multiplexing approach [274,410]. A recent article on detection of multiple liver cancer biomarkers, human tissue transglutaminase 2 (TGM2) and heterogeneous nuclear ribonucleoprotein A1 (hnRNP A1), focusses on development of a Fe_3O_4/MIL-101(Fe)-(NH)(CO)-COOH (FO/MOF) adorned with alkaline phosphatase (ALP)-labelled detection antibodies [410]. In a single chip, a spatially separated array of eight distinct electrodes was screen-printed in parallel fashion where each electrode comprised of two carbon-ink WE and CE electrodes, and an Ag/AgCl ink RE. Sandwich assays comprising of anti-TGM2 (JU30–02)-FO/MOF/TGM2/ALP-anti-TGM2 (2F4) and hnRNP A1 aptamer-FO/MOF/hnRNP A1/ALP-anti-hnRNP A1 were magnetically assembled onto each WE (**Figure 1.15A-ii**). The ALP present on them could enzymatically convert 4-aminophenyl phosphate (APP) producing electroactive species thereby releasing $2e^-$ and $2H^+$ which facilitated the quantitative analysis of both the biomarkers. The developed probe was designed to detect two biomarkers at a time but the model could be well deployed for detection of up to eight biomarkers simultaneously. The DPV based assay also demonstrated results in clinical undiluted serum samples with promising results for future liver cancer diagnostics however, lacked an upscaling device fabrication approach. An attempt towards solving this was made by Zhang et al. where ZIF-90-ZnO-MoS_2 nanohybrid-based integrated electrochemical liquid biopsy (ELB) platform was developed for direct profiling cancer exosomes from blood [411]. The multiplexed point-of-care ELB platform comprised of three WE, one CE and one RE printed on a polyethylene terephthalate substrate sealed with PDMS. Solid-phase redox chemical species (silver/carbon band) were placed underneath the WE to facilitate Ag^0/Ag^+ redox reaction to eliminate external redox chemicals and matrix effects. ZIF-90-ZnO-MoS_2 was hierarchically grown over the substrate which were immobilized with exosome recognition antibodies through the MOFs -CHO groups. BSA was interlaced for its antifouling property to detect exosomes from culture supernatant of human non-small cell lung cancer cell line (A549) through DPV (**Figure 1.15B**). The developed sensors could efficiently sense trace amounts of CD9, CD63 and CD81 with an LOD of 10fg/mL, 1fg/ mL and, 1fg/mL, respectively. Practical application of the microchip was evaluated by also considering healthy and diseased blood samples generating higher current values for normal samples. Such rational engineering approaches could pioneer clinically significant MOF-based multiplexing sensing platforms in coming years. These recently reported MOF-based biosensors for diagnosis of cancer using its specific biomarkers can be further complimented with other studies elaborately discussed in **Table 1.9** with their respective target analytes, detection techniques, sensor composite, fabrication strategies, mechanistic role of MOF, real samples considerations and detection efficiency parameters (LDR and LOD).

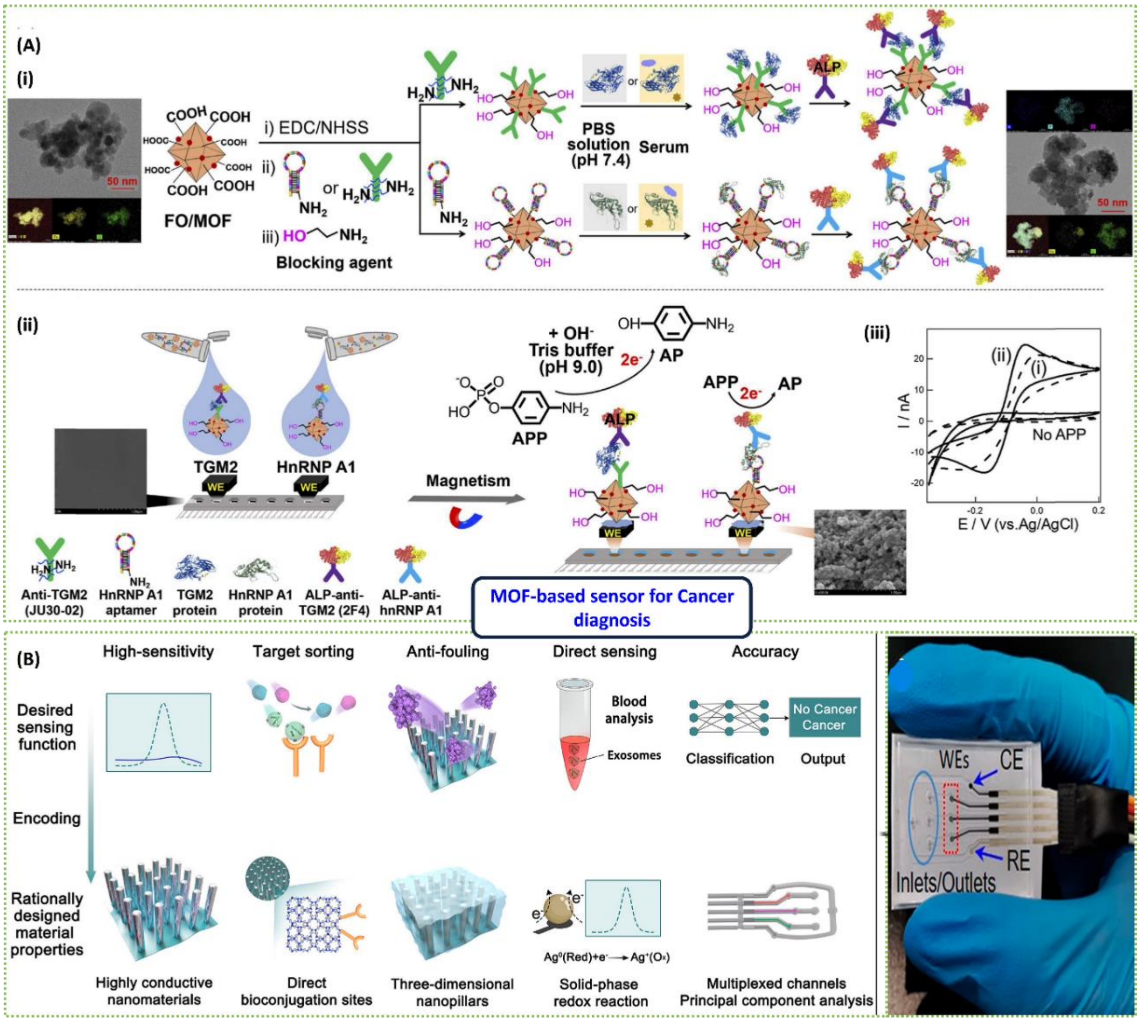

Figure 1.15. *A)-i) Representative scheme illustrating the entire process for fabrication of two types of signalling systems, where the first one comprises of FO/MOF conjugated with capturing bioreceptors and the second comprises of ALP-labeled specific antibodies. TEM and EDS mapping of FO/MOF (left inset box) and FO/MOF/hnRNP A1/ALP-anti-hnRNP A1 (right inset box). ii) Representative mechanism of simultaneous detection of TGM2 and hnRNP A1 on fabricated electrode surface. SEM images of bare (left inset box) and final probe (right inset box). iii) CV data corresponding to target protein detection in alkaline medium (pH 9.0), reproduced with permission from J. Li et al., copyright 2023. B) Schematic representation of strategy to impart sensing properties to ZIF-90-ZnO-MoS_2 based integrated electrochemical liquid biopsy platform for effective screening of cancer exosomes (adopted from Y. Zhang et al., copyright 2022).*

Table 1.9. *Detailed list of latest MOF-based electrochemical biosensors for cancer detection*

S.No.	Target Analyte	Detection Technique	Sensor Composite	Fabrication Strategy	Mechanistic Role of MOF	Real Sample	LDR	LOD	Reference
1.	i) Human Epidermal Growth Factor-2 (HER-2) ii) Estrogen receptor	SWV	ZIF-8/Co-MOF	Co-MOF nanosheets were synthesized hydrothermally. ITO was chosen as the WE and was immersed in a solution of ZIF-8 precursors to coat its surface with a thin film. It was further coated with a drop-casted layer of Co-MOF followed by coating it with labeled ssDNA aptamers. The fabricated electrode was incubated with PBS solution containing the target proteins.	High surface area with increased conductivity and also provide adsorption of aptamer	Human serum spiked with HER2 and ER	0-15 pg mL^{-1}	i) 3.8 fg/mL ii)6.8 fg/mL	[412]
2.	Circulating tumor DNA (ctDNA)	SWV	Nd-MOF	Template-assisted reagent substitution reaction was used for the synthesis of nanosheets of Nd-MOF which was then integrated with AuNPs to coat onto the GCE electrode surface. The surface was then further functionalized with thiol functionalized capture probes (CPs). On encountering the Fc-labeled signaling probes, the ctDNA-probe hybridization leads to signal generation.	Large surface area providing site to adsorb AuNPs	Healthy human serum	1.0 fM-1.0 nM	0.30 fM	[413]
3.	HER-2	DPV	La-MOF-PbO_2	GCE electrode was drop-casted with Polyethyleneimine functionalized MoS_2NFs (PEI-MoS_2NFs) then electrocoated with Au nanocrystals. It was followed by electrode incubation with Ab_1 and thereby treatment with HER2 samples of varying concentrations.	High specific surface area providing large number of active sites	Human serum	100 fg mL^{-1}- 10 µg mL^{-1}	15.64 fM	[414]
4.	Matrix metalloproteinase-9	CV, DPV	Fe-MOF	Fe-MOF was synthesized and functionalized with AuNPs and then with peptide2 through sulfhydryl bonding. In another process Au electrode was immobilized with peptide 1. Then the two peptides could integrate with cucurbit[8] uril to complete the probe fabrication.	Increase in conductivity	Serum from metastatic liver cancer patients	0.5 pg·mL^{-1}- 500 ng·mL^{-1}	1.30 pg·mL^{-1}	[415]
5.	Alpha-fetoprotein (AFP) Cancer embryo antigen (CEA)	DPV	Cu-UMOFNs@Au NPs and Co-UMOFNs@Au NPs	Cleaned GCE electrode surface was casted with Au@Fe_3O_4 NPs dispersed in 0.5% Nafion solution. It was followed by immersion of the electrode in the mixture of 0.1 mg mL^{-1} anti-AFP and 0.1 mg mL^{-1} anti-CEA, incubation and later immobilization with Ab_1 at RT. The last step was blocking of non-specific binding sites using BSA.	Both MOFs are providing high surface area, chemical stability and are carrier for antibodies	Human serum	AFP: 0.001-100 ng mL^{-1} CEA: 0.001-80 ng mL^{-1}	AFP: 0.28 pg mL^{-1} CEA: 0.31 pg mL^{-1}	[416]
6.	Programmed death Ligand 1 (PD-L1)	EIS	Cu-F/Hs (Copper MOF)	Gold was chosen as the working electrode which was polished and treated with piranha solution followed by washing and drying under N_2 atmosphere. To fabricate the electrode, it was cycled in 0.5 M H_2SO_4 to remove any oxide layer. Then, PD-L1 aptamer was mixed with TCEP followed by modification with MCH to avoid any unspecific binding. Then, PD-L1 and Ab-Cu-F/Hs were	Cu-F/Hs shows oxidase like activity and enhance catalytic activity	Serum	0.5 ng/mL-200 ng/mL	0.11 ng/mL	[417]

				subsequently added to the electrode surface to form sandwich-like arrangement. Finally, the probe was completed post addition and incubation by DA and ODA.					
7.	HER-2	DPV	Zn–Co-MOF@ferrocene (Fc) and Fe–Co-MOF@methylene blue (MB)	Zn-Co-MOF film was electrodeposited onto the electrode surface as a thin film. The formed bimetallic MOF film was used for immobilization of aptamer doped with Fc which acts as a capture probe. In a parallel setup, Fe-Co MOF was synthesized through the hydrothermal route which encapsulated the MB signal molecule. The two MOFs jointly acted as ratiometric sensor probe against target analyte.	Provide active surface for aptamer attachment	Human serum	0.75-250 pg/mL	0.37 pg/mL	418
8.	Interleukin-1 receptor antagonist (IL-1RA)	EIS	FeCo-MOF/NF	Sliced commercial NF was treated and dried to use as FeCo MOF growth substrate in hydrothermal setup. Functionalization of the formed material was done by initial incubation in EDC-NHS followed by IL-1RA antibody at 4 °C. It was followed by washing in Tween 20-PBS solution and blocking of unwanted sites through BSA. It was then refrigerated for further usage.	Large surface area providing site to adsorb AuNPs	Human serum	10 fg/mL-10 ng/mL	PBS Buffer: 7.30 fg/mL Serum: 7.22 fg/mL	419
9.	Mucin1	DPV CA	Mn-MOF-74	The aptasensor was constructed with GCE as the WE being electrodeposited with AgNPs followed by coating it with aptamer solution aided by thiol bonding. Later, MCH solution was used to block the non-specific sites followed by functionalizing with varying concentrations of MUC1. Then, Apt/MnO@C@AuNPs were dropped onto the modified electrode surface and was washed with PBS. The probe was stored at 4 °C to finish the final probe.	High specific surface area providing large number of active sites	Human serum	DPV: 0.001 nM-100 nM CA: 0.001 nM-10 nM	DPV:0.31 pM CA:0.25 pM	420
10.	microRNA 155	DPV	Cu-MOF	At first, magnetic rod carbon paste electrodes (MCPE) were prepared. In a separate setup, CNF was dispersed in 0.5% Nafion solution to obtain a homogeneous mixture. This mixture was dropped onto the surface of the MCPE followed by dropping CuBTC-AIA solution over it. It was followed by dispersion of Fe@rGO and PANHS solution and further saturation with DMF vapour. The modified probe was immobilized with miR-155 capture probe to obtain the final sensing probe.	Platform for microRNA binding	Human serum	0.2 fM–500 pM	0.08 fM	421

***Abbreviations:** GCE: Glassy Carbon Electrode; CV: Cyclic Voltammetry; DPV: Differential Pulse Voltammetry; CA: Chronoamperometry; CC: Carbon cloth; CNF: Carbon nanofibers; PANHS: 1-pyrenebutyric acid-N-hydroxysuccinimide ester; AIA: 5-aminoisophthalic acid; NR: Not Reported*

REFERENCES

(1) Li, H.; Eddaoudi, M.; O'Keeffe, M.; Yaghi, O. M. Design and Synthesis of an Exceptionally Stable and Highly Porous Metal- Organic Framework. *Nature* **1999**, *402* (6759), 276–279. https://doi.org/10.1038/46248.

(2) Kim, M.; Xin, R.; Earnshaw, J.; Tang, J.; Hill, J. P.; Ashok, A.; Nanjundan, A. K.; Kim, J.; Young, C.; Sugahara, Y.; Na, J.; Yamauchi, Y. MOF-Derived Nanoporous Carbons with Diverse Tunable Nanoarchitectures. *Nat. Protoc.* **2022**, *17* (12), 2990–3027. https://doi.org/10.1038/s41596-022-00718-2.

(3) Mao, Y.; Li, J.; Cao, W.; Ying, Y.; Hu, P.; Liu, Y.; Sun, L.; Wang, H.; Jin, C.; Peng, X. General Incorporation of Diverse Components inside Metal-Organic Framework Thin Films at Room Temperature. *Nat. Commun.* **2014**, *5*. https://doi.org/10.1038/ncomms6532.

(4) Bux, H.; Liang, F.; Li, Y.; Cravillon, J.; Wiebcke, M.; Caro, J. Zeolitic Imidazolate Framework Membrane with Molecular Sieving Properties by Microwave-Assisted Solvothermal Synthesis. *J. Am. Chem. Soc.* **2009**, *131* (44), 16000–16001. https://doi.org/10.1021/ja907359t.

(5) Guo, H.; Zhu, G.; Hewitt, I. J.; Qiu, S. Twin Copper Source" Growth of Metal-Organic Framework Membrane: Cu3(BTC)2 with High Permeability and Selectivity for Recycling H2. *J. Am. Chem. Soc.* **2009**, *131* (5), 1646–1647. https://doi.org/10.1021/ja8074874.

(6) Huang, A.; Caro, J. Covalent Post-Functionalization of Zeolitic Imidazolate Framework ZIF-90 Membrane for Enhanced Hydrogen Selectivity. *Angew. Chemie - Int. Ed.* **2011**, *50* (21), 4979–4982. https://doi.org/10.1002/anie.201007861.

(7) Li, Y. S.; Liang, F. Y.; Bux, H.; Feldhoff, A.; Yang, W. S.; Caro, J. Molecular Sieve Membrane: Supported Metal-Organic Framework with High Hydrogen Selectivity. *Angew. Chemie - Int. Ed.* **2010**, *49* (3), 548–551. https://doi.org/10.1002/anie.200905645.

(8) Sumida, K.; Rogow, D. L.; Mason, J. A.; McDonald, T. M.; Bloch, E. D.; Herm, Z. R.; Bae, T. H.; Long, J. R. Carbon Dioxide Capture in Metal-Organic Frameworks. *Chem. Rev.* **2012**, *112* (2), 724–781. https://doi.org/10.1021/cr2003272.

(9) Fujita, M.; Washizu, S.; Ogura, K.; Kwon, Y. J. Preparation, Clathration Ability, and Catalysis of a Two-Dimensional Square Network Material Composed of Cadmium(II) and 4, 4′-Bipyridine. *J. Am. Chem. Soc.* **1994**, *116* (3), 1151–1152. https://doi.org/10.1021/ja00082a055.

(13) Gao, W. Y.; Chrzanowski, M.; Ma, S. Metal-Metalloporphyrin Frameworks: A Resurging Class of Functional Materials. *Chemical Society Reviews*. 2014, pp 5841–5866. https://doi.org/10.1039/c4cs00001c.

(14) Yang, Q. Y.; Li, K.; Luo, J.; Pan, M.; Su, C. Y. A Simple Topological Identification Method for Highly (3,12)-Connected 3D MOFs Showing Anion Exchange and Luminescent Properties. *Chem. Commun.* **2011**, *47* (14), 4234–4236. https://doi.org/10.1039/c0cc05464j.

(15) Lei, J.; Qian, R.; Ling, P.; Cui, L.; Ju, H. Design and Sensing Applications of Metal-Organic Framework Composites. *TrAC - Trends in Analytical Chemistry*. 2014, pp 71–78. https://doi.org/10.1016/j.trac.2014.02.012.

(16) Chen, L.; Zheng, H.; Zhu, X.; Lin, Z.; Guo, L.; Qiu, B.; Chen, G.; Chen, Z. N. Metal-Organic Frameworks-Based Biosensor for Sequence-Specific Recognition of Double-Stranded DNA. *Analyst* **2013**, *138* (12), 3490–3493. https://doi.org/10.1039/c3an00426k.

(17) Wu, Y.; Han, J.; Xue, P.; Xu, R.; Kang, Y. Nano Metal-Organic Framework (NMOF)-Based Strategies for Multiplexed MicroRNA Detection in Solution and Living Cancer Cells. *Nanoscale* **2015**, *7* (5), 1753–1759. https://doi.org/10.1039/c4nr05447d.

(18) Li, B.; Chen, D.; Wang, J.; Yan, Z.; Jiang, L.; Duan, D.; He, J.; Luo, Z.; Zhang, J.; Yuan, F. MOFzyme: Intrinsic Protease-like Activity of Cu-MOF. *Sci. Rep.* **2014**, *4*. https://doi.org/10.1038/srep06759.

(19) Wang, J.; Hu, Y.; Zhou, Q.; Hu, L.; Fu, W.; Wang, Y. Peroxidase-like Activity of Metal-Organic Framework [Cu(PDA)(DMF)] and Its Application for Colorimetric Detection of Dopamine. *ACS Appl. Mater. Interfaces* **2019**, *11* (47), 44466–44473. https://doi.org/10.1021/acsami.9b17488.

(20) Liang, H.; Lin, F.; Zhang, Z.; Liu, B.; Jiang, S.; Yuan, Q.; Liu, J. Multicopper Laccase Mimicking Nanozymes with Nucleotides as Ligands. *ACS Appl. Mater. Interfaces* **2017**, *9* (2), 1352–1360. https://doi.org/10.1021/acsami.6b15124.

(21) Bai, Y.; Dou, Y.; Xie, L. H.; Rutledge, W.; Li, J. R.; Zhou, H. C. Zr-Based Metal-Organic Frameworks: Design, Synthesis, Structure, and Applications. *Chemical Society Reviews*. 2016, pp 2327–2367. https://doi.org/10.1039/c5cs00837a.

(22) Baranwal, A.; Srivastava, A.; Kumar, P.; Bajpai, V. K.; Maurya, P. K.; Chandra, P. Prospects of Nanostructure Materials and Their Composites as Antimicrobial Agents. *Front. Microbiol.* **2018**, *9* (MAR). https://doi.org/10.3389/fmicb.2018.00422.

(23) Luo, N.; Shu, Y.; Zhu, C.; Cheng, X.; Chen, L.; Wang, J.; Liu, R.; Ju, H.; Cheng, W.; Xia, Q. Surface Plasma Resonance Biosensing of Phosphorylated Proteins via PH-Adjusted Specific Binding of Phosphate Residues with UiO-66. *Chem. Eng. J.* **2022**, *446*. https://doi.org/10.1016/j.cej.2022.137000.

(24) Song, X.; Zhao, L.; Zhang, N.; Liu, L.; Ren, X.; Ma, H.; Luo, C.; Li, Y.; Wei, Q. Zinc-Based Metal-Organic Framework with MLCT Properties as an Efficient Electrochemiluminescence Probe for Trace Detection of Trenbolone. *Anal. Chem.* **2022**, *94* (40), 14054–14060. https://doi.org/10.1021/acs.analchem.2c03615.

(25) Wen, L.; Wang, N.; Liu, Z.; Tao, C.-A.; Zou, X.; Wang, F.; Wang, J. Acetylcholinesterase Immobilization on ZIF-8/Graphene Composite Engenders High Sensitivity Electrochemical Sensing for Organophosphorus Pesticides. *Chemosensors* **2022**, *10* (10). https://doi.org/10.3390/chemosensors10100418.

(26) Lai, X.; Shen, Y.; Gao, S.; Chen, Y.; Cui, Y.; Ning, D.; Ji, X.; Liu, Z.; Wang, L. The Mn-Modified Porphyrin Metal-Organic Framework with Enhanced Oxidase-like Activity for Sensitively Colorimetric Detection of Glutathione. *Biosens. Bioelectron.* **2022**, *213*. https://doi.org/10.1016/j.bios.2022.114446.

(27) Kulandaivel, S.; Lo, W.-C.; Lin, C.-H.; Yeh, Y.-C. Cu-PyC MOF with Oxidoreductase-like Catalytic Activity Boosting Colorimetric Detection of Cr(VI) on Paper. *Anal. Chim. Acta* **2022**, *1227*. https://doi.org/10.1016/j.aca.2022.340335.

(28) Freund, R.; Zaremba, O.; Arnauts, G.; Ameloot, R.; Skorupskii, G.; Dincă, M.; Bavykina, A.; Gascon, J.; Ejsmont, A.; Goscianska, J.; Kalmutzki, M.; Lächelt, U.; Ploetz, E.; Diercks, C. S.; Wuttke, S. The Current Status of MOF and COF Applications. *Angew. Chemie - Int. Ed.* **2021**, *60* (45), 23975–24001. https://doi.org/10.1002/anie.202106259.

(29) Shu, Y.; Ye, Q.; Tan, J.; Lv, H.; Liu, Z.; Mo, Q. Metalloporphyrin-Based Metal-Organic Framework Nanorods for Peroxidase-Like Catalysis. *ACS Appl. Nano Mater.* **2022**, *5* (12), 17909–17918. https://doi.org/10.1021/acsanm.2c03871.

(30) Dai, W.; Wang, X.; Chen, G.; Wang, X.; Hu, C.; Zhen, S.; Huang, C.; Li, Y. Facile Synthesis of 2D Europium-Metal Organic Frameworks Nanosheets for Highly Efficient Electrochemiluminescence in DNA Detection. *Chem. Eng. J.* **2023**, *465*. https://doi.org/10.1016/j.cej.2023.143037.

(31) Chen, C.; Xu, H.; Zhan, Q.; Zhang, Y.; Wang, B.; Chen, C.; Tang, H.; Xie, Q. Preparation of Novel HKUST-1-Glucose Oxidase Composites and Their Application in Biosensing. *Microchim. Acta* **2023**, *190* (1). https://doi.org/10.1007/s00604-022-05563-4.

(32) Pashazadeh-Panahi, P.; Belali, S.; Sohrabi, H.; Oroojalian, F.; Hashemzaei, M.; Mokhtarzadeh, A.; de la Guardia, M. Metal-Organic Frameworks Conjugated with Biomolecules as Efficient Platforms for Development of Biosensors. *TrAC - Trends in Analytical Chemistry*. 2021. https://doi.org/10.1016/j.trac.2021.116285.

(33) Paul, A.; Banga, I. K.; Muthukumar, S.; Prasad, S. Engineering the ZIF-8 Pore for Electrochemical Sensor Applications-A Mini Review. *ACS Omega*. 2022, pp 26993–27003. https://doi.org/10.1021/acsomega.2c00737.

(34) Sun, Z.; Li, J.; Tong, Y.; Han, H.; Yang, Y.; Wang, C.; Li, H.; Du, L.; Jiang, Y. A Ratiometric Fluorescent Biosensor Based on Self-Fluorescent MOF and Target-Triggered Rolling Circle Amplification for Sensitive Detection of Exosome-Derived MiRNA. *Anal. Chim. Acta* **2022**, *1221*. https://doi.org/10.1016/j.aca.2022.340136.

(35) Yang, X.; Cui, A.; Zhang, Y.; Li, S.; Li, Y. Electrogenerated Chemiluminescence Biosensor for MicroRNA Detection Incorporating Enzyme-Free Dual DNA Cyclic Amplification and Ru(Bpy)32+-Functionalized Metal-Organic Framework. *Talanta* **2022**, *245*. https://doi.org/10.1016/j.talanta.2022.123458.

(36) Mashkoori, A.; Mostafavi, A.; Shamspur, T.; Torkzadeh-Mahani, M. Electrochemical Enzyme-Based Blood Uric Acid Biosensor: New Insight into the Enzyme Immobilization on the Surface of Electrode via Poly-Histidine Tag. *Microchim. Acta* **2022**, *189* (9). https://doi.org/10.1007/s00604-022-05408-0.

(37) Huang, S.; Liu, Z.; Yan, Y.; Chen, J.; Yang, R.; Huang, Q.; Jin, M.; Shui, L. Triple Signal-Enhancing Electrochemical Aptasensor Based on Rhomboid Dodecahedra Carbonized-ZIF<inf>67</Inf> for Ultrasensitive CRP Detection. *Biosens. Bioelectron.* **2022**, *207*. https://doi.org/10.1016/j.bios.2022.114129.

(38) Kong, W.; Zhu, D.; Luo, R.; Yu, S.; Ju, H. Framework-Promoted Charge Transfer for Highly Selective Photoelectrochemical Biosensing of Dopamine. *Biosens. Bioelectron.* **2022**, *211*. https://doi.org/10.1016/j.bios.2022.114369.

(39) Zhong, Y. F.; Bao, G. M.; Qiu, M.; Xia, Y. F.; Li, W.; Tao, Y. Q.; Liu, S. Y.; Li, S. H.; Xiao, W.; Zhang, Y.; Yuan, H. Q. Highly Selective and Sensitive Fluorescent Biosensor for the Detection of Serotonin and Its Metabolite by Eu3+-Doped Metal-Organic Framework. *Chem. Eng. J.* **2022**, *442*. https://doi.org/10.1016/j.cej.2022.136272.

(40) Bieniek, A.; Terzyk, A. P.; Wiśniewski, M.; Roszek, K.; Kowalczyk, P.; Sarkisov, L.; Keskin, S.; Kaneko, K. MOF Materials as Therapeutic Agents, Drug Carriers, Imaging Agents and Biosensors in Cancer Biomedicine: Recent Advances and Perspectives. *Progress in Materials Science*. 2021. https://doi.org/10.1016/j.pmatsci.2020.100743.

(41) Jia, Y.; Yan, B. Visual Ratiometric Fluorescence Sensing of L-Lactate in Sweat by Eu-Mof and the Design of Logic Devices. *SSRN Electron. J.* **2023**. https://doi.org/10.2139/ssrn.4347405.

(42) Mathew, G.; Daniel, M.; Peramaiah, K.; Ganesh, M.-R.; Neppolian, B. Real-Time Electrochemical Quantification of H<inf>2</Inf>O<inf>2</Inf> in Living Cancer Cells Using Bismuth Based MOF. *J. Electroanal. Chem.* **2022**, *914*. https://doi.org/10.1016/j.jelechem.2022.116255.

(43) Wang, Y.; Zhou, Y.; Chen, Y.; Yin, Z.; Hao, J.; Li, H.; Liu, K. Simple and Sensitive Nitric Oxide Biosensor Based on the Electrocatalysis of Horseradish Peroxidase on AuNPs@metal–Organic Framework Composite-Modified Electrode. *Microchim. Acta* **2022**, *189* (4). https://doi.org/10.1007/s00604-022-05268-8.

(44) Sikka, R.; Kumar, P.; Lee, J.; Sonne, C. Aqueous-Phase Biofunctionalized NH2-MIL-53(Al) MOF for Biosensing Applications. *J. Porous Mater.* **2022**, *29* (2), 515–522. https://doi.org/10.1007/s10934-021-01192-z.

(45) Wang, Y.; Jin, D.; Zhang, X.; Zhao, J.; Hun, X. Self-Enhancement Photoelectrochemical Strategy for Kanamycin Determination with Amino Functionalized MOFs. *Microchim. Acta* **2022**, *189* (5). https://doi.org/10.1007/s00604-022-05266-w.

(46) Rabiee, N.; Fatahi, Y.; Ahmadi, S.; Abbariki, N.; Ojaghi, A.; Rabiee, M.; Radmanesh, F.; Dinarvand, R.; Bagherzadeh, M.; Mostafavi, E.; Ashrafizadeh, M.; Makvandi, P.; Lima, E. C.; Saeb, M. R. Bioactive Hybrid Metal-Organic Framework (MOF)-Based Nanosensors for Optical Detection of Recombinant SARS-CoV-2 Spike Antigen. *Sci. Total Environ.* **2022**, *825*. https://doi.org/10.1016/j.scitotenv.2022.153902.

(47) Wang, Z.; Zhou, X.; Han, J.; Xie, G.; Liu, J. DNA Coated CoZn-ZIF Metal-Organic Frameworks for Fluorescent Sensing Guanosine Triphosphate and Discrimination of Nucleoside Triphosphates. *Anal. Chim. Acta* **2022**, *1207*. https://doi.org/10.1016/j.aca.2022.339806.

(48) Peng, M.; Lin, S.; Lin, Z.; Zheng, D.; Song, Y.; Lu, F.; Chen, Y.; Gao, W. Rationally Constructed ZnCdS-HDCs@In<inf>2</Inf>S<inf>3</Inf>-HNRs Double-Hollow Heterojunction with Promoted Light Capture Capability for Photoelectrochemical Biosensing. *Biosens. Bioelectron.* **2022**, *201*. https://doi.org/10.1016/j.bios.2021.113957.

(49) Du, Q.; Liao, Y.; Shi, N.; Sun, S.; Liao, X.; Yin, G.; Huang, Z.; Pu, X.; Wang, J. Facile Synthesis of Bimetallic Metal–Organic Frameworks on Nickel Foam for a High Performance Non-Enzymatic Glucose Sensor. *J. Electroanal. Chem.* **2022**, *904*. https://doi.org/10.1016/j.jelechem.2021.115887.

(50) Aina, N.; Ruzniza, I. M. M.; Wan, M. Z.; Nor, M. K. *Electrochemical and Optical Sensors Made of Composites of Metal – Organic Frameworks and Carbon - Based Materials . A Review*; Springer International Publishing, 2022; Vol. 20. https://doi.org/10.1007/s10311-022-01403-2.

(51) Zuliani, A.; Khiar, N.; Carrillo, C. Recent Progress of Metal – Organic Frameworks as Sensors in (Bio) Analytical Fields : Towards Real - World Applications. *Anal. Bioanal. Chem.* **2023**, 2005–2023. https://doi.org/10.1007/s00216-022-04493-7.

(52) Ghosh, A.; Fathima, S.; Kallungal, T. Applications in Electrochemical and Optical Biosensors. **2023**.

(53) Rezaee, T.; Fazel-zarandi, R.; Karimi, A.; Ensafi, A. A. Journal of Pharmaceutical and Biomedical Analysis Metal-Organic Frameworks for Pharmaceutical and Biomedical Applications. *J. Pharm. Biomed. Anal.* **2022**, *221* (September), 115026. https://doi.org/10.1016/j.jpba.2022.115026.

(54) Pashazadeh-panahi, P.; Belali, S.; Sohrabi, H.; Oroojalian, F.; Hashemzaei, M.; Mokhtarzadeh, A.; De, M. Trends in Analytical Chemistry Metal-Organic Frameworks Conjugated with Biomolecules as Ef Fi Cient Platforms for

Development of Biosensors. *Trends Anal. Chem.* **2021**, *141*, 116285. https://doi.org/10.1016/j.trac.2021.116285.

(55) Shah, B. B.; Kundu, T.; Zhao, D. Mechanical Properties of Shaped Metal–Organic Frameworks. *Topics in Current Chemistry*. 2019. https://doi.org/10.1007/s41061-019-0250-7.

(56) Tan, J. C.; Furman, J. D.; Cheetham, A. K. Relating Mechanical Properties and Chemical Bonding in an Inorganic−Organic Framework Material: A Single−Crystal Nanoindentation Study. *J. Am. Chem. Soc.* **2009**, *131* (40), 14252–14254. https://doi.org/10.1021/jz4013849.

(57) Coudert, F. X.; Boutin, A.; Fuchs, A. H.; Neimark, A. V. Adsorption Deformation and Structural Transitions in Metal-Organic Frameworks: From the Unit Cell to the Crystal. *J. Phys. Chem. Lett.* **2013**, *4* (19), 3198–3205. https://doi.org/10.1021/jz4013849.

(58) Rabiee, N.; Ghadiri, A. M.; Alinezhad, V.; Sedaghat, A.; Ahmadi, S.; Fatahi, Y.; Makvandi, P.; Saeb, M. R.; Bagherzadeh, M.; Asadnia, M.; Varma, R. S.; Lima, E. C. Synthesis of Green Benzamide-Decorated UiO-66-NH<inf>2</Inf> for Biomedical Applications. *Chemosphere* **2022**, *299*. https://doi.org/10.1016/j.chemosphere.2022.134359.

(59) Kuc, A.; Enyashin, A.; Seifert, G. Metal - Organic Frameworks : Structural , Energetic , Electronic , and Mechanical Properties. **2007**, 8179–8186.

(60) Hsieh, C. T.; Ariga, K.; Shrestha, L. K.; Hsu, S. H. Development of MOF Reinforcement for Structural Stability and Toughness Enhancement of Biodegradable Bioinks. *Biomacromolecules* **2021**, *22* (3), 1053–1064. https://doi.org/10.1021/acs.biomac.0c00920.

(61) Burtch, N. C.; Heinen, J.; Bennett, T. D.; Dubbeldam, D.; Allendorf, M. D. Mechanical Properties in Metal–Organic Frameworks: Emerging Opportunities and Challenges for Device Functionality and Technological Applications. *Advanced Materials*. 2018. https://doi.org/10.1002/adma.201704124.

(62) Allendorf, M. D.; Bauer, C. A.; Bhakta, R. K.; Houk, R. J. T. Luminescent Metal-Organic Frameworks. *Chem. Soc. Rev.* **2009**, *38* (5), 1330–1352. https://doi.org/10.1039/b802352m.

(63) Jiang, Y. P.; Fang, X. H.; Wang, Q.; Huo, J. Z.; Liu, Y. Y.; Wang, X. R.; Ding, B. Near-Infrared Magnetic Core-Shell Nanoparticles Based on Lanthanide Metal-Organic Frameworks as a Ratiometric Felodipine Sensing Platform. *Commun. Chem.* **2023**, *6* (1), 1–10. https://doi.org/10.1038/s42004-023-00893-7.

(64) Li, Z.; Dong, J.; Wang, Q.; Chen, N.; Cui, W.; He, Y.; Chen, B.; Zhao, D. Ratiometric Fluorescence Temperature Sensing Based on Thermal Coupling Energy Levels of a Single-Lanthanide Dysprosium MOF. *J. Lumin.* **2023**, *263*, 120070. https://doi.org/10.1016/J.JLUMIN.2023.120070.

(65) Mahata, P.; Mondal, S. K.; Singha, D. K.; Majee, P. Luminescent Rare-Earth-

Based MOFs as Optical Sensors. *Dalton Trans.* **2017**, *46* (2), 301–328. https://doi.org/10.1039/c6dt03419e.

(66) Luo, Y.; Ahmad, M.; Schug, A.; Tsotsalas, M. Rising Up: Hierarchical Metal–Organic Frameworks in Experiments and Simulations. *Advanced Materials*. 2019. https://doi.org/10.1002/adma.201901744.

(67) Xia, H.; Zhang, J.; Yang, Z.; Guo, S.; Guo, S.; Xu, Q. 2D MOF Nanoflake-Assembled Spherical Microstructures for Enhanced Supercapacitor and Electrocatalysis Performances. *Nano-Micro Lett.* **2017**, *9* (4). https://doi.org/10.1007/s40820-017-0144-6.

(68) Jamali, S.; Kazemzad, M.; Naderi, N.; Eshraghi, M. J.; Sabzehmeidani, M. M. Preparation of Hierarchical MOF-5 Films Using Morphology Controlled ZnO Coatings for Temperature Dependent Optical Sensors Application. *Mater. Chem. Phys.* **2023**, *304*, 127775. https://doi.org/10.1016/j.matchemphys.2023.127775.

(69) Oladipo, A. A.; Oskouei, S. D.; Gazi, M. Metal-Organic Framework-Based Nanomaterials as Opto-Electrochemical Sensors for the Detection of Antibiotics and Hormones : A Review. **2023**, 631–673. https://doi.org/10.3762/bjnano.14.52.

(70) Sun, L.; Campbell, M. G.; Dincă, M. Electrically Conductive Porous Metal-Organic Frameworks. *Angew. Chem. Int. Ed. Engl.* **2016**, *55* (11), 3566–3579. https://doi.org/10.1002/anie.201506219.

(71) Zhang, X.; Wang, P.; Liang, Z.; Zhong, W.; Ma, Q. A Novel Cu-MOFs Nanosheet/BiVO4 Nanorod-Based ECL Sensor for Colorectal Cancer Diagnosis. *Talanta* **2024**, *266*, 124952. https://doi.org/10.1016/J.TALANTA.2023.124952.

(72) Li, J.; Kumar, A.; Johnson, B. A.; Ott, S. Experimental Manifestation of Redox-Conductivity in Metal-Organic Frameworks and Its Implication for Semiconductor/Insulator Switching. *Nat. Commun.* **2023**, *14* (1), 1–10. https://doi.org/10.1038/s41467-023-40110-6.

(73) Lim, H.; Kwon, H.; Kang, H.; Jang, J. E.; Kwon, H. J. Semiconducting MOFs on Ultraviolet Laser-Induced Graphene with a Hierarchical Pore Architecture for NO2 Monitoring. *Nat. Commun.* **2023**, *14* (1). https://doi.org/10.1038/s41467-023-38918-3.

(74) Sundriyal, S.; Kaur, H.; Bhardwaj, S. K.; Mishra, S.; Kim, K. H.; Deep, A. Metal-Organic Frameworks and Their Composites as Efficient Electrodes for Supercapacitor Applications. *Coord. Chem. Rev.* **2018**, *369*, 15–38. https://doi.org/10.1016/J.CCR.2018.04.018.

(75) Ghorbani-Choghamarani, A.; Kakakhani, Z.; Taherinia, Z. 4,6-Diamino-2-Thiopyrimidine-Based Cobalt Metal Organic Framework (Co-DAT-MOF): Green, Efficient, Novel and Reusable Nanocatalyst for Synthesis of Multicomponent Reactions. *Sci. Rep.* **2023**, *13* (1), 7502. https://doi.org/10.1038/s41598-023-34001-5.

(76) Do, H. H.; Tekalgne, M. A.; Le, Q. Van; Cho, J. H.; Ahn, S. H.; Kim, S. Y. Hollow

Ni/NiO/C Composite Derived from Metal-Organic Frameworks as a High-Efficiency Electrocatalyst for the Hydrogen Evolution Reaction. *Nano Converg.* **2023**, *10* (1). https://doi.org/10.1186/s40580-023-00354-w.

(77) Zou, N.; Qiu, T.; Zheng, Y. Synthesis of MOFs Catalyst Containing Cu(I) Sites for CO2 Hydrogenation: Room-Temperature Controlled Reduction via Plasma Reducing Treatment Strategy. *Catal. Today* **2023**, *421* (1), 114176. https://doi.org/10.1016/j.cattod.2023.114176.

(78) Chen, S. S.; Hu, C.; Liu, C. H.; Chen, Y. H.; Ahamad, T.; Alshehri, S. M.; Huang, P. H.; Wu, K. C. W. De Novo Synthesis of Platinum-Nanoparticle-Encapsulated UiO-66-NH2 for Photocatalytic Thin Film Fabrication with Enhanced Performance of Phenol Degradation. *J. Hazard. Mater.* **2020**, *397*. https://doi.org/10.1016/j.jhazmat.2020.122431.

(79) Chueh, C. C.; Chen, C. I.; Su, Y. A.; Konnerth, H.; Gu, Y. J.; Kung, C. W.; Wu, K. C. W. Harnessing MOF Materials in Photovoltaic Devices: Recent Advances, Challenges, and Perspectives. *J. Mater. Chem. A* **2019**, *7* (29), 17079–17095. https://doi.org/10.1039/c9ta03595h.

(80) Yaghi, O. M.; Li, G.; Li, H. Selective Binding and Removal of Guests in a Microporous Metal–Organic Framework. *Nature* **1995**, *378* (6558), 703–706. https://doi.org/10.1038/378703a0.

(81) Yaghi, O. M.; Li, H. Hydrothermal Synthesis of a Metal-Organic Framework Containing Large Rectangular Channels. *J. Am. Chem. Soc.* **1995**, *117* (41), 10401–10402. https://doi.org/10.1021/ja00146a033.

(82) Bian, Y.; Xiong, N.; Zhu, G. Technology for the Remediation of Water Pollution: A Review on the Fabrication of Metal Organic Frameworks. *Processes* **2018**, *6* (8). https://doi.org/10.3390/pr6080122.

(83) Solís, R. R.; Peñas-Garzón, M.; Belver, C.; Rodriguez, J. J.; Bedia, J. Highly Stable UiO-66-NH2 by the Microwave-Assisted Synthesis for Solar Photocatalytic Water Treatment. *J. Environ. Chem. Eng.* **2022**, *10* (2). https://doi.org/10.1016/j.jece.2021.107122.

(84) Yang, H. M.; Liu, X.; Song, X. L.; Yang, T. L.; Liang, Z. H.; Fan, C. M. In Situ Electrochemical Synthesis of MOF-5 and Its Application in Improving Photocatalytic Activity of BiOBr. *Trans. Nonferrous Met. Soc. China (English Ed.* **2015**, *25* (12), 3987–3994. https://doi.org/10.1016/S1003-6326(15)64047-X.

(85) Borse, R. A.; Kale, M. B.; Srinivasan, S.; Sonawane, S. H.; Wang, Y. Sonochemical Approach of Highly Thermal, Mechanical, and Corrosion Inhibition Performance of Metal–Organic Framework (ZIF-8)-Decorated Waterborne Polyurethane Nanocomposite. *Adv. Eng. Mater.* **2022**, *2201484*, 1–11. https://doi.org/10.1002/adem.202201484.

(86) Wang, Y.; Lu, Y.; Li, Z.; Sun, X. W.; Zhang, W. Y.; Zhang, S.; Wang, J.; Dang, T. Y.; Zhang, Z.; Liu, S. X. One-Pot Mechanochemical Synthesis to Encapsulate

Functional Guests into a Metal-Organic Framework for Proton Conduction. *Chem. Commun.* **2021**, *57* (71), 8933–8936. https://doi.org/10.1039/d1cc03482k.

(87) Lu, N.; Zhou, F.; Jia, H.; Wang, H.; Fan, B.; Li, R. Dry-Gel Conversion Synthesis of Zr-Based Metal-Organic Frameworks. *Ind. Eng. Chem. Res.* **2017**, *56* (48), 14155–14163. https://doi.org/10.1021/acs.iecr.7b04010.

(88) Zhao, Y.; Song, Z.; Li, X.; Sun, Q.; Cheng, N.; Lawes, S.; Sun, X. Metal Organic Frameworks for Energy Storage and Conversion. *Energy Storage Mater.* **2016**, *2*, 35–62. https://doi.org/10.1016/j.ensm.2015.11.005.

(89) Rabenau, A. The Role of Hydrothermal Synthesis in Preparative Chemistry. *Angewandte Chemie International Edition in English*. 1985, pp 1026–1040. https://doi.org/10.1002/anie.198510261.

(90) Chen, M.; Wei, S.; Wu, J.; Li, J.; Fu, B.; Zhu, X. Sulfur Doped Bi-MOF with Adjustable Band Gap for Tetracycline Removal under Visible Light. *Colloids Surfaces A Physicochem. Eng. Asp.* **2023**, *664*. https://doi.org/10.1016/j.colsurfa.2023.131186.

(91) Mukherjee, D.; Das, P.; Kundu, S.; Mohan Kundu, L.; Mandal, B. Graphene Quantum Dots Decorated MIL-100(Fe) Composites for Dye Degradation. *J. Photochem. Photobiol. A Chem.* **2023**, *442*, 114776. https://doi.org/10.1016/j.jphotochem.2023.114776.

(92) Hu, D. C.; Lin, X. R.; Gao, Q.; Zhang, J. M.; Feng, H.; Liu, J. C. Synthesis of Novel Coordination Polymer Cd-MOF and Fluorescence Recognition of Tryptophan. *J. Mol. Struct.* **2023**, *1284*, 135389. https://doi.org/10.1016/j.molstruc.2023.135389.

(93) Stock, N.; Biswas, S. Synthesis of Metal-Organic Frameworks (MOFs): Routes to Various MOF Topologies, Morphologies, and Composites. *Chemical Reviews*. 2012, pp 933–969. https://doi.org/10.1021/cr200304e.

(94) Wang, J.; Zhu, W.; Ma, M. For Superior Glucose Sensing. *J. Alloys Compd.* **2022**, *923*, 166418. https://doi.org/10.1016/j.jallcom.2022.166418.

(95) Van Assche, T. R. C.; Desmet, G.; Ameloot, R.; De Vos, D. E.; Terryn, H.; Denayer, J. F. M. Electrochemical Synthesis of Thin HKUST-1 Layers on Copper Mesh. *Microporous Mesoporous Mater.* **2012**, *158* (3), 209–213. https://doi.org/10.1016/j.micromeso.2012.03.029.

(96) Martinez Joaristi, A.; Juan-Alcañiz, J.; Serra-Crespo, P.; Kapteijn, F.; Gascon, J. Electrochemical Synthesis of Some Archetypical Zn 2+ , Cu 2+ , and Al 3+ Metal Organic Frameworks. *Cryst. Growth Des.* **2012**, *12* (7), 3489–3498. https://doi.org/10.1021/cg300552w.

(97) Senthil Kumar, R.; Senthil Kumar, S.; Anbu Kulandainathan, M. Efficient Electrosynthesis of Highly Active Cu3(BTC) 2-MOF and Its Catalytic Application to Chemical Reduction. *Microporous Mesoporous Mater.* **2013**, *168*, 57–64. https://doi.org/10.1016/j.micromeso.2012.09.028.

(98) Ameloot, R.; Stappers, L.; Fransaer, J.; Alaerts, L.; Sels, B. F.; De Vos, D. E. Patterned Growth of Metal-Organic Framework Coatings by Electrochemical Synthesis. *Chem. Mater.* **2009**, *21* (13), 2580–2582. https://doi.org/10.1021/cm900069f.

(99) Ploskonka, A. M.; Marzen, S. E.; DeCoste, J. B. Facile Synthesis and Direct Activation of Zirconium Based Metal-Organic Frameworks from Acetone. *Ind. Eng. Chem. Res.* **2017**, *56* (6), 1478–1484. https://doi.org/10.1021/acs.iecr.6b04361.

(100) Bazzi, L.; Ayouch, I.; Tachallait, H.; EL Hankari, S. Ultrasound and Microwave Assisted-Synthesis of ZIF-8 from Zinc Oxide for the Adsorption of Phosphate. *Results Eng.* **2022**, *13* (March), 100378. https://doi.org/10.1016/j.rineng.2022.100378.

(101) Li, X.; Dong, H.; Fan, Q.; Chen, K.; Sun, D.; Hu, T.; Ni, Z. One-Pot, Rapid Microwave-Assisted Synthesis of Bimetallic Metal–Organic Framework for Efficient Enzyme-Free Glucose Detection. *Microchem. J.* **2022**, *179* (April), 107468. https://doi.org/10.1016/j.microc.2022.107468.

(102) Zhao, Z.; Li, H.; Zhao, K.; Wang, L.; Gao, X. Microwave-Assisted Synthesis of MOFs: Rational Design via Numerical Simulation. *Chem. Eng. J.* **2022**, *428* (March 2021), 131006. https://doi.org/10.1016/j.cej.2021.131006.

(103) Lee, J. H.; Ahn, Y.; Kwak, S. Y. Facile Sonochemical Synthesis of Flexible Fe-Based Metal-Organic Frameworks and Their Efficient Removal of Organic Contaminants from Aqueous Solutions. *ACS Omega* **2022**, *7* (27), 23213–23222. https://doi.org/10.1021/acsomega.2c01068.

(104) Vaitsis, C.; Kanellou, E.; Pandis, P. K.; Papamichael, I.; Sourkouni, G.; Zorpas, A. A.; Argirusis, C. Sonochemical Synthesis of Zinc Adipate Metal-Organic Framework (MOF) for the Electrochemical Reduction of CO2: MOF and Circular Economy Potential. *Sustain. Chem. Pharm.* **2022**, *29* (April), 100786. https://doi.org/10.1016/j.scp.2022.100786.

(105) Bui, T. T.; Nguyen, D. C.; Hua, S. H.; Chun, H.; Kim, Y. S. Sonochemical Preparation of a Magnet-Responsive Fe 3 O 4 @ ZIF-8 Adsorbent for Efficient Cu 2 + Removal. **2022**, 1–12.

(106) Imawaka, K.; Sugita, M.; Takewaki, T.; Tanaka, S. Mechanochemical Synthesis of Bimetallic CoZn-ZIFs with Sodalite Structure. *Polyhedron* **2019**, *158*, 290–295. https://doi.org/10.1016/j.poly.2018.11.018.

(107) Crawford, D.; Casaban, J.; Haydon, R.; Giri, N.; McNally, T.; James, S. L. Synthesis by Extrusion: Continuous, Large-Scale Preparation of MOFs Using Little or No Solvent. *Chem. Sci.* **2015**, *6* (3), 1645–1649. https://doi.org/10.1039/c4sc03217a.

(108) Koekkoek, A. J. J.; Degirmenci, V.; Hensen, E. J. M. Dry Gel Conversion of Organosilane Templated Mesoporous Silica: From Amorphous to Crystalline

Catalysts for Benzene Oxidation. *J. Mater. Chem.* **2011**, *21* (25), 9279–9289. https://doi.org/10.1039/c1jm10779h.

(109) Matsukata, M.; Ogura, M.; Osaki, T.; Hari Prasad Rao, P. R.; Nomura, M.; Kikuchi, E. Conversion of Dry Gel to Microporous Crystals in Gas Phase. *Top. Catal.* **1999**, *9* (1–2), 77–92. https://doi.org/10.1023/a:1019106421183.

(110) Kim, J.; Lee, Y. R.; Ahn, W. S. Dry-Gel Conversion Synthesis of Cr-MIL-101 Aided by Grinding: High Surface Area and High Yield Synthesis with Minimum Purification. *Chem. Commun.* **2013**, *49* (69), 7647–7649. https://doi.org/10.1039/c3cc44559c.

(111) Pezhhanfar, S.; Farajzadeh, M. A.; Hosseini-Yazdi, S. A.; Mogaddam, M. R. A. Synthesis of MOF-70 Based on Diffusion Method; Microgram Amount Application as a Highly Efficient Sorbent in Dispersive Micro Solid Phase Extraction Prior to Dispersive Liquid–Liquid Microextraction for the Preconcentration and Extraction of Pesticides Fr. *J. Iran. Chem. Soc.* **2022**, *19* (6), 2407–2419. https://doi.org/10.1007/s13738-021-02456-w.

(112) Haldar, R.; Bonakala, S.; Kanoo, P.; Balasubramanian, S.; Maji, T. K. Two 3D Metal-Organic Frameworks of Cd(Ii): Modulation of Structures and Porous Properties Based on Linker Functionalities. *CrystEngComm* **2014**, *16* (22), 4877–4885. https://doi.org/10.1039/c4ce00190g.

(113) Teixeira, M.; Maia, R. A.; Karmazin, L.; Louis, B.; Baudron, S. A. Ionothermal Synthesis of Calcium-Based Metal-Organic Frameworks in a Deep Eutectic Solvent. *CrystEngComm* **2022**, *24* (3), 601–608. https://doi.org/10.1039/d1ce01497h.

(114) Azbell, T. J.; Pitt, T. A.; Bollmeyer, M. M.; Cong, C.; Lancaster, K. M.; Milner, P. J. Ionothermal Synthesis of Metal-Organic Frameworks Using Low-Melting Metal Salt Precursors**. *Angew. Chemie - Int. Ed.* **2023**, *08544*. https://doi.org/10.1002/anie.202218252.

(115) Xiao, F.; Wang, L.; Duan, H. Nanomaterial Based Electrochemical Sensors for in Vitro Detection of Small Molecule Metabolites. *Biotechnology Advances*. 2016, pp 234–249. https://doi.org/10.1016/j.biotechadv.2016.01.006.

(116) Purohit, B.; Mahato, K.; Kumar, A.; Chandra, P. Sputtering Enhanced Peroxidase like Activity of a Dendritic Nanochip for Amperometric Determination of Hydrogen Peroxide in Blood Samples. *Microchim. Acta* **2019**, *186* (9), 658. https://doi.org/10.1007/s00604-019-3773-2.

(117) Patella, B.; Buscetta, M.; Di Vincenzo, S.; Ferraro, M.; Aiello, G.; Sunseri, C.; Pace, E.; Inguanta, R.; Cipollina, C. Electrochemical Sensor Based on RGO/Au Nanoparticles for Monitoring H2O2 Released by Human Macrophages. *Sensors Actuators, B Chem.* **2021**, *327*. https://doi.org/10.1016/j.snb.2020.128901.

(118) Wang, Y.; Zhang, D.; Zeng, Y.; Sun, Y.; Qi, P. Simultaneous Ultrasensitive ADP and ATP Quantification Based on CRISPR/Cas12a Integrated ZIF-

90@Ag3AuS2@Fe3O4 Nanocomposites. *Biosens. Bioelectron.* **2022**, *218*. https://doi.org/10.1016/j.bios.2022.114784.

(119) Huang, W.; Xu, Y.; Wang, Z.; Liao, K.; Zhang, Y.; Sun, Y. Dual Nanozyme Based on Ultrathin 2D Conductive MOF Nanosheets Intergraded with Gold Nanoparticles for Electrochemical Biosensing of H<inf>2</Inf>O<inf>2</Inf> in Cancer Cells. *Talanta* **2022**, *249*. https://doi.org/10.1016/j.talanta.2022.123612.

(120) Xie, Y.; Shi, X.; Chen, L.; Lu, J.; Lu, X.; Sun, D.; Zhang, L. Direct Electrodeposition of Bimetallic Nanostructures on Co-Based MOFs for Electrochemical Sensing of Hydrogen Peroxide. *Front. Chem.* **2022**, *10* (March), 1–11. https://doi.org/10.3389/fchem.2022.856003.

(121) Xiong, L.; Zhang, Y.; Wu, S.; Chen, F.; Lei, L.; Yu, L.; Li, C. Co3O4 Nanoparticles Uniformly Dispersed in Rational Porous Carbon Nano-Boxes for Significantly Enhanced Electrocatalytic Detection of H2O2 Released from Living Cells. *Int. J. Mol. Sci.* **2022**, *23* (7). https://doi.org/10.3390/ijms23073799.

(122) Chen, Y.; Huang, W.; Wang, C.; Zhai, X.; Zhang, T.; Wang, Y.; Hu, X. Direct Growth of Poly-Glutamic Acid Film on Peroxidase Mimicking PCN-222(Mn) for Constructing a Novel Sensitive Nonenzymatic Electrochemical Hydrogen Peroxide Biosensor. *ACS Sustain. Chem. Eng.* **2020**, *8* (35), 13226–13235. https://doi.org/10.1021/acssuschemeng.0c03000.

(123) Ma, X.; Tang, K.-L.; Yang, M.; Shi, W.; Zhao, W. Metal–Organic Framework-Derived Yolk–Shell Hollow Ni/NiO@C Microspheres for Bifunctional Non-Enzymatic Glucose and Hydrogen Peroxide Biosensors. *J. Mater. Sci.* **2021**, *56* (1), 442–456. https://doi.org/10.1007/s10853-020-05236-8.

(124) Li, X.; Zhao, Y.; Hao, X.; Wang, X.; Luan, F.; Tian, C.; Zhang, Z.; Yu, S.; Zhuang, X. Self-Luminescent Europium Based Metal Organic Frameworks Nanorods as a Novel Electrochemiluminescence Chromophore for Sensitive Ulinastatin Detection in Biological Samples. *Talanta* **2022**, *250*. https://doi.org/10.1016/j.talanta.2022.123726.

(125) Yu, H.; Wu, H.; Tian, X.; Zhou, Y.; Ren, C.; Wang, Z. A Nano-Sized Cu-MOF with High Peroxidase-like Activity and Its Potential Application in Colorimetric Detection of H2O2and Glucose. *RSC Adv.* **2021**, *11* (43), 26963–26973. https://doi.org/10.1039/d1ra04877e.

(126) Cui, H.; Cui, S.; Zhang, S.; Tian, Q.; Liu, Y.; Zhang, P.; Wang, M.; Zhang, J.; Li, X. Cu-MOF/Hemin: A Bionic Enzyme with Excellent Dispersity for the Determination of Hydrogen Peroxide Released from Living Cells. *Analyst* **2021**, *146* (19), 5951–5961. https://doi.org/10.1039/d1an01323h.

(127) Tan, B.; Zhang, S.; Wang, K.; Yan, Y.; Chu, Z.; Wang, Q.; Li, X.; Zhu, G.; Fan, J.; Zhao, H. Moisture-Resistant and Green Cyclodextrin Metal–Organic Framework Nanozyme Based on Cross-Linkage for Visible Detection of Cellular

Hydrogen Peroxide. *Microchim. Acta* **2022**, *189* (8). https://doi.org/10.1007/s00604-022-05389-0.

(128) Chen, Q.; Hu, C.; Liu, Y.; Liu, Y.; Wang, W.; Zheng, H.; Rong, L.; Jia, J.; Sun, S.; Yu, C.; Liu, Y. M. Safety and Tolerability of High-Dose Ulinastatin after 2-Hour Intravenous Infusion in Adult Healthy Chinese Volunteers: A Randomized, Double-Blind, Placebo-Controlled, Ascending-Dose Study. *PLoS One* **2017**, *12* (5), e0177425. https://doi.org/10.1371/journal.pone.0177425.

(129) El-Kenawi, A.; Ruffell, B. Inflammation, ROS, and Mutagenesis. *Cancer Cell* **2017**, *32* (6), 727–729. https://doi.org/10.1016/j.ccell.2017.11.015.

(130) Shanmugapriya, J.; Rajaguru, K.; Sivaraman, G.; Muthusubramanian, S.; Bhuvanesh, N. Boranil Dye Based "Turn-on" Fluorescent Probes for Detection of Hydrogen Peroxide and Their Cell Imaging Application. *RSC Adv.* **2016**, *6* (89), 85838–85843. https://doi.org/10.1039/c6ra17863d.

(131) Srinivas, U. S.; Tan, B. W. Q.; Vellayappan, B. A.; Jeyasekharan, A. D. ROS and the DNA Damage Response in Cancer. *Redox Biol.* **2019**, *25*, 101084. https://doi.org/10.1016/j.redox.2018.101084.

(132) Zhang, J.; Duan, D.; Song, Z.-L.; Liu, T.; Hou, Y.; Fang, J. Small Molecules Regulating Reactive Oxygen Species Homeostasis for Cancer Therapy. *Med. Res. Rev.* **2021**, *41* (1), 342–394. https://doi.org/10.1002/med.21734.

(133) Valko, M.; Leibfritz, D.; Moncol, J.; Cronin, M. T. D.; Mazur, M.; Telser, J. Free Radicals and Antioxidants in Normal Physiological Functions and Human Disease. *Int. J. Biochem. Cell Biol.* **2007**, *39* (1), 44–84. https://doi.org/https://doi.org/10.1016/j.biocel.2006.07.001.

(134) Liu, F.; Jiang, X.; He, N.; Yu, R.; Xue, Z.; Liu, X. Electrochemical Investigation for Enhancing Cellular Antioxidant Defense System Based on a Superoxide Anion Sensor. *Sensors Actuators B Chem.* **2022**, *368* (967), 132190. https://doi.org/10.1016/j.snb.2022.132190.

(135) Huang, S.; Han, X.; Liu, Y.; Huang, P.; Deng, K. Y.; Wu, F. Y. A Reversible Fluorescent Probe Based on a Redox-Switchable Excited-State Intramolecular Proton-Transfer Active Metal-Organic Framework for Detection and Imaging of Highly Reactive Oxygen Species in Live Cells. *ACS Appl. Bio Mater.* **2022**, *5* (11), 5165–5173. https://doi.org/10.1021/acsabm.2c00541.

(136) Zhang, Y.; Guo, C. X.; Du, H.; Wang, X.; Liu, L.; Li, C. M. Solvent-Engineered Morphologies of Mn-MOF toward Ultrasensitive Sensing Cell Superoxide. *Electrochim. Acta* **2022**, *431*. https://doi.org/10.1016/j.electacta.2022.141147.

(137) Kim, H. S.; Kim, Y. J.; Seo, Y. R. An Overview of Carcinogenic Heavy Metal: Molecular Toxicity Mechanism and Prevention. *J. cancer Prev.* **2015**, *20* (4), 232–240. https://doi.org/10.15430/JCP.2015.20.4.232.

(138) Kim, K.-H.; Kabir, E.; Jahan, S. A. A Review on the Distribution of Hg in the Environment and Its Human Health Impacts. *J. Hazard. Mater.* **2016**, *306*, 376–

385. https://doi.org/10.1016/j.jhazmat.2015.11.031.

(139) Uttam, B.; Polepalli, S.; Sinha, S.; Majumder, A.; Rao, C. P. Selective Sensing and Removal of Mercury Ions by Encapsulating Dansyl Appended Calix[4]Conjugate in a Zeolitic Imidazolate Framework as an Organic-Inorganic Hybrid Nanomaterial. *ACS Appl. Nano Mater.* **2022**, *5* (8), 11371–11380. https://doi.org/10.1021/acsanm.2c02459.

(140) Diaz, L. A.; Lister, T. E.; Parkman, J. A.; Clark, G. G. Comprehensive Process for the Recovery of Value and Critical Materials from Electronic Waste. *J. Clean. Prod.* **2016**, *125*, 236–244. https://doi.org/10.1016/j.jclepro.2016.03.061.

(141) Awual, M. R. Innovative Composite Material for Efficient and Highly Selective Pb(II) Ion Capturing from Wastewater. *J. Mol. Liq.* **2019**, *284*, 502–510. https://doi.org/https://doi.org/10.1016/j.molliq.2019.03.157.

(142) Awual, M. R.; Kobayashi, T.; Shiwaku, H.; Miyazaki, Y.; Motokawa, R.; Suzuki, S.; Okamoto, Y.; Yaita, T. Evaluation of Lanthanide Sorption and Their Coordination Mechanism by EXAFS Measurement Using Novel Hybrid Adsorbent. *Chem. Eng. J.* **2013**, *225*, 558–566. https://doi.org/https://doi.org/10.1016/j.cej.2013.04.015.

(143) Alharbi, A.; Al-Ahmed, Z. A.; El-Metwaly, N. M.; Shahat, A.; El-Bindary, M. A. A Novel Strategy for Preparing Metal-Organic Framework as a Smart Material for Selective Detection and Efficient Extraction of Pd(II) and Au(III) Ions from E-Wastes. *J. Mol. Liq.* **2023**, *369*, 120862. https://doi.org/https://doi.org/10.1016/j.molliq.2022.120862.

(144) Nandhini, C.; Arul, P.; Huang, S.-T.; Tominaga, M.; Huang, C.-H. Electrochemical Sensing of Dual Biomolecules in Live Cells and Whole Blood Samples: A Flexible Gold Wire-Modified Copper-Organic Framework-Based Hybrid Composite. *Bioelectrochemistry* **2023**, *152*. https://doi.org/10.1016/j.bioelechem.2023.108434.

(145) Arul, P.; Huang, S.-T.; Mani, V.; Huang, C.-H. Graphene Quantum Dots-Based Nanocomposite for Electrocatalytic Application of L-Cysteine in Whole Blood and Live Cells. *Electrochim. Acta* **2022**, *428*. https://doi.org/10.1016/j.electacta.2022.140937.

(146) Yang, H.; Dong, J.; Li, Q.; Wen, L.; Qi, N.; Wang, X.; Xu, F.; Huo, D.; Hou, C. Au and Pt Nanoparticles Grown on Flexible Carbon Fiber Cloth Supports Decorated with Cerium Metal Organic Frameworks for the Real-Time Detection of H2O2in Live Cancer Tissue. *ACS Appl. Nano Mater.* **2022**, *5* (12), 18328–18336. https://doi.org/10.1021/acsanm.2c04176.

(147) Mu, S.; Deng, Y.; Xing, Z.; Rong, X.; He, C.; Cao, S.; Ma, T.; Cheng, C.; Wang, Y. Ir Cluster-Anchored MOFs as Peroxidase-Mimetic Nanoreactors for Diagnosing Hydrogen Peroxide-Related Biomarkers. *ACS Appl. Mater. Interfaces* **2022**, *14* (51), 56635–56643. https://doi.org/10.1021/acsami.2c18676.

(148) Shu, Y.; Ye, Q.; Tan, J.; Lv, H.; Liu, Z.; Mo, Q. Metalloporphyrin-Based Metal-Organic Framework Nanorods for Peroxidase-Like Catalysis. *ACS Appl. Nano Mater.* **2022**, *5* (12), 17909–17918. https://doi.org/10.1021/acsanm.2c03871.

(149) Liu, S.; Huo, Y.; Deng, S.; Li, G.; Li, S.; Huang, L.; Ren, S.; Gao, Z. A Facile Dual-Mode Aptasensor Based on AuNPs@MIL-101 Nanohybrids for Ultrasensitive Fluorescence and Surface-Enhanced Raman Spectroscopy Detection of Tetrodotoxin. *Biosens. Bioelectron.* **2022**, *201*. https://doi.org/10.1016/j.bios.2021.113891.

(150) Zhang, S.; Chen, K.; Zhu, L.; Xu, M.; Song, Y.; Zhang, Z.; Du, M. Direct Growth of Two-Dimensional Phthalocyanine-Based COF on Cu-MOF to Construct a Photoelectrochemical-Electrochemical Dual-Mode Biosensing Platform for High-Efficiency Determination of Cr(Iii). *Dalt. Trans.* **2021**, *50* (40), 14285–14295. https://doi.org/10.1039/d1dt02710g.

(151) Bhowal, S.; Ghosh, A. Highly Selective Fluorescent Turn-on-off Sensing of OH−, Al3+and Fe3+ions by Tuning ESIPT in Metal Organic Frameworks and Mitochondria Targeted Bio-Imaging. *RSC Adv.* **2021**, *11* (45), 27787–27800. https://doi.org/10.1039/d1ra03078g.

(152) Li, J.; Zhu, Y.; Xu, H.; Zheng, T.-F.; Liu, S.-J.; Wu, Y.; Chen, J.-L.; Chen, Y.-Q.; Wen, H.-R. A Benzothiadiazole-Based Eu3+ Metal–Organic Framework as the Turn-On Luminescent Sensor toward Al3+ and Ga3+ with Potential Bioimaging Application. *Inorg. Chem.* **2022**, *61* (8), 3607–3615. https://doi.org/10.1021/acs.inorgchem.1c03661.

(153) Zhang, Y.; Zhang, L. Designed Multifunctional Ratiometric Fluorescent Probe for Directly Detecting Fluoride Ion/ Dichromate and Indirectly Monitoring Urea. *J. Hazard. Mater.* **2021**, *418*, 126271. https://doi.org/https://doi.org/10.1016/j.jhazmat.2021.126271.

(154) Zhang, X.; Feng, L.; Ma, S.; Xia, T.; Jiao, F.; Kong, Z.; Duan, X. A Microporous Tb-Based MOF for Multifunctional Detection of the α-CHC, Cu2+ and Fe3+. *J. Solid State Chem.* **2022**, *312*, 123232. https://doi.org/https://doi.org/10.1016/j.jssc.2022.123232.

(155) Yu, F.; Du, T.; Wang, Y.; Li, C.; Qin, Z.; Jiang, H.; Wang, X. Ratiometric Fluorescence Sensing of UiO-66-NH2 toward Hypochlorite with Novel Dual Emission in Vitro and in Vivo. *Sensors Actuators B Chem.* **2022**, *353*, 131032. https://doi.org/https://doi.org/10.1016/j.snb.2021.131032.

(156) Kumar, A.; Purohit, B.; Mahato, K.; Chandra, P. Advance Engineered Nanomaterials in Point-of-Care Immunosensing for Biomedical Diagnostics. In *Immunosensors*; The Royal Society of Chemistry, 2019. https://doi.org/10.1039/9781788016162-00238.

(157) Kumar, A.; Roy, S.; Srivastava, A.; Naikwade, M. M.; Purohit, B.; Mahato, K.; Naidu, V. G. M.; Chandra, P. Chapter 10 - Nanotherapeutics: A Novel and

Powerful Approach in Modern Healthcare System. In *Nanotechnology in Modern Animal Biotechnology*; Maurya, P. K., Singh, S., Eds.; Elsevier, 2019; pp 149–161. https://doi.org/https://doi.org/10.1016/B978-0-12-818823-1.00010-7.

(158) John, H.; Thiermann, H. Poisoning by Organophosphorus Nerve Agents and Pesticides: An Overview of the Principle Strategies and Current Progress of Mass Spectrometry-Based Procedures for Verification. *Journal of Mass Spectrometry and Advances in the Clinical Lab*. 2021, pp 20–31. https://doi.org/10.1016/j.jmsacl.2021.01.002.

(159) Vale, A.; Marrs, T. C.; Rice, P. Chemical Terrorism and Nerve Agents. *Medicine*. 2012, pp 77–79. https://doi.org/10.1016/j.mpmed.2011.11.017.

(160) Niu, Z.; Liu, Y.; Li, X.; Yan, K.; Chen, H. Electrochemical Sensor for Ultrasensitive Detection of Paraquat Based on Metal-Organic Frameworks and Para-Sulfonatocalix[4]Arene-AuNPs Composite. *Chemosphere* **2022**, *307*. https://doi.org/10.1016/j.chemosphere.2022.135570.

(161) Niu, K.; Sun, P.; Chen, J.; Lu, X. Dense Conductive Metal-Organic Frameworks as Robust Electrocatalysts for Biosensing. *Anal. Chem.* **2022**, *94* (49), 17177–17185. https://doi.org/10.1021/acs.analchem.2c03766.

(162) Garabrant, D. H.; Philbert, M. A. Review of 2,4-Dichlorophenoxyacetic Acid (2,4-D) Epidemiology and Toxicology. *Critical Reviews in Toxicology*. 2002, pp 233–257. https://doi.org/10.1080/20024091064237.

(163) Ding, M.; Chen, W.; Xu, H.; Shen, Z.; Lin, T.; Hu, K.; Kong, Q.; Yang, G.; Xie, Z. Heterogeneous Fe2CoTi3O10-MXene Composite Catalysts: Synergistic Effect of the Ternary Transition Metals in the Degradation of 2,4-Dichlorophenoxyacetic Acid Based on Peroxymonosulfate Activation. *Chem. Eng. J.* **2019**, *378*. https://doi.org/10.1016/j.cej.2019.122177.

(164) Li, K.; Wu, J. Q.; Jiang, L. L.; Shen, L. Z.; Li, J. Y.; He, Z. H.; Wei, P.; Lv, Z.; He, M. F. Developmental Toxicity of 2,4-Dichlorophenoxyacetic Acid in Zebrafish Embryos. *Chemosphere* **2017**, *171*, 40–48. https://doi.org/10.1016/j.chemosphere.2016.12.032.

(165) Chen, H.; Zhang, Z.; Yang, Z.; Yang, Q.; Li, B.; Bai, Z. Heterogeneous Fenton-like Catalytic Degradation of 2,4-Dichlorophenoxyacetic Acid in Water with FeS. *Chem. Eng. J.* **2015**, *273*, 481–489. https://doi.org/https://doi.org/10.1016/j.cej.2015.03.079.

(166) Kermani, M.; Mohammadi, F.; Kakavandi, B.; Esrafili, A.; Rostamifasih, Z. Simultaneous Catalytic Degradation of 2,4-D and MCPA Herbicides Using Sulfate Radical-Based Heterogeneous Oxidation over Persulfate Activated by Natural Hematite (α-Fe2O3/PS). *J. Phys. Chem. Solids* **2018**, *117*, 49–59. https://doi.org/https://doi.org/10.1016/j.jpcs.2018.02.009.

(167) Yi, J.; Han, X.; Zhu, Q.; Wu, L.; Wang, Y.; Xue, J.; Lai, X.; Zhou, H. A Novel Metal-Organic Framework of Co-Hemin for Portable and Visual Colorimetric

Detection of 2,4-Dichlorophenoxyacetic Acid. *Anal. Methods* **2022**, *15* (1), 63–69. https://doi.org/10.1039/d2ay01694j.

(168) Lee, H.; Yuh, Y.; Kim, S. Serum Lactate Dehydrogenase (LDH) Level as a Prognostic Factor for the Patients with Advanced Gastric Cancer. *J. Clin. Oncol.* **2009**, *27* (15_suppl), e15621–e15621. https://doi.org/10.1200/jco.2009.27.15_suppl.e15621.

(169) Sohrabi, H.; Dezhakam, E.; Nozohouri, E.; Majidi, M. R.; Orooji, Y.; Yoon, Y.; Khataee, A. Advances in Layered Double Hydroxide Based Labels for Signal Amplification in Ultrasensitive Electrochemical and Optical Affinity Biosensors of Glucose. *Chemosphere* **2022**, *309*. https://doi.org/10.1016/j.chemosphere.2022.136633.

(170) Gao, W.; Emaminejad, S.; Nyein, H. Y. Y.; Challa, S.; Chen, K.; Peck, A.; Fahad, H. M.; Ota, H.; Shiraki, H.; Kiriya, D.; Lien, D. H.; Brooks, G. A.; Davis, R. W.; Javey, A. Fully Integrated Wearable Sensor Arrays for Multiplexed in Situ Perspiration Analysis. *Nature* **2016**, *529* (7587), 509–514. https://doi.org/10.1038/nature16521.

(171) Lipani, L.; Dupont, B. G. R.; Doungmene, F.; Marken, F.; Tyrrell, R. M.; Guy, R. H.; Ilie, A. Non-Invasive, Transdermal, Path-Selective and Specific Glucose Monitoring via a Graphene-Based Platform. *Nat. Nanotechnol.* **2018**, *13* (6), 504–511. https://doi.org/10.1038/s41565-018-0112-4.

(172) Ma, C.; Zhao, X.; Wang, P.; Jia, P.; Zhao, X.; Xiao, C.; Zheng, X. Metabolite Characterization of Penta- O -Galloyl-β- D -Glucose in Rat Biofluids by HPLC-QTOF-MS. *Chinese Herb. Med.* **2018**, *10* (1), 73–79. https://doi.org/10.1016/j.chmed.2018.01.002.

(173) Kristensen, K.; Wangel, A.-M.; Katsarou, A.; Shaat, N.; Simmons, D.; Fadl, H.; Berntorp, K. Diagnosis of Gestational Diabetes Mellitus with Point-of-Care Methods for Glucose versus Hospital Laboratory Method Using Isotope Dilution Gas Chromatography-Mass Spectrometry as Reference. *J. Diabetes Res.* **2020**, *2020* (2), 1–10. https://doi.org/10.1155/2020/7937403.

(174) Švecová, P.; Petr, J. Separation of Cetirizine Enantiomers by Capillary Electrophoresis with a Dual Selector System Based on Borate-Glucose Complexes and Sulfated-β-Cyclodextrin. *Talanta* **2019**, *198*, 154–158. https://doi.org/10.1016/j.talanta.2019.01.097.

(175) Wei, H.; Wang, E. Fe3O4 Magnetic Nanoparticles as Peroxidase Mimetics and Their Applications in H2O2 and Glucose Detection. *Anal. Chem.* **2008**, *80* (6), 2250–2254. https://doi.org/10.1021/ac702203f.

(176) Kadian, S.; Arya, D.; Kumar, S.; Sharma, S. N.; Chauhan, P. Synthesis and Application of PHT-TiO 2 Nanohybrid for Amperometric Glucose Detection in Human Saliva Sample. **2018**, 2793–2802. https://doi.org/10.1002/elan.201800207.

(177) Zhao, Z.; Li, Q.; Sun, Y.; Zhao, C.; Guo, Z.; Gong, W.; Hu, J.; Chen, Y. Highly Sensitive and Portable Electrochemical Detection System Based on AuNPs@CuO NWs/Cu2O/CF Hierarchical Nanostructures for Enzymeless Glucose Sensing. *Sensors Actuators, B Chem.* **2021**, *345*. https://doi.org/10.1016/j.snb.2021.130379.

(178) Sun, Y.; Li, P.; Zhu, Y.; Zhu, X.; Zhang, Y.; Liu, M.; Liu, Y. In Situ Growth of TiO2 Nanowires on Ti3C2 MXenes Nanosheets as Highly Sensitive Luminol Electrochemiluminescent Nanoplatform for Glucose Detection in Fruits, Sweat and Serum Samples. *Biosens. Bioelectron.* **2021**, *194*. https://doi.org/10.1016/j.bios.2021.113600.

(179) Tonyushkina, K.; Nichols, J. H. Glucose Meters: A Review of Technical Challenges to Obtaining Accurate Results. *J. Diabetes Sci. Technol.* **2009**, *3* (4), 971–980. https://doi.org/10.1177/193229680900300446.

(180) WU, Y.; ZHOU, J.-M.; JIANG, Y.-S.; LI, W.; HE, M.-J.; XIAO, Y.; CHEN, J.-Y. Silver Nanoparticles@metal-Organic Framework as Peroxidase Mimics for Colorimetric Determination of Hydrogen Peroxide and Blood Glucose. *Chinese J. Anal. Chem.* **2022**, *50* (12). https://doi.org/10.1016/j.cjac.2022.100187.

(181) Zhong, N.; Gao, R.; Shen, Y.; Kou, X.; Wu, J.; Huang, S.; Chen, G.; Ouyang, G. Enzymes-Encapsulated Defective Metal-Organic Framework Hydrogel Coupling with a Smartphone for a Portable Glucose Biosensor. *Anal. Chem.* **2022**, *94* (41), 14385–14393. https://doi.org/10.1021/acs.analchem.2c03138.

(182) Zhou, R.; Zhuang, X.; Wu, Q.; Jin, M.; Zheng, C.; Jiang, Y.; Lou, Y.; Zheng, L. Cu-MOF@Pt 3D Nanocomposites Prepared by One-Step Wrapping Method with Peroxidase-like Activity for Colorimetric Detection of Glucose. *Colloids Surfaces B Biointerfaces* **2022**, *216*, 112601. https://doi.org/https://doi.org/10.1016/j.colsurfb.2022.112601.

(183) Kaur, B.; Kumar, S.; Kaushik, B. K. Recent Advancements in Optical Biosensors for Cancer Detection. *Biosens. Bioelectron.* **2022**, *197*, 113805. https://doi.org/10.1016/j.bios.2021.113805.

(184) Nandhini, C.; Arul, P.; Huang, S.-T.; Tominaga, M.; Huang, C.-H. Electrochemical Sensing of Dual Biomolecules in Live Cells and Whole Blood Samples: A Flexible Gold Wire-Modified Copper-Organic Framework-Based Hybrid Composite. *Bioelectrochemistry* **2023**, *152*. https://doi.org/10.1016/j.bioelechem.2023.108434.

(185) Zha, X.; Yang, W.; Shi, L.; Zeng, Q.; Xu, J.; Yang, Y. 2D Bimetallic Organic Framework Nanosheets for High-Performance Wearable Power Source and Real-Time Monitoring of Glucose. *Dalt. Trans.* **2023**, *52* (9), 2631–2640. https://doi.org/10.1039/d2dt03311a.

(186) Wang, Q.; Jiao, C.; Wang, X.; Wang, Y.; Sun, K.; Li, L.; Fan, Y.; Hu, L. A Hydrogel-Based Biosensor for Stable Detection of Glucose. *Biosens. Bioelectron.*

2023, *221*. https://doi.org/10.1016/j.bios.2022.114908.

(187) Asaduzzaman, M.; Zahed, M. A.; Sharifuzzaman, M.; Reza, M. S.; Hui, X.; Sharma, S.; Shin, Y. D.; Park, J. Y. A Hybridized Nano-Porous Carbon Reinforced 3D Graphene-Based Epidermal Patch for Precise Sweat Glucose and Lactate Analysis. *Biosens. Bioelectron.* **2023**, *219*. https://doi.org/10.1016/j.bios.2022.114846.

(188) Gumilar, G.; Chowdhury, S.; Shukri, G.; Patah, A.; Nugraha, N.; Henzie, J.; Anshori, I.; Kaneti, Y. V; Yuliarto, B. The Revelation of Glucose Adsorption Mechanisms on Hierarchical Metal-Organic Frameworks Using a Surface Plasmon Resonance Sensor. *J. Mater. Chem. B* **2023**. https://doi.org/10.1039/d3tb00138e.

(189) Arul, P.; Nandhini, C.; Huang, S.-T.; Gowthaman, N. S. K.; Huang, C.-H. Tailoring of Peroxidase Mimetics Bifunctional Nanocomposite: Dual Mode Electro-Spectroscopic Screening of Cholesterol and Hydrogen Peroxide in Real Food Samples and Live Cells. *Food Chem.* **2023**, *414*. https://doi.org/10.1016/j.foodchem.2023.135747.

(190) Wang, N.; Zhang, L.; Li, Z.; Zhou, C.; Lv, Y.; Su, X. A Sensing Platform for On-Site Detection of Glutathione S-Transferase Using Oxidized Pi@Ce-Doped Zr-Based Metal-Organic Frameworks(MOFs). *Talanta* **2023**, *259*. https://doi.org/10.1016/j.talanta.2023.124537.

(191) Ke, X.; Zhao, Z.; Huang, J.; Liu, C.; Huang, G.; Tan, J.; Zhu, H.; Xiao, Z.; Liu, X.; Mei, Y.; Chu, J. Growth Control of Metal-Organic Framework Films on Marine Biological Carbon and Their Potential-Dependent Dopamine Sensing. *ACS Appl. Mater. Interfaces* **2023**, *15* (9), 12005–12016. https://doi.org/10.1021/acsami.2c20517.

(192) Fu, H.; Xu, Z.; Liu, T.; Lei, J. In Situ Coordination Interactions between Metal-Organic Framework Nanoemitters and Coreactants for Enhanced Electrochemiluminescence in Biosensing. *Biosens. Bioelectron.* **2023**, *222*. https://doi.org/10.1016/j.bios.2022.114920.

(193) Kıyıkçı, H. F.; Avcı, O.; Tepeli Büyüksünetçi, Y.; Timur, S.; Anık, Ü. Oxidase Mimicking Co/2Fe MOF Included Biosensor for Sialic Acid Detection. *Talanta* **2023**, *254*. https://doi.org/10.1016/j.talanta.2022.124166.

(194) Cheng, Y.; Kong, R.-M.; Hu, W.; Tian, X.; Zhang, L.; Xia, L.; Qu, F. Colorimetric-Assisted Photoelectrochemical Sensing for Dual-Model Detection of Sialic Acid via Oxidation-Power Mediator Integration. *Chinese Chem. Lett.* **2023**, *34* (3). https://doi.org/10.1016/j.cclet.2022.05.016.

(195) Peng, L.; Wang, L.; Wu, K.; Deng, A.; Li, J. A Resonant Energy Transfer Electrochemiluminescence Immunosensor Based on Low Trigger Potential of Zn-Metal Organic Framework and CoOOH Nanosheets for 5-Fluorouracil Detection. *Biosens. Bioelectron.* **2023**, *231*. https://doi.org/10.1016/j.bios.2023.115261.

(196) Wang, Y.-Y.; Zhang, H.-F.; Wang, D.-H.; Sheng, N.; Zhang, G.-G.; Yin, L.; Sha, J.-Q. Development of a Uricase-Free Colorimetric Biosensor for Uric Acid Based on PPy-Coated Polyoxometalate-Encapsulated Fourfold Helical Metal-Organic Frameworks. *ACS Biomater. Sci. Eng.* **2020**, *6* (3), 1438–1448. https://doi.org/10.1021/acsbiomaterials.9b01922.

(197) Ma, R.; Jiang, J.; Ya, Y.; Lin, Y.; Zhou, Y.; Wu, Y.; Tan, X.; Huang, K.; Du, F.; Xu, J. A Carbon Dot-Based Nanoscale Covalent Organic Framework as a New Emitter Combined with a CRISPR/Cas12a-Mediated Electrochemiluminescence Biosensor for Ultrasensitive Detection of Bisphenol A. *Analyst* **2023**, *148* (6), 1362–1370. https://doi.org/10.1039/d3an00024a.

(198) Ma, J.; Yuan, J.; Xu, Y.; Jiang, Y.; Bai, W.; Zheng, J. Ultrasensitive Electrochemical Determination of Bisphenol A in Food Samples Based on a Strategy for Activity Enhancement of Enzyme: Layer-by-Layer Self-Assembly of Tyrosinase between Two-Dimensional Porphyrin Metal–Organic Framework Nanofilms. *Chem. Eng. J.* **2022**, *446*. https://doi.org/10.1016/j.cej.2022.137001.

(199) Zhao, L.; Song, X.; Li, Y.; Jia, H.; Zhang, N.; Wei, Q.; Wu, D.; Ju, H. Europium-Based Metal-Organic Framework with Acid-Base Buffer Structure as Electrochemiluminescence Luminophore for Hyperstatic Trenbolone Trace Monitoring under Wide PH Range. *Biosens. Bioelectron.* **2023**, *221*. https://doi.org/10.1016/j.bios.2022.114925.

(200) Wang, Y.; Tu, R.; Hou, C.; Wang, Z. Zn–Porphyrin Metal–Organic Framework–Based Photoelectrochemical Enzymatic Biosensor for Hypoxanthine. *J. Solid State Electrochem.* **2022**, *26* (2), 565–572. https://doi.org/10.1007/s10008-021-05111-9.

(201) Guan, Y.; Si, P.-B.; Yang, T.; Wu, Y.; Yang, Y.-H.; Hu, R. A Novel Method for Detection of Ochratoxin A in Foods—Co-MOFs Based Dual Signal Ratiometric Electrochemical Aptamer Sensor Coupled with DNA Walker. *Food Chem.* **2023**, *403*. https://doi.org/10.1016/j.foodchem.2022.134316.

(202) Wei, Q.; Huang, C.; Lu, P.; Zhang, X.; Chen, Y. Combining Magnetic MOFs as a Highly Adsorbent with Homogeneous Chemiluminescent Immunosensor for Rapid and Ultrasensitive Determination of Ochratoxin A. *J. Hazard. Mater.* **2023**, *441*. https://doi.org/10.1016/j.jhazmat.2022.129960.

(203) Duan, X.; Zhang, N.; Li, Z.; Zhang, L.; Sun, F.; Zhou, Z.; Liu, H.; Guo, Y.; Sun, X.; Jiang, J.; Jiang, J.; Zhang, D. Ultrasensitive Electrochemiluminescent Aptasensor for Trace Detection of Kanamycin Based-on Novel Semi-Sandwich Gadolinium Phthalocyanine Complex and Dysprosium Metal-Organic Framework. *J. Colloid Interface Sci.* **2023**, *632*, 171–178. https://doi.org/10.1016/j.jcis.2022.11.016.

(204) Du, H.; Yin, T.; Wang, J.; Jie, G. Multifunctional Photoelectrochemical Biosensor Based on ZnIn2S4/ZnS QDs@Au-Ag-Reversed Photocurrent of Cu-Metal-Organic Framework Coupled with CRISPR/Cas-12a-Shearing for Assay of Dual

Targets. *Anal. Chem.* **2023**. https://doi.org/10.1021/acs.analchem.3c00846.

(205) Gao, X.; Sun, G.; Wang, X.; Lin, X.; Wang, S.; Liu, Y. RhB/UiO-66-N3 MOF-Based Ratiometric Fluorescent Detection and Intracellular Imaging of Hydrogen Sulfide. *Sensors Actuators B Chem.* **2021**, *331*, 129448. https://doi.org/https://doi.org/10.1016/j.snb.2021.129448.

(206) Purohit, B.; Vernekar, P. R.; Shetti, N. P.; Chandra, P. Biosensor Nanoengineering: Design, Operation, and Implementation for Biomolecular Analysis. *Sensors Int.* **2020**, *1*, 100040. https://doi.org/https://doi.org/10.1016/j.sintl.2020.100040.

(207) Levine, A. J.; Momand, J.; Finlay, C. A. The P53 Tumour Suppressor Gene. *Nature* **1991**, *351* (6326), 453–456. https://doi.org/10.1038/351453a0.

(208) Assah, E.; Goh, W.; Zheng, X. T.; Lim, T. X.; Li, J.; Lane, D.; Ghadessy, F.; Tan, Y. N. Rapid Colorimetric Detection of P53 Protein Function Using DNA-Gold Nanoconjugates with Applications for Drug Discovery and Cancer Diagnostics. *Colloids Surfaces B Biointerfaces* **2018**, *169*, 214–221. https://doi.org/https://doi.org/10.1016/j.colsurfb.2018.05.007.

(209) Wang, Z.; Xia, J.; Song, D.; Zhang, F.; Yang, M.; Gui, R.; Xia, L.; Bi, S.; Xia, Y. Lable-Free Quadruple Signal Amplification Strategy for Sensitive Electrochemical P53 Gene Biosensing. *Biosens. Bioelectron.* **2016**, *77*, 157–163. https://doi.org/https://doi.org/10.1016/j.bios.2015.09.011.

(210) Cheng, H.; Li, W.; Duan, S.; Peng, J.; Liu, J.; Ma, W.; Wang, H.; He, X.; Wang, K. Mesoporous Silica Containers and Programmed Catalytic Hairpin Assembly/Hybridization Chain Reaction Based Electrochemical Sensing Platform for MicroRNA Ultrasensitive Detection with Low Background. *Anal. Chem.* **2019**, *91* (16), 10672–10678. https://doi.org/10.1021/acs.analchem.9b01947.

(211) Lv, M.; Cao, X.; Tian, M.; Jiang, R.; Gao, C.; Xia, J.; Wang, Z. A Novel Electrochemical Biosensor Based on MIL-101-NH<inf>2</Inf> (Cr) Combining Target-Responsive Releasing and Self-Catalysis Strategy for P53 Detection. *Biosens. Bioelectron.* **2022**, *214*. https://doi.org/10.1016/j.bios.2022.114518.

(212) Wilcox, G. Insulin and Insulin Resistance. *Clin. Biochem. Rev.* **2005**, *26* (2), 19–39.

(213) Taib, M.; Tan, L. L.; Abd Karim, N. H.; Ta, G. C.; Heng, L. Y.; Khalid, B. Reflectance Aptasensor Based on Metal Salphen Label for Rapid and Facile Determination of Insulin. *Talanta* **2020**, *207*, 120321. https://doi.org/https://doi.org/10.1016/j.talanta.2019.120321.

(214) Cha, T.-G.; Baker, B. A.; Sauffer, M. D.; Salgado, J.; Jaroch, D.; Rickus, J. L.; Porterfield, D. M.; Choi, J. H. Optical Nanosensor Architecture for Cell-Signaling Molecules Using DNA Aptamer-Coated Carbon Nanotubes. *ACS Nano* **2011**, *5* (5), 4236–4244. https://doi.org/10.1021/nn201323h.

(215) Moein, M. M.; Javanbakht, M.; Akbari-adergani, B. Molecularly Imprinted Polymer Cartridges Coupled On-Line with High Performance Liquid Chromatography for Simple and Rapid Analysis of Human Insulin in Plasma and Pharmaceutical Formulations. *Talanta* **2014**, *121*, 30–36. https://doi.org/https://doi.org/10.1016/j.talanta.2013.12.011.

(216) Sakthivel, R.; Lin, L.-Y.; Duann, Y.-F.; Chen, H.-H.; Su, C.; Liu, X.; He, J.-H.; Chung, R.-J. MOF-Derived Cu-BTC Nanowire-Embedded 2D Leaf-like Structured ZIF Composite-Based Aptamer Sensors for Real-Time In Vivo Insulin Monitoring. *ACS Appl. Mater. Interfaces* **2022**, *14* (25), 28639–28650. https://doi.org/10.1021/acsami.2c06785.

(217) Bartel, D. P. MicroRNAs: Genomics, Biogenesis, Mechanism, and Function. *Cell* **2004**, *116* (2), 281–297. https://doi.org/https://doi.org/10.1016/S0092-8674(04)00045-5.

(218) Ambros, V. The Functions of Animal MicroRNAs. *Nature* **2004**, *431* (7006), 350–355. https://doi.org/10.1038/nature02871.

(219) Moltzahn, F.; Olshen, A. B.; Baehner, L.; Peek, A.; Fong, L.; Stöppler, H.; Simko, J.; Hilton, J. F.; Carroll, P.; Blelloch, R. Microfluidic-Based Multiplex QRT-PCR Identifies Diagnostic and Prognostic MicroRNA Signatures in the Sera of Prostate Cancer Patients. *Cancer Res.* **2011**, *71* (2), 550–560. https://doi.org/10.1158/0008-5472.CAN-10-1229.

(220) Iorio, M. V; Ferracin, M.; Liu, C.-G.; Veronese, A.; Spizzo, R.; Sabbioni, S.; Magri, E.; Pedriali, M.; Fabbri, M.; Campiglio, M.; Ménard, S.; Palazzo, J. P.; Rosenberg, A.; Musiani, P.; Volinia, S.; Nenci, I.; Calin, G. A.; Querzoli, P.; Negrini, M.; Croce, C. M. MicroRNA Gene Expression Deregulation in Human Breast Cancer. *Cancer Res.* **2005**, *65* (16), 7065–7070. https://doi.org/10.1158/0008-5472.CAN-05-1783.

(221) Ahmadi Najafabadi, M.; Yousefi, F.; Rasaee, M. J.; Soleimani, M.; Kazemzad, M. Metal-Organic Frameworks-Based Biosensor for MicroRNA Detection in Prostate Cancer Cell Lines. *RSC Adv.* **2022**, *12* (54), 35170–35180. https://doi.org/10.1039/d2ra04959g.

(222) Zha, R.; Wu, R.; Zong, Y.; Wang, Z.; Wu, T.; Zhong, Y.; Liang, H.; Chen, L.; Li, C.; Wang, Y. A High Performance Dual-Mode Biosensor Based on Nd-MOF Nanosheets Functionalized with Ionic Liquid and Gold Nanoparticles for Sensing of CtDNA. *Talanta* **2023**, *258*. https://doi.org/10.1016/j.talanta.2023.124377.

(223) Zhang, Q. F. Ulinastatin Inhibits Renal Tubular Epithelial Apoptosis and Interstitial Fibrosis in Rats with Unilateral Ureteral Obstruction. *Mol. Med. Rep.* **2017**, *16* (6), 8916–8922. https://doi.org/10.3892/mmr.2017.7692.

(224) Valkanova, V.; Ebmeier, K. P.; Allan, C. L. CRP, IL-6 and Depression: A Systematic Review and Meta-Analysis of Longitudinal Studies. *J. Affect. Disord.* **2013**, *150* (3), 736–744. https://doi.org/https://doi.org/10.1016/j.jad.2013.06.004.

(225) Ria, R.; Reale, A.; Vacca, A.; Internal, S. World Journal of Methodology © 2014. **2014**, *4* (2), 73–91.

(226) Mahato, K.; Kumar, A.; Maurya, P. K.; Chandra, P. Shifting Paradigm of Cancer Diagnoses in Clinically Relevant Samples Based on Miniaturized Electrochemical Nanobiosensors and Microfluidic Devices. *Biosens. Bioelectron.* **2018**, *100*, 411–428. https://doi.org/https://doi.org/10.1016/j.bios.2017.09.003.

(227) Agrawal, A. CRP after 2004. *Mol. Immunol.* **2005**, *42* (8), 927–930. https://doi.org/https://doi.org/10.1016/j.molimm.2004.09.028.

(228) Bansal, T.; Pandey, A.; D, D.; Asthana, A. K. C-Reactive Protein (CRP) and Its Association with Periodontal Disease: A Brief Review. *J. Clin. Diagn. Res.* **2014**, *8* (7), ZE21-4. https://doi.org/10.7860/JCDR/2014/8355.4646.

(229) Yang, L.; Liu, S.; Liu, J.; Zhang, Z.; Wan, X.; Huang, B.; Chen, Y.; Zhang, Y. COVID-19: Immunopathogenesis and Immunotherapeutics. *Signal Transduct. Target. Ther.* **2020**, *5* (1), 128. https://doi.org/10.1038/s41392-020-00243-2.

(230) Ali, G. K.; Omer, K. M. Ultrasensitive Aptamer-Functionalized Cu-MOF Fluorescent Nanozyme as an Optical Biosensor for Detection of C-Reactive Protein. *Anal. Biochem.* **2022**, *658*. https://doi.org/10.1016/j.ab.2022.114928.

(231) Lüftner, D.; Lüke, C.; Possinger, K. Serum HER-2/Neu in the Management of Breast Cancer Patients. *Clin. Biochem.* **2003**, *36* (4), 233–240. https://doi.org/https://doi.org/10.1016/S0009-9120(03)00026-2.

(232) Zhang, M.; Gao, G.; Ding, Y.; Deng, C.; Xiang, J.; Wu, H. A Fluorescent Aptasensor for the Femtomolar Detection of Epidermal Growth Factor Receptor-2 Based on the Proximity of G-Rich Sequences to Ag Nanoclusters. *Talanta* **2019**, *199*, 238–243. https://doi.org/https://doi.org/10.1016/j.talanta.2019.02.014.

(233) Shen, C.; Zeng, K.; Luo, J.; Li, X.; Yang, M.; Rasooly, A. Self-Assembled DNA Generated Electric Current Biosensor for HER2 Analysis. *Anal. Chem.* **2017**, *89* (19), 10264–10269. https://doi.org/10.1021/acs.analchem.7b01747.

(234) Xie, J.; Mu, Z.; Qing, M.; Zhou, J.; Sun, S.; Bai, L. A Novel Binary Luminophore Based High-Efficient Electrochemiluminescence Biosensor for Ultrasensitive Detection of Human Epidermal Growth Factor Receptor-2. *Chem. Eng. J.* **2022**, *450*. https://doi.org/10.1016/j.cej.2022.138362.

(235) Zhang, R.; Zheng, D.; Chen, J.; Zhang, C.; Wang, C. Design of NiS@Ni3S2/CdS Heterostructure with Intimate Contact Interface for Sensitive Photoelectrochemical Detection of Lincomycin. *Food Chem.* **2023**, *418*. https://doi.org/10.1016/j.foodchem.2023.136028.

(236) You, S.; Chen, L.; Li, D.; Yang, W.; Chen, L. Construction of a Novel “Self-Regenerative” Electrochemical Biosensor Based on Metal–Organic Frameworks and Its Application to the Detection of Mycoplasma Ovine Pneumonia. *Bioelectrochemistry* **2023**, *152*. https://doi.org/10.1016/j.bioelechem.2023.108409.

(237) Zhao, C.; Ma, C.; Zhang, F.; Li, W.; Hong, C.; Qi, Y. Two–Dimensional Metal–Organic Framework Nanosheets: An Efficient Two–Electron Oxygen Reduction Reaction Electrocatalyst for Boosting Cathodic Luminol Electrochemiluminescence. *Chem. Eng. J.* **2023**, *466*. https://doi.org/10.1016/j.cej.2023.143156.

(238) Dai, W.; Wang, X.; Chen, G.; Wang, X.; Hu, C.; Zhen, S.; Huang, C.; Li, Y. Facile Synthesis of 2D Europium-Metal Organic Frameworks Nanosheets for Highly Efficient Electrochemiluminescence in DNA Detection. *Chem. Eng. J.* **2023**, *465*. https://doi.org/10.1016/j.cej.2023.143037.

(239) Tong, Y.; Guan, B.; Sun, Z.; Dong, X.; Chen, Y.; Li, Y.; Jiang, Y.; Li, J. Ratiometric Fluorescent Detection of Exosomal PiRNA-823 Based on Au NCs/UiO-66-NH2 and Target-Triggered Rolling Circle Amplification. *Talanta* **2023**, *257*. https://doi.org/10.1016/j.talanta.2023.124307.

(240) Zhang, J.-L.; Gao, S.; Yang, Y.; Liang, W.-B.; Lu, M.-L.; Zhang, X.-Y.; Xiao, H.-X.; Li, Y.; Yuan, R.; Xiao, D.-R. Ruthenium(II) Complex-Grafted Conductive Metal-Organic Frameworks with Conductivity- and Confinement-Enhanced Electrochemiluminescence for Ultrasensitive Biosensing Application. *Biosens. Bioelectron.* **2023**, *227*. https://doi.org/10.1016/j.bios.2023.115157.

(241) Hu, L.; Shi, T.; Chen, J.; Cui, Q.; Yu, H.; Wu, D.; Ma, H.; Wei, Q.; Ju, H. Dual-Quenching Electrochemiluminescence Resonance Energy Transfer System from CoPd Nanoparticles Enhanced Porous g-C<inf>3</Inf>N<inf>4</Inf> to FeMOFs-SCuO for Neuron-Specific Enolase Immunosensing. *Biosens. Bioelectron.* **2023**, *226*. https://doi.org/10.1016/j.bios.2023.115132.

(242) Li, C.; Liu, C.; Liu, R.; Wang, Y.; Li, A.; Tian, S.; Cheng, W.; Ding, S.; Li, W.; Zhao, M.; Zhao, M.; Xia, Q. A Novel CRISPR/Cas14a-Based Electrochemical Biosensor for Ultrasensitive Detection of Burkholderia Pseudomallei with PtPd@PCN-224 Nanoenzymes for Signal Amplification. *Biosens. Bioelectron.* **2023**, *225*. https://doi.org/10.1016/j.bios.2023.115098.

(243) Wang, Y.; Shu, J.; Lyu, A.; Wang, M.; Hu, C.; Cui, H. Zn2+-Modified Nonmetal Porphyrin-Based Metal-Organic Frameworks with Improved Electrochemiluminescence for Nanoscale Exosome Detection. *ACS Appl. Nano Mater.* **2023**, *6* (6), 4214–4223. https://doi.org/10.1021/acsanm.2c05273.

(244) Mehmandoust, M.; Erk, E. E.; Soylak, M.; Erk, N.; Karimi, F. Metal-Organic Framework Based Electrochemical Immunosensor for Label-Free Detection of Glial Fibrillary Acidic Protein as a Biomarker. *Ind. Eng. Chem. Res.* **2023**, *62* (11), 4532–4539. https://doi.org/10.1021/acs.iecr.2c01445.

(245) Guan, Y.; Wang, F. P.; Chen, Z. X.; Yang, Y. H.; Yang, T.; Hu, R. Ratiometrically Homogeneous Electrochemical Biosensor Based on the Signal Amplified Strategy of Dual DNA Nanomachines for MicroRNA Analysis. *Talanta* **2023**, *254*. https://doi.org/10.1016/j.talanta.2022.124191.

(246) Liu, W.; Zhang, D.; Zhang, F.; Hao, Z.; Li, Y.; Shao, M.; Zhang, R.; Li, X.; Zhang, L. Self-Enhanced Peroxidase-like Activity in a Wide PH Range Enabled by Heterostructured Au/MOF Nanozymes for Multiple Ascorbic Acid-Related Bioenzyme Analyses. *Analyst* **2023**, *148* (7), 1579–1586. https://doi.org/10.1039/d3an00017f.

(247) Wang, F.; Liu, M.; Niu, X.; Xia, L.; Qu, F. Dextran-Assisted Ultrasonic Exfoliation of Two-Dimensional Metal-Organic Frameworks to Evaluate Acetylcholinesterase Activity and Inhibitor Screening. *Anal. Chim. Acta* **2023**, *1243*. https://doi.org/10.1016/j.aca.2023.340815.

(248) Tang, J.; Qin, J.; Li, J.; Liu, L.; Zeng, H. Cu^{2+}@NMOFs-to-Bimetallic CuFe PBA Transformation: An Instant Catalyst with Oxidase-Mimicking Activity for Highly Sensitive Impedimetric Biosensor. *Biosens. Bioelectron.* **2023**, *222*. https://doi.org/10.1016/j.bios.2022.114961.

(249) Yan, Y.; Guo, L.; Geng, H.; Bi, S. Hierarchical Porous Metal-Organic Framework as Biocatalytic Microreactor for Enzymatic Biofuel Cell-Based Self-Powered Biosensing of MicroRNA Integrated with Cascade Signal Amplification. *Small* **2023**. https://doi.org/10.1002/smll.202301654.

(250) Yang, J.; Qin, D.; Wang, N.; Wu, Y.; Fang, K.; Deng, B. Aggregation-Induced Electrochemiluminescence Based on a Zinc-Based Metal-Organic Framework and a Double Quencher Au@UiO-66-NH2 for the Sensitive Detection of Amyloid β 42 via Resonance Energy Transfer. *Anal. Chem.* **2023**. https://doi.org/10.1021/acs.analchem.3c00729.

(251) Chen, G.; Wang, X.; Dai, W.; Liang, L.; Luo, Z.; Chen, C.; Zhen, S.; Huang, C.; Li, Y. High-Efficiency Aluminum-Metal Organic Framework/HEPES Electrochemiluminescence System for Ultrasensitive Detection of HBV DNA. *Anal. Chem.* **2023**. https://doi.org/10.1021/acs.analchem.3c00687.

(252) Fan, Y.; Wu, W.; Xie, N.; Huang, Y.; Wu, H.; Zhang, J.; Guo, X.; Ding, S.; Guo, B. Biocompatible Engineered Erythrocytes as Plasmonic Sensor Initiators for High-Sensitive Screening of Non-Small Cell Lung Cancer-Derived Exosomal MiRNA in an Integrated System. *Biosens. Bioelectron.* **2023**, *219*. https://doi.org/10.1016/j.bios.2022.114802.

(253) Rabiee, N.; Rabiee, M.; Sojdeh, S.; Fatahi, Y.; Dinarvand, R.; Safarkhani, M.; Ahmadi, S.; Daneshgar, H.; Radmanesh, F.; Maghsoudi, S.; Varma, R. S.; Mostafavi, E. Porphyrin Molecules Decorated on Metal–Organic Frameworks for Multi-Functional Biomedical Applications. *Biomolecules* **2021**, *11* (11). https://doi.org/10.3390/biom11111714.

(254) Zhong, Y.; Zha, R.; Li, W.; Lu, C.; Zong, Y.; Sun, D.; Li, C.; Wang, Y. Signal-On Near-Infrared Photoelectrochemical Aptasensors for Sensing VEGF165 Based on Ionic Liquid-Functionalized Nd-MOF Nanorods and In-Site Formation of Gold Nanoparticles. *Anal. Chem.* **2022**, *94* (51), 17835–17842. https://doi.org/10.1021/acs.analchem.2c03583.

(255) Liu, Z.; Wang, T.; He, L.; Nan, X.; Sun, X.; Bai, P. A Double Emission Turn-on Eu-MOF-Based Luminescent Sensor towards an Anthrax Biomarker. *Microchem. J.* **2022**, *180*, 107618. https://doi.org/https://doi.org/10.1016/j.microc.2022.107618.

(256) Wang, Y.; Chen, R.; Shen, B.; Li, C.; Chen, J.; Wang, Y.; Tian, S.; Li, X.; Luo, N.; Liu, R.; Zhu, C.; Xia, Q. Electrochemiluminescent (ECL) Biosensor for Burkholderia Pseudomallei Based on Cobalt-Doped MOF Decorated with Gold Nanoparticles and N-(4-Aminobutyl)-N-(Ethylisoluminol). *Microchim. Acta* **2022**, *189* (9). https://doi.org/10.1007/s00604-022-05402-6.

(257) Zhang, H.; Ma, X.; Liu, Y.; Duan, N.; Wu, S.; Wang, Z.; Xu, B. Gold Nanoparticles Enhanced SERS Aptasensor for the Simultaneous Detection of Salmonella Typhimurium and Staphylococcus Aureus. *Biosens. Bioelectron.* **2015**, *74*, 872–877. https://doi.org/https://doi.org/10.1016/j.bios.2015.07.033.

(258) Chen, Y.; Chen, Y.; Yi, H.-C.; Gu, H.-W.; Yin, X.-L.; Xiang, D.-L.; Zou, P. An Electrochemical and Colorimetric Dual-Mode Aptasensor for Staphylococcus Aureus Based on a Multifunctional MOF and Magnetic Separation Technique. *Microchem. J.* **2023**, *190*, 108681. https://doi.org/https://doi.org/10.1016/j.microc.2023.108681.

(259) Zhu, Y.; Chandra, P.; Shim, Y. B. Ultrasensitive and Selective Electrochemical Diagnosis of Breast Cancer Based on a Hydrazine-Au Nanoparticle-Aptamer Bioconjugate. *Anal. Chem.* **2013**, *85* (2), 1058–1064. https://doi.org/10.1021/ac302923k.

(260) Chandra, P. HER2 Protein Biomarker Based Sensor Systems for Breast Cancer Diagnosis. *J. Mol. Biomark. Diagn.* **2013**, *05* (01). https://doi.org/10.4172/2155-9929.1000e119.

(261) Chandra, P.; Noh, H. B.; Shim, Y. B. Cancer Cell Detection Based on the Interaction between an Anticancer Drug and Cell Membrane Components. *Chem. Commun.* **2013**, *49* (19), 1900–1902. https://doi.org/10.1039/c2cc38235k.

(262) Dong, W.; Pan, Q.; Liu, Z.; Sun, H. ScienceDirect Electrodeposition of Defect-Rich High Entropy ZIF and Its Application in Water Oxidation. *Int. J. Hydrogen Energy* **2023**, No. xxxx. https://doi.org/10.1016/j.ijhydene.2023.05.333.

(263) Wang, L.; Xie, H.; Zhou, X.; Lin, Y.; Qin, Y.; Yang, J.; Zhao, J.; Li, G. An Electrochemical Biosensor to Identify the Phenotype of Aggressive Breast Cancer Cells. *Chem. Commun.* **2023**, *59* (26), 3890–3893. https://doi.org/10.1039/d3cc00611e.

(264) Ilkhani, H.; Sarparast, M.; Noori, A.; Zahra Bathaie, S.; Mousavi, M. F. Electrochemical Aptamer/Antibody Based Sandwich Immunosensor for the Detection of EGFR, a Cancer Biomarker, Using Gold Nanoparticles as a Signaling Probe. *Biosens. Bioelectron.* **2015**, *74*, 491–497. https://doi.org/https://doi.org/10.1016/j.bios.2015.06.063.

(265) Vivek, R.; Thangam, R.; NipunBabu, V.; Rejeeth, C.; Sivasubramanian, S.; Gunasekaran, P.; Muthuchelian, K.; Kannan, S. Multifunctional HER2-Antibody Conjugated Polymeric Nanocarrier-Based Drug Delivery System for Multi-Drug-Resistant Breast Cancer Therapy. *ACS Appl. Mater. Interfaces* **2014**, *6* (9), 6469–6480. https://doi.org/10.1021/am406012g.

(266) Gu, C.; Guo, C.; Li, Z.; Wang, M.; Zhou, N.; He, L.; Zhang, Z.; Du, M. Bimetallic ZrHf-Based Metal-Organic Framework Embedded with Carbon Dots: Ultra-Sensitive Platform for Early Diagnosis of HER2 and HER2-Overexpressed Living Cancer Cells. *Biosens. Bioelectron.* **2019**, *134*, 8–15. https://doi.org/https://doi.org/10.1016/j.bios.2019.03.043.

(267) Liu, X.; Hu, M.; Wang, M.; Song, Y.; Zhou, N.; He, L.; Zhang, Z. Novel Nanoarchitecture of Co-MOF-on-TPN-COF Hybrid: Ultralowly Sensitive Bioplatform of Electrochemical Aptasensor toward Ampicillin. *Biosens. Bioelectron.* **2019**, *123*, 59–68. https://doi.org/https://doi.org/10.1016/j.bios.2018.09.089.

(268) Chung, S.; Chandra, P.; Koo, J. P.; Shim, Y.-B. Development of a Bifunctional Nanobiosensor for Screening and Detection of Chemokine Ligand in Colorectal Cancer Cell Line. *Biosens. Bioelectron.* **2018**, *100*, 396–403. https://doi.org/https://doi.org/10.1016/j.bios.2017.09.031.

(269) He, L.; Li, Z.; Guo, C.; Hu, B.; Wang, M.; Zhang, Z.; Du, M. Bifunctional Bioplatform Based on NiCo Prussian Blue Analogue: Label-Free Impedimetric Aptasensor for the Early Detection of Carcino-Embryonic Antigen and Living Cancer Cells. *Sensors Actuators B Chem.* **2019**, *298*, 126852. https://doi.org/https://doi.org/10.1016/j.snb.2019.126852.

(270) Ghorbani, F.; Abbaszadeh, H.; Dolatabadi, J. E. N.; Aghebati-Maleki, L.; Yousefi, M. Application of Various Optical and Electrochemical Aptasensors for Detection of Human Prostate Specific Antigen: A Review. *Biosens. Bioelectron.* **2019**, *142*, 111484. https://doi.org/10.1016/j.bios.2019.111484.

(271) Duan, F.; Hu, M.; Guo, C.; Song, Y.; Wang, M.; He, L.; Zhang, Z.; Pettinari, R.; Zhou, L. Chromium-Based Metal-Organic Framework Embedded with Cobalt Phthalocyanine for the Sensitively Impedimetric Cytosensing of Colorectal Cancer (CT26) Cells and Cell Imaging. *Chem. Eng. J.* **2020**, *398*. https://doi.org/10.1016/j.cej.2020.125452.

(272) Xu, J.; Wang, Y.-H.; Wei, Z.; Wang, F.-T.; Huang, K.-J. Significantly Improving the Performance of Self-Powered Biosensor by Effectively Combining with High-Energy Enzyme Biofuel Cells, N-Doped Graphene, and Ultrathin Hollow Carbon Shell. *Sensors Actuators B Chem.* **2021**, *327*, 128933. https://doi.org/https://doi.org/10.1016/j.snb.2020.128933.

(273) Purohit, B.; Kumar, A.; Mahato, K.; Roy, S.; Chandra, P. Chapter 9 - Cancer Cytosensing Approaches in Miniaturized Settings Based on Advanced Nanomaterials and Biosensors. In *Nanotechnology in Modern Animal*

Biotechnology; Maurya, P. K., Singh, S., Eds.; Elsevier, 2019; pp 133–147. https://doi.org/https://doi.org/10.1016/B978-0-12-818823-1.00009-0.

(274) Zhang, Y.; Liu, X.; Li, N.; Xu, Y.; Ma, Y.; Huang, Z.; Luo, H.; Hou, C.; Huo, D. Typing of Cancer Cells by Microswimmer Based on Co-Fe-MOF for One-Step Simultaneously Detect Multiple Biomarkers. *Biosens. Bioelectron.* **2023**, *230*, 115263. https://doi.org/https://doi.org/10.1016/j.bios.2023.115263.

(275) Zhang, Y.; Zhang, Z.; Pan, H.; Chang, D.; Lin, Y. Colorimetric and Fluorescence Detection of Circulating Tumor Cells Based on a Bimetallic-Organic Framework. *Microchem. J.* **2023**, *190*, 108621. https://doi.org/https://doi.org/10.1016/j.microc.2023.108621.

(276) Yuan, J.; Duan, H.; Wang, L.; Wang, S.; Li, Y.; Lin, J. A Three-in-One Hybrid Nanozyme for Sensitive Colorimetric Biosensing of Pathogens. *Food Chem.* **2023**, *408*. https://doi.org/10.1016/j.foodchem.2022.135212.

(277) Qi, X.; Xia, L.; Li, Y.; Wang, T.; Zhang, X.; Chen, J.; Zhang, L.; Fu, Y. The Fabrication of 2D Cu-Based MOF Nanosheets for DNA Detection. *Aust. J. Chem.* **2019**, *72* (12), 939–944. https://doi.org/10.1071/CH19312.

(278) Mirsadoughi, E.; Pebdeni, A. B.; Hosseini, M. Sensitive Colorimetric Aptasensor Based on Peroxidase-like Activity of ZrPr-MOF to Detect Salmonella Typhimurium in Water and Milk. *Food Control* **2023**, *146*. https://doi.org/10.1016/j.foodcont.2022.109500.

(279) Wang, M.; Wang, M.; Huang, S.; Zhang, S.; Zhang, Z.; He, L.; Du, M. Confinement of Defect-Rich Bimetallic In<inf>2</Inf>O<inf>3</Inf>/CeO<inf>2</Inf> Nanocrystals in Mesoporous Nitrogen-Doped Carbon as a Sensitive Platform for Photoelectrochemical Aptasensing of Escherichia Coli. *Anal. Chim. Acta* **2023**, *1248*. https://doi.org/10.1016/j.aca.2023.340893.

(280) Bhatt, D.; Singh, S.; Singhal, N.; Bhardwaj, N.; Deep, A. Glyco-Conjugated Metal–Organic Framework Biosensor for Fluorescent Detection of Bacteria. *Anal. Bioanal. Chem.* **2023**, *415* (4), 659–667. https://doi.org/10.1007/s00216-022-04455-z.

(281) Zuo, W.; Liang, L.; Ye, F.; Zhao, S. An Integrated Platform for Label-Free Fluorescence Detection and Inactivation of Bacteria Based on Boric Acid Functionalized Zr-MOF. *Sensors Actuators B Chem.* **2021**, *345*, 130345. https://doi.org/https://doi.org/10.1016/j.snb.2021.130345.

(282) Tian, J.-Y.; Liu, X.; Zhang, S.; Chen, K.; Zhu, L.; Song, Y.; Wang, M.; Zhang, Z.; Du, M. Novel Aptasensing Strategy for Efficiently Quantitative Analyzing Staphylococcus Aureus Based on Defective Copper-Based Metal–Organic Framework. *Food Chem.* **2023**, *402*. https://doi.org/10.1016/j.foodchem.2022.134357.

(283) Zhao, X.; Yang, Z.; Niu, R.; Tang, Y.; Wang, H.; Gao, R.; Zhao, Y.; Jing, X.;

Wang, D.; Lin, P.; Guan, H.; Meng, L. MIL-101(CuFe) Nanozymes with Excellent Peroxidase-like Activity for Simple, Accurate, and Visual Naked-Eye Detection of SARS-CoV-2. *Anal. Chem.* **2023**, *95* (2), 1731–1738. https://doi.org/10.1021/acs.analchem.2c05043.

(284) Liu, Y.; Zhou, S.; Dong, J.; Sun, H.; Deng, L.; Ma, Y.; Zhao, D.; Huo, D.; Hou, C. Rapid and Ultrasensitive Fluorescence Sensing Platform Based on Nanometer-Sized Metal-Organic Frameworks for Transgenic CaMV 35S Promoter Detection. *ACS Appl. Nano Mater.* **2023**. https://doi.org/10.1021/acsanm.3c01091.

(285) Huang, X.; Zhu, Y.; Kianfar, E. Nano Biosensors: Properties, Applications and Electrochemical Techniques. *J. Mater. Res. Technol.* **2021**, *12*, 1649–1672. https://doi.org/10.1016/J.JMRT.2021.03.048.

(286) BioSensing, Theranostics, and Medical Devices. *BioSensing, Theranostics, Med. Devices* **2022**. https://doi.org/10.1007/978-981-16-2782-8.

(287) Mahato, K.; Prasad, A.; Maurya, P. K.; Chandra, P. Nanobiosensors: Next Generation Point-of-Care Biomedical Devices for Personalized Diagnosis. *J. Anal. Bioanal. Tech.* **2016**, *7* (2). https://doi.org/10.4172/2155-9872.1000e125.

(288) Mehrotra, P. Biosensors and Their Applications – A Review. *J. Oral Biol. Craniofacial Res.* **2016**, *6* (2), 153. https://doi.org/10.1016/J.JOBCR.2015.12.002.

(289) Divya; Darshna; Sammi, A.; Chandra, P. Design and Development of Opto-Electrochemical Biosensing Devices for Diagnosing Chronic Kidney Disease. *Biotechnol. Bioeng.* **2023**, *120* (11), 3116–3136. https://doi.org/10.1002/BIT.28490.

(290) Kumari, R.; Singh, A.; Azad, U. P.; Chandra, P. Insights into the Fabrication and Electrochemical Aspects of Paper Microfluidics-Based Biosensor Module. *Biosensors*. 2023. https://doi.org/10.3390/bios13090891.

(291) Kajal, N.; Singh, V.; Gupta, R.; Gautam, S. Metal Organic Frameworks for Electrochemical Sensor Applications: A Review. *Environ. Res.* **2022**, *204*, 112320. https://doi.org/10.1016/J.ENVRES.2021.112320.

(292) Chen, Y.; Yang, Z.; Hu, H.; Zhou, X.; You, F.; Yao, C.; Liu, F. J.; Yu, P.; Wu, D.; Yao, J.; Hu, R.; Jiang, X.; Yang, H. Advanced Metal–Organic Frameworks-Based Catalysts in Electrochemical Sensors. *Front. Chem.* **2022**, *10*, 881172. https://doi.org/10.3389/FCHEM.2022.881172/BIBTEX.

(293) Naser, S. A. E.; Badmus, K. O.; Khotseng, L. Synthesis, Properties, and Applications of Metal Organic Frameworks Supported on Graphene Oxide. *Coatings 2023, Vol. 13, Page 1456* **2023**, *13* (8), 1456. https://doi.org/10.3390/COATINGS13081456.

(294) Baumann, A. E.; Burns, D. A.; Liu, B.; Thoi, V. S. Metal-Organic Framework Functionalization and Design Strategies for Advanced Electrochemical Energy Storage Devices. *Commun. Chem. 2019 21* **2019**, *2* (1), 1–14.

https://doi.org/10.1038/s42004-019-0184-6.

(295) Sharabati, M. Al; Sabouni, R.; Husseini, G. A. Biomedical Applications of Metal−Organic Frameworks for Disease Diagnosis and Drug Delivery: A Review. *Nanomaterials* **2022**, *12* (2), 277. https://doi.org/10.3390/NANO12020277.

(296) Ma, Z. Z.; Wang, Y. S.; Liu, B.; Jiao, H.; Xu, L. A Non–Enzymatic Electrochemical Sensor of Cu@Co–MOF Composite for Glucose Detection with High Sensitivity and Selectivity. *Chemosensors* **2022**, *10* (10), 416. https://doi.org/10.3390/CHEMOSENSORS10100416/S1.

(297) Divya; Chandra, P. ZIF-67-MWCNT Nanohybrid Based Electrochemical Immunosensing Device for Diagnosing Kidney Dysfunction. *Proc. IEEE Sensors* **2023**. https://doi.org/10.1109/SENSORS56945.2023.10324879.

(298) Sheta, S. M.; El-Sheikh, S. M.; Osman, D. I.; Salem, A. M.; Ali, O. I.; Harraz, F. A.; Shousha, W. G.; Shoeib, M. A.; Shawky, S. M.; Dionysiou, D. D. A Novel HCV Electrochemical Biosensor Based on a Polyaniline@Ni-MOF Nanocomposite. *Dalt. Trans.* **2020**, *49* (26), 8918–8926. https://doi.org/10.1039/D0DT01408G.

(299) Dourandish, Z.; Tajik, S.; Beitollahi, H.; Jahani, P. M.; Nejad, F. G.; Sheikhshoaie, I.; Di Bartolomeo, A. A Comprehensive Review of Metal–Organic Framework: Synthesis, Characterization, and Investigation of Their Application in Electrochemical Biosensors for Biomedical Analysis. *Sensors (Basel).* **2022**, *22* (6). https://doi.org/10.3390/S22062238.

(300) Ren, J.; Dyosiba, X.; Musyoka, N. M.; Langmi, H. W.; Mathe, M.; Liao, S. Review on the Current Practices and Efforts towards Pilot-Scale Production of Metal-Organic Frameworks (MOFs). *Coord. Chem. Rev.* **2017**, *352*, 187–219. https://doi.org/https://doi.org/10.1016/j.ccr.2017.09.005.

(301) Mansour, F. R.; Hammad, S. F.; Abdallah, I. A.; Bedair, A.; Abdelhameed, R. M.; Locatelli, M. Applications of Metal Organic Frameworks in Point of Care Testing. *TrAC Trends Anal. Chem.* **2024**, *172*, 117596. https://doi.org/https://doi.org/10.1016/j.trac.2024.117596.

(302) Yan, T.; Zhang, G.; Yu, K.; Chai, H.; Tian, M.; Qu, L.; Dong, H.; Zhang, X. Smartphone Light-Driven Zinc Porphyrinic MOF Nanosheets-Based Enzyme-Free Wearable Photoelectrochemical Sensor for Continuous Sweat Vitamin C Detection. *Chem. Eng. J.* **2023**, *455*, 140779. https://doi.org/10.1016/J.CEJ.2022.140779.

(303) Baker, R. E.; Mahmud, A. S.; Miller, I. F.; Rajeev, M.; Rasambainarivo, F.; Rice, B. L.; Takahashi, S.; Tatem, A. J.; Wagner, C. E.; Wang, L. F.; Wesolowski, A.; Metcalf, C. J. E. Infectious Disease in an Era of Global Change. *Nat. Rev. Microbiol. 2021 204* **2021**, *20* (4), 193–205. https://doi.org/10.1038/s41579-021-00639-z.

(304) Li, Z.; Zeng, W.; Li, Y. Recent Progress in MOF-Based Electrochemical Sensors

for Non-Enzymatic Glucose Detection. *Mol. 2023, Vol. 28, Page 4891* **2023**, *28* (13), 4891. https://doi.org/10.3390/MOLECULES28134891.

(305) Wang, Y.; Hu, Y.; He, Q.; Yan, J.; Xiong, H.; Wen, N.; Cai, S.; Peng, D.; Liu, Y.; Liu, Z. Metal-Organic Frameworks for Virus Detection. *Biosens. Bioelectron.* **2020**, *169*, 112604. https://doi.org/10.1016/J.BIOS.2020.112604.

(306) Li, M.; Zhang, G.; Boakye, A.; Chai, H.; Qu, L.; Zhang, X. Recent Advances in Metal-Organic Framework-Based Electrochemical Biosensing Applications. *Front. Bioeng. Biotechnol.* **2021**, *9*, 797067. https://doi.org/10.3389/FBIOE.2021.797067/BIBTEX.

(307) Nandi, I.; Rai, S. K.; Chandra, P. Talanta MOF-Based Nanocomposites as Transduction Matrices for Optical and Electrochemical Sensing. *Talanta* **2024**, *266* (P2), 125124. https://doi.org/10.1016/j.talanta.2023.125124.

(308) Saeedi, P.; Salpea, P.; Karuranga, S.; Petersohn, I.; Malanda, B.; Gregg, E. W.; Unwin, N.; Wild, S. H.; Williams, R. Mortality Attributable to Diabetes in 20–79 Years Old Adults, 2019 Estimates: Results from the International Diabetes Federation Diabetes Atlas, 9th Edition. *Diabetes Res. Clin. Pract.* **2020**, *162*, 108086. https://doi.org/https://doi.org/10.1016/j.diabres.2020.108086.

(309) Lovic, D.; Piperidou, A.; Zografou, I.; Grassos, H.; Pittaras, A.; Manolis, A. The Growing Epidemic of Diabetes Mellitus. *Curr. Vasc. Pharmacol.* **2020**, *18* (2), 104–109. https://doi.org/10.2174/1570161117666190405165911.

(310) Naikoo, G. A.; Bano, M.; Arshad, F.; Hassan, I. U.; BaOmar, F.; Alfagih, I. M.; Tambuwala, M. M. Non-Enzymatic Glucose Sensors Composed of Trimetallic CuO/Ag/NiO Based Composite Materials. *Sci. Rep.* **2023**, *13* (1), 6210. https://doi.org/10.1038/s41598-023-32719-w.

(311) Zhang, Y.; Lin, Q.; Song, Y.; Huang, J.; Chen, M.; Ouyang, R.; Liu, S. Y.; Dai, Z. MOF-Based Materials for Glucose Detection. *Chemosensors* **2023**, *11* (8). https://doi.org/10.3390/chemosensors11080429.

(312) Xu, T.; Zhang, Y.; Liu, M.; Wang, H.; Ren, J.; Tian, Y.; Liu, X.; Zhou, Y.; Wang, J.; Zhu, W.; Ma, M. In-Situ Two-Step Electrodeposition of α-CD-RGO/Ni-MOF Composite Film for Superior Glucose Sensing. *J. Alloys Compd.* **2022**, *923*, 166418. https://doi.org/https://doi.org/10.1016/j.jallcom.2022.166418.

(313) Koukouviti, E.; Plessas, A. K.; Pagkali, V.; Economou, A.; Papaefstathiou, G. S.; Kokkinos, C. 3D-Printed Electrochemical Glucose Device with Integrated Fe(II)-MOF Nanozyme. *Microchim. Acta* **2023**, *190* (7), 9–15. https://doi.org/10.1007/s00604-023-05860-6.

(314) Xia, Y.; Su, T.; Mi, Z.; Feng, Z.; Hong, Y.; Hu, X.; Shu, Y. Wearable Electrochemical Sensor Based on Bimetallic MOF Coated CNT/PDMS Film Electrode via a Dual-Stamping Method for Real-Time Sweat Glucose Analysis. *Anal. Chim. Acta* **2023**, *1278*, 341754. https://doi.org/https://doi.org/10.1016/j.aca.2023.341754.

(315) Kuppuswamy, G. P.; Shabanur Matada, M. S.; Marappan, G.; Mulla, M. Y.; Velappa Jayaraman, S.; Di Natale, C.; Sivalingam, Y. NiOX Template-Grown Ni-MOF-Coated Carbon Paper Electrode Embedded Extended Gate Field Effect Transistor for Glucose Detection in Saliva: En Route toward the Noninvasive Diagnosis of Diabetes Mellitus. *ACS Appl. Electron. Mater.* **2023**, *5* (6), 3268–3279. https://doi.org/10.1021/acsaelm.3c00339.

(316) Yuan, M.; Wang, L.; Li, K.; Zhang, Q.; Li, Y.; Hou, C.; Wang, H. Non-Enzyme Electrochemical Sensing Fabrics and Wearable Applications Based on Bimetallic NiCo-MOFs. *Electroanalysis* **2023**, No. December 2022, 1–12. https://doi.org/10.1002/elan.202200556.

(317) Lu, J.; Cheng, C.; Cao, Y.; Hou, X.; Li, H.; Yin, X. MOFs-Derived Core-Shell Structured NiCo2O4NWs@Co3O4NPs for Non-Enzymatic Glucose Detection. *Ceram. Int.* **2023**, *49* (14, Part A), 23958–23966. https://doi.org/https://doi.org/10.1016/j.ceramint.2023.04.245.

(318) Wei, Y.; Hui, Y.; Lu, X.; Liu, C.; Zhang, Y.; Fan, Y.; Chen, W. One-Pot Preparation of NiMn Layered Double Hydroxide-MOF Material for Highly Sensitive Electrochemical Sensing of Glucose. *J. Electroanal. Chem.* **2023**, *933*, 117276. https://doi.org/https://doi.org/10.1016/j.jelechem.2023.117276.

(319) Xu, Z.; Wang, Q.; Zhangsun, H.; Zhao, S.; Zhao, Y.; Wang, L. Carbon Cloth-Supported Nanorod-like Conductive Ni/Co Bimetal MOF: A Stable and High-Performance Enzyme-Free Electrochemical Sensor for Determination of Glucose in Serum and Beverage. *Food Chem.* **2021**, *349*, 129202. https://doi.org/https://doi.org/10.1016/j.foodchem.2021.129202.

(320) Ezzati, M.; Shahrokhian, S.; Hosseini, H. In Situ Two-Step Preparation of 3D NiCo-BTC MOFs on a Glassy Carbon Electrode and a Graphitic Screen Printed Electrode as Nonenzymatic Glucose-Sensing Platforms. *ACS Sustain. Chem. Eng.* **2020**, *8* (38), 14340–14352. https://doi.org/10.1021/acssuschemeng.0c03806.

(321) Shu, Y.; Shang, Z.; Su, T.; Zhang, S.; Lu, Q.; Xu, Q.; Hu, X. A Highly Flexible Ni-Co MOF Nanosheet Coated Au/PDMS Film Based Wearable Electrochemical Sensor for Continuous Human Sweat Glucose Monitoring. *Analyst* **2022**, *147* (7), 1440–1448. https://doi.org/10.1039/d1an02214h.

(322) Zha, X.; Yang, W.; Shi, L.; Li, Y.; Zeng, Q.; Xu, J.; Yang, Y. Morphology Control Strategy of Bimetallic MOF Nanosheets for Upgrading the Sensitivity of Noninvasive Glucose Detection. *ACS Appl. Mater. Interfaces* **2022**, *14* (33), 37843–37852. https://doi.org/10.1021/acsami.2c10760.

(323) Shu, Y.; Su, T.; Lu, Q.; Shang, Z.; Xu, Q.; Hu, X. Highly Stretchable Wearable Electrochemical Sensor Based on Ni-Co MOF Nanosheet-Decorated Ag/RGO/PU Fiber for Continuous Sweat Glucose Detection. *Anal. Chem.* **2021**, *93* (48), 16222–16230. https://doi.org/10.1021/acs.analchem.1c04106.

(324) Gumilar, G.; Kaneti, Y. V.; Henzie, J.; Chatterjee, S.; Na, J.; Yuliarto, B.;

Nugraha, N.; Patah, A.; Bhaumik, A.; Yamauchi, Y. General Synthesis of Hierarchical Sheet/Plate-like M-BDC (M = Cu, Mn, Ni, and Zr) Metal-Organic Frameworks for Electrochemical Non-Enzymatic Glucose Sensing. *Chem. Sci.* **2020**, *11* (14), 3644–3655. https://doi.org/10.1039/c9sc05636j.

(325) Xiao, L.; Fang, X.; Cao, Y.; Hu, L.; Jiang, J. Ni-MOF Derived Rod-like Nickel Hydroxide through Controllable Hydrolysis for Efficient Electrocatalytic Glucose Oxidation. *Microchem. J.* **2023**, *190*, 108694. https://doi.org/https://doi.org/10.1016/j.microc.2023.108694.

(326) Feng, L.; Lin, X.; Feng, J.; Min, X.; Ni, Y. NiNP/Cu-MOF-C/GCE for the the Noninvasive Detection of Glucose in Natural Saliva Samples. *Microchem. J.* **2023**, *190*, 108657. https://doi.org/https://doi.org/10.1016/j.microc.2023.108657.

(327) Hekmat, F.; Ataei Kachouei, M.; Taghaddosi Foshtomi, S.; Shahrokhian, S.; Zhu, Z. Direct Decoration of Commercial Cotton Fabrics by Binary Nickel-Cobalt Metal-Organic Frameworks for Flexible Glucose Sensing in next-Generation Wearable Sensors. *Talanta* **2023**, *257*, 124375. https://doi.org/https://doi.org/10.1016/j.talanta.2023.124375.

(328) Baranwal, A.; Mahapatra, S.; Purohit, B.; Roy, S.; Chandra, P. Insights into Novel Coronavirus and COVID-19 Outbreak BT - Diagnostic Strategies for COVID-19 and Other Coronaviruses; Chandra, P., Roy, S., Eds.; Springer Singapore: Singapore, 2020; pp 1–17. https://doi.org/10.1007/978-981-15-6006-4_1.

(329) Dhar Chowdhury Anu Mary, S. O. Epidemiology of COVID-19. *J. Dig. Endosc.* **2020**, *11* (01), 3–7. https://doi.org/10.1055/s-0040-1712187.

(330) Huang, X.; Wei, F.; Hu, L.; Wen, L.; Chen, K. Epidemiology and Clinical Characteristics of COVID-19. *Arch. Iran. Med.* **2020**, *23* (4), 268–271. https://doi.org/10.34172/aim.2020.09.

(331) Goud, K. Y.; Reddy, K. K.; Khorshed, A.; Kumar, V. S.; Mishra, R. K.; Oraby, M.; Ibrahim, A. H.; Kim, H.; Gobi, K. V. Electrochemical Diagnostics of Infectious Viral Diseases: Trends and Challenges. *Biosens. Bioelectron.* **2021**, *180*, 113112. https://doi.org/https://doi.org/10.1016/j.bios.2021.113112.

(332) Ioos, S.; Mallet, H.-P.; Leparc Goffart, I.; Gauthier, V.; Cardoso, T.; Herida, M. Current Zika Virus Epidemiology and Recent Epidemics. *Médecine Mal. Infect.* **2014**, *44* (7), 302–307. https://doi.org/https://doi.org/10.1016/j.medmal.2014.04.008.

(333) MacLachlan, J. H.; Cowie, B. C. Hepatitis B Virus Epidemiology. *Cold Spring Harb. Perspect. Med.* **2015**, *5* (5), a021410. https://doi.org/10.1101/cshperspect.a021410.

(334) Heintges, T.; Wands, J. R. Hepatitis C Virus: Epidemiology and Transmission. *Hepatology* **1997**, *26* (3).

(335) Kaushik, A.; Yndart, A.; Jayant, R. D.; Sagar, V.; Atluri, V.; Bhansali, S.; Nair, M. Electrochemical Sensing Method for Point-of-Care Cortisol Detection in

Human Immunodeficiency Virus-Infected Patients. *Int. J. Nanomedicine* **2015**, *10*, 677–685. https://doi.org/10.2147/IJN.S75514.

(336) Lo Presti, A.; Lai, A.; Cella, E.; Zehender, G.; Ciccozzi, M. Chikungunya Virus, Epidemiology, Clinics and Phylogenesis: A Review. *Asian Pac. J. Trop. Med.* **2014**, *7* (12), 925–932. https://doi.org/https://doi.org/10.1016/S1995-7645(14)60164-4.

(337) Roy, S. K.; Bhattacharjee, S. Dengue Virus: Epidemiology, Biology, and Disease Aetiology. *Can. J. Microbiol.* **2021**, *67* (10), 687–702. https://doi.org/10.1139/cjm-2020-0572.

(338) Liesegang, T. J. Herpes Simplex Virus Epidemiology and Ocular Importance. *Cornea* **2001**, *20* (1).

(339) Lunn, R. M.; Jahnke, G. D.; Rabkin, C. S. Tumour Virus Epidemiology. *Philos. Trans. R. Soc. B Biol. Sci.* **2017**, *372* (1732). https://doi.org/10.1098/rstb.2016.0266.

(340) Mahapatra, S.; Chandra, P. Clinically Practiced and Commercially Viable Nanobio Engineered Analytical Methods for COVID-19 Diagnosis. *Biosens. Bioelectron.* **2020**, *165*, 112361. https://doi.org/https://doi.org/10.1016/j.bios.2020.112361.

(341) Chandra, P. Miniaturized Label-Free Smartphone Assisted Electrochemical Sensing Approach for Personalized COVID-19 Diagnosis. *Sensors Int.* **2020**, *1*, 100019. https://doi.org/https://doi.org/10.1016/j.sintl.2020.100019.

(342) Wang, Y.; Hu, Y.; He, Q.; Yan, J.; Xiong, H.; Wen, N.; Cai, S.; Peng, D.; Liu, Y.; Liu, Z. Metal-Organic Frameworks for Virus Detection. *Biosens. Bioelectron.* **2020**, *169*. https://doi.org/10.1016/j.bios.2020.112604.

(343) Benjamin, S. R.; Ribeiro Júnior, E. J. M.; De Andrade, G. M.; Oriá, R. B. *Metal-Organic Framework–Based Electrochemical Immunosensors for Virus Detection*; 2023. https://doi.org/10.10.1201/9781003252061-12.

(344) Lin, X.; Lian, X.; Luo, B.; Huang, X.-C. A Highly Sensitive and Stable Electrochemical HBV DNA Biosensor Based on ErGO-Supported Cu-MOF. *Inorg. Chem. Commun.* **2020**, *119*. https://doi.org/10.1016/j.inoche.2020.108095.

(345) Qian, X.; Tan, S.; Li, Z.; Qu, Q.; Li, L.; Yang, L. A Robust Host-Guest Interaction Controlled Probe Immobilization Strategy for the Ultrasensitive Detection of HBV DNA Using Hollow HP5–Au/CoS Nanobox as Biosensing Platform. *Biosens. Bioelectron.* **2020**, *153*. https://doi.org/10.1016/j.bios.2020.112051.

(346) Allel, K.; Stone, J.; Undurraga, E. A.; Day, L.; Moore, C. E.; Lin, L.; Furuya-Kanamori, L.; Yakob, L. *The Impact of Inpatient Bloodstream Infections Caused by Antibiotic-Resistant Bacteria in Low- and Middle-Income Countries: A Systematic Review and Meta-Analysis*; 2023; Vol. 20. https://doi.org/10.1371/journal.pmed.1004199.

(347) García-Rodríguez, J. F.; Mariño-Callejo, A. The Factors Associated with the Trend in Incidence of Bacteraemia and Associated Mortality over 30 Years. *BMC Infect. Dis.* **2023**, *23* (1), 69. https://doi.org/10.1186/s12879-023-08018-0.

(348) Ohnuma, T.; Chihara, S.; Costin, B.; Treggiari, M.; Bartz, R. R.; Raghunathan, K.; Krishnamoorthy, V. Epidemiology, Resistance Profiles, and Outcomes of Bloodstream Infections in Community-Onset Sepsis in the United States*. *Crit. Care Med.* **2023**, *51* (9).

(349) Yoon, Y.; So, H.; Lee, J. K.; Kim, D.; Jo, K. J.; Kim, H. H.; Kim, Y.-J.; Lee, J.; Jo, D. S.; Kim, Y.-K.; Park, S. E.; Chang, Y. S.; Kim, Y.-J. Microbiologic Epidemiology of Early-Onset Sepsis in Neonates Born at ≥35 0/7 Weeks' Gestation in Korea During 2009–2018. *Pediatr. Infect. Dis. J.* **2023**, *42* (8).

(350) Shan, X.; Xie, H.; Zhou, T.; Wu, M.; Yang, J. Dual DNA Recycling Amplifications Coupled with Au NPs@ZIF-MOF Accelerator for Enhanced Electrochemical Ratiometric Sensing of Pathogenic Bacteria. *Talanta* **2023**, *263*, 124751. https://doi.org/https://doi.org/10.1016/j.talanta.2023.124751.

(351) Ye, Y.; Yan, W.; Wang, T.; Zhang, C.; Wang, K.; Lu, Y.; Zheng, H.; Tao, Y.; Cao, X.; He, S.; Li, Y. Dual-Channel Biosensor for Simultaneous Detection of S. Typhimurium and L. Monocytogenes Using Nanotags of Gold Nanoparticles Loaded Metal-Organic Frameworks. *Anal. Chim. Acta* **2023**, *1279* (September), 341816. https://doi.org/10.1016/j.aca.2023.341816.

(352) Kumari, R.; Rai, S. K.; Chandra, P. Electrochemical Assembly of Nickel Metal Organic Framework- Decorated Nanoimprinted Gold Dendrites as Peroxidase Mimic for High-Performance Hydrogen Peroxide Sensing. **2023**. https://doi.org/10.1021/acsanm.3c05396.

(353) Hu, W. C.; Pang, J.; Biswas, S.; Wang, K.; Wang, C.; Xia, X. H. Ultrasensitive Detection of Bacteria Using a 2D MOF Nanozyme-Amplified Electrochemical Detector. *Anal. Chem.* **2021**, *93* (24), 8544–8552. https://doi.org/10.1021/acs.analchem.1c01261.

(354) Palanisamy, S.; Lee, L.-Y.; Kao, C.-F.; Chen, W.-L.; Wang, H.-C.; Shen, S.-T.; Jian, J.-W.; Yuan, S.-S. F.; Kung, Y.-A.; Wang, Y.-M. One-Step-One-Pot Hydrothermally Derived Metal-Organic-Framework-Nanohybrids for Integrated Point-of-Care Diagnostics of SARS-CoV-2 Viral Antigen/Pseudovirus Utilizing Electrochemical Biosensor Chip. *Sensors Actuators B Chem.* **2023**, *390*. https://doi.org/10.1016/j.snb.2023.133960.

(355) Jia, Z.; Ma, Y.; Yang, L.; Guo, C.; Zhou, N.; Wang, M.; He, L.; Zhang, Z. NiCo <inf>2</Inf> O <inf>4</Inf> Spinel Embedded with Carbon Nanotubes Derived from Bimetallic NiCo Metal-Organic Framework for the Ultrasensitive Detection of Human Immune Deficiency Virus-1 Gene. *Biosens. Bioelectron.* **2019**, *133*, 55–63. https://doi.org/10.1016/j.bios.2019.03.030.

(356) Rahmati, Z.; Roushani, M. SARS-CoV-2 Virus Label-Free Electrochemical

Nanohybrid MIP-Aptasensor Based on Ni<inf>3</Inf>(BTC)<inf>2</Inf> MOF as a High-Performance Surface Substrate. *Microchim. Acta* **2022**, *189* (8). https://doi.org/10.1007/s00604-022-05357-8.

(357) Sheta, S. M.; El-Sheikh, S. M.; Osman, D. I.; Salem, A. M.; Ali, O. I.; Harraz, F. A.; Shousha, W. G.; Shoeib, M. A.; Shawky, S. M.; Dionysiou, D. D. A Novel HCV Electrochemical Biosensor Based on a Polyaniline@Ni-MOF Nanocomposite. *Dalt. Trans.* **2020**, *49* (26), 8918–8926. https://doi.org/10.1039/d0dt01408g.

(358) Yiwei, X.; Yahui, L.; Weilong, T.; Jiyong, S.; Xiaobo, Z.; Wen, Z.; Xinai, Z.; Yanxiao, L.; Changqiang, Z.; Lele, A.; Hong, L.; Tingting, S. Electrochemical Determination of Hantavirus Using Gold Nanoparticle-Modified Graphene as an Electrode Material and Cu-Based Metal-Organic Framework Assisted Signal Generation. *Mikrochim. Acta* **2021**, *188* (4), 112. https://doi.org/10.1007/s00604-021-04769-2.

(359) El-Sheikh, S. M.; Osman, D. I.; Ali, O. I.; Shousha, W. G.; Shoeib, M. A.; Shawky, S. M.; Sheta, S. M. A Novel Ag/Zn Bimetallic MOF as a Superior Sensitive Biosensing Platform for HCV-RNA Electrochemical Detection. *Appl. Surf. Sci.* **2021**, *562*, 150202. https://doi.org/https://doi.org/10.1016/j.apsusc.2021.150202.

(360) Qin, X.; Wang, B.; Li, X.; Ding, Y.; Yang, X.; Zhou, Y.; Xu, W.; Xu, M.; Gu, C. Toluidine Blue-Assisted Synthesis of Functionalized M (M = Cu, Co, Zn)-Metal-Organic Frameworks for Electrochemical Immunoassay of Proteins. *J. Electroanal. Chem.* **2022**, *911*, 116186. https://doi.org/https://doi.org/10.1016/j.jelechem.2022.116186.

(361) Su, Z.; Tang, D.; Yang, X.; Peng, Y.; Wang, B.; Li, X.; Chen, J.; Hu, Y.; Qin, X. Selective and Fast Growth of CdS Nanocrystals on Zinc (II) Metal–Organic Framework Architectures for Photoelectrochemical Response and Electrochemical Immunosensor of Foot-and-Mouth Disease Virus. *Microchem. J.* **2022**, *174*, 107038. https://doi.org/https://doi.org/10.1016/j.microc.2021.107038.

(362) Zhang, X.; Xie, G.; Gou, D.; Luo, P.; Yao, Y.; Chen, H. A Novel Enzyme-Free Electrochemical Biosensor for Rapid Detection of Pseudomonas Aeruginosa Based on High Catalytic Cu-ZrMOF and Conductive Super P. *Biosens. Bioelectron.* **2019**, *142*. https://doi.org/10.1016/j.bios.2019.111486.

(363) Zhong, M.; Yang, L.; Yang, H.; Cheng, C.; Deng, W.; Tan, Y.; Xie, Q.; Yao, S. An Electrochemical Immunobiosensor for Ultrasensitive Detection of Escherichia Coli O157:H7 Using CdS Quantum Dots-Encapsulated Metal-Organic Frameworks as Signal-Amplifying Tags. *Biosens. Bioelectron.* **2019**, *126*, 493–500. https://doi.org/10.1016/j.bios.2018.11.001.

(364) Lou, Y.; Jia, Q.; Rong, F.; Zhang, S.; Zhang, Z.; Du, M. Universal Biosensing Platform Based on PolyMn-MOF Nanosheets for Efficient Analysis of Foodborne Pathogens from Diverse Foodstuffs. *Food Chem.* **2022**, *395*, 133618.

https://doi.org/https://doi.org/10.1016/j.foodchem.2022.133618.

(365) Chen, Y.; Liu, X.; Guo, S.; Cao, J.; Zhou, J.; Zuo, J.; Bai, L. A Sandwich-Type Electrochemical Aptasensor for Mycobacterium Tuberculosis MPT64 Antigen Detection Using C(60)NPs Decorated N-CNTs/GO Nanocomposite Coupled with Conductive PEI-Functionalized Metal-Organic Framework. *Biomaterials* **2019**, *216*, 119253. https://doi.org/10.1016/j.biomaterials.2019.119253.

(366) Hu, W.-C.; Pang, J.; Biswas, S.; Wang, K.; Wang, C.; Xia, X.-H. Ultrasensitive Detection of Bacteria Using a 2D MOF Nanozyme-Amplified Electrochemical Detector. *Anal. Chem.* **2021**, *93* (24), 8544–8552. https://doi.org/10.1021/acs.analchem.1c01261.

(367) Gupta, A.; Bhardwaj, S. K.; Sharma, A. L.; Kim, K.-H.; Deep, A. Development of an Advanced Electrochemical Biosensing Platform for E. Coli Using Hybrid Metal-Organic Framework/Polyaniline Composite. *Environ. Res.* **2019**, *171*, 395–402. https://doi.org/10.1016/j.envres.2019.01.049.

(368) Dai, G.; Li, Z.; Luo, F.; Lu, Y.; Chu, Z.; Zhang, J.; Zhang, F.; Wang, Q.; He, P. Simultaneous Electrochemical Determination of Nuc and MecA Genes for Identification of Methicillin-Resistant Staphylococcus Aureus Using N-Doped Porous Carbon and DNA-Modified MOF. *Microchim. Acta* **2021**, *188* (2), 39. https://doi.org/10.1007/s00604-020-04698-6.

(369) Meng, Y.; Ma, Z.; Huang, Y.; Song, Y. Construction of MOF@COF Composite-Based Electrochemical Aptasensor for Detection of Staphylococcus Aureus. *Anal. Sci.* **2023**, *39* (6), 901–909. https://doi.org/10.1007/s44211-023-00295-8.

(370) Scott, D.; Atkin, A. E.; Granley, A.; Singhal, A. The Utility of Cognitive Testing to Predict Real World Commercial Driving Risk. *Transp. Res. Interdiscip. Perspect.* **2023**, *18*, 100783. https://doi.org/https://doi.org/10.1016/j.trip.2023.100783.

(371) Dumurgier, J.; Tzourio, C. Epidemiology of Neurological Diseases in Older Adults. *Rev. Neurol. (Paris).* **2020**, *176* (9), 642–648. https://doi.org/https://doi.org/10.1016/j.neurol.2020.01.356.

(372) Dugger, B. N.; Dickson, D. W. Pathology of Neurodegenerative Diseases. *Cold Spring Harb. Perspect. Biol.* **2017**, *9* (7). https://doi.org/10.1101/cshperspect.a028035.

(373) Sun, W.; Liu, J.; Zha, X.; Sun, G.; Wang, Y. Triple Microenvironment Modulation of Zeolite Imidazolate Framework (ZIF) Nanocages for Boosting Dopamine Electrocatalysis. *J. Colloid Interface Sci.* **2024**, *654,* 1–12. https://doi.org/https://doi.org/10.1016/j.jcis.2023.10.022.

(374) Hira, S. A.; Nagappan, S.; Yusuf, M.; Chen, A.; Lee, J. M.; Hyun Park, K. L-Cysteine Anchored Co-MOF Derived Cobalt-Nitrogen-Carbon Hierarchical Architecture as an Efficient Sensor for the Electrochemical Detection of Catecholamine. *Microchem. J.* **2023**, *190* (April), 108748.

https://doi.org/10.1016/j.microc.2023.108748.

(375) Klein, M. O.; Battagello, D. S.; Cardoso, A. R.; Hauser, D. N.; Bittencourt, J. C.; Correa, R. G. Dopamine: Functions, Signaling, and Association with Neurological Diseases. *Cell. Mol. Neurobiol.* **2019**, *39* (1), 31–59. https://doi.org/10.1007/s10571-018-0632-3.

(376) Zhou, Y.; Tian, M.; Li, R.; Zhang, Y.; Zhang, G.; Zhang, C.; Shuang, S. Ultrasensitive Electrochemical Platform for Dopamine Detection Based on CoNi-MOF@ERGO Composite. *ACS Biomater. Sci. Eng.* **2023**, *9* (10), 5599–5609. https://doi.org/10.1021/acsbiomaterials.3c00740.

(377) Ding, Y.; Zhao, X.; Wu, P.; Wang, R.; Xie, L.; Li, Z.; Zhu, Z.; Zhao, H.; Lan, M. ZIF-67 MOF Derived Co-Based CeO2 Electrochemical Sensor for Dopamine. *Electrochim. Acta* **2023**, *463* (June), 142802. https://doi.org/10.1016/j.electacta.2023.142802.

(378) Baranwal, A.; Chandra, P. Clinical Implications and Electrochemical Biosensing of Monoamine Neurotransmitters in Body Fluids, in Vitro, in Vivo, and Ex Vivo Models. *Biosens. Bioelectron.* **2018**, *121*, 137–152. https://doi.org/https://doi.org/10.1016/j.bios.2018.09.002.

(379) Chen, J.; Yang, J.; Chen, Y.; Dong, J.; Deng, R.; Zhu, L. Multiwalled Carbon Nanotubes Modified with Nickel-Zinc Bis(Dithiolene) Metal-Organic Frameworks for Electrochemical Detection of 5-Hydroxytryptamine. *J. Electroanal. Chem.* **2023**, *949*, 117851. https://doi.org/https://doi.org/10.1016/j.jelechem.2023.117851.

(380) Dong, Y.; Zhang, L. Coupling Surfactants with 3D Hollow Raspberry-like NiS/Carbon Microsphere with S Vacancies for Enhanced Sensitivity Monitoring of Serotonin and L-Tryptophan. *Sensors Actuators B Chem.* **2022**, *368*, 132140. https://doi.org/https://doi.org/10.1016/j.snb.2022.132140.

(381) Leite, J. P.; Figueira, F.; Mendes, R. F.; Almeida Paz, F. A.; Gales, L. Metal–Organic Frameworks as Sensors for Human Amyloid Diseases. *ACS Sensors* **2023**, *8* (3), 1033–1053. https://doi.org/10.1021/acssensors.2c02741.

(382) Shetty, S. S.; Moosa, B.; Zhang, L.; Alshankiti, B.; Baslyman, W.; Mani, V.; Khashab, N. M.; Salama, K. N. Polyoxometalate-Cyclodextrin Supramolecular Entities for Real-Time in Situ Monitoring of Dopamine Released from Neuroblastoma Cells. *Biosens. Bioelectron.* **2023**, *229* (March), 115240. https://doi.org/10.1016/j.bios.2023.115240.

(383) Huang, Z.; Zhang, L.; Cao, P.; Wang, N.; Lin, M. Electrochemical Sensing of Dopamine Using a Ni-Based Metal-Organic Framework Modified Electrode. *Ionics (Kiel).* **2021**, *27* (3), 1339–1345. https://doi.org/10.1007/s11581-020-03857-2.

(384) Chen, S.; Zhou, D.; Yu, J.; Huang, Z.; Wang, L. Porous Carbon Nanosheets Derived from Two-Dimensional Fe-MOF for Simultaneous Voltammetric

Sensing of Dopamine and Uric Acid. *Nanotechnology* **2023**, *34* (49). https://doi.org/10.1088/1361-6528/acf225.

(385) Wang, X.; Ma, Y.; Zhou, Z.; Zhang, Z.; Zhang, J.; Fan, L.; Du, X.; Lu, X. Ultrarapid Synthesis of Dumbbell-Shaped Carbon Black-Doped Ce (III, IV)-MOF Composites for Fabrication of Simultaneous Electrochemical Sensor of Dopamine and Acetaminophen. *Microchem. J.* **2023**, *195*, 109430. https://doi.org/https://doi.org/10.1016/j.microc.2023.109430.

(386) Chen, C.; Ren, J.; Zhao, P.; Zhang, J.; Hu, Y.; Fei, J. A Novel Dopamine Electrochemical Sensor Based on a β-Cyclodextrin/Ni-MOF/Glassy Carbon Electrode. *Microchem. J.* **2023**, *194*, 109328. https://doi.org/https://doi.org/10.1016/j.microc.2023.109328.

(387) Mukundan, G.; Ganapathy, N.; Badhulika, S. ZnO Nanoparticles-Copper Metal-Organic Framework Composite on 3D Porous Nickel Foam: A Novel Electrochemical Sensing Platform to Detect Serotonin in Blood Serum. *Nanotechnology* **2023**, *34* (40). https://doi.org/10.1088/1361-6528/ace368.

(388) Zhou, Y.; Huang, Z.; Liu, J.; Dong, H.; Zhang, Y.; Xu, M.; Bi, Y. Tyrosine-Conjugation Method for Evaluating BACE1 Activity Based on Silver Nanoparticles/Metal-Organic Framework Composites as Electrochemical Tags. *Chemistry* **2023**, *29* (28), e202300450. https://doi.org/10.1002/chem.202300450.

(389) Zhou, Y.; Li, C.; Li, X.; Zhu, X.; Ye, B.; Xu, M. A Sensitive Aptasensor for the Detection of β-Amyloid Oligomers Based on Metal-Organic Frameworks as Electrochemical Signal Probes. *Anal. Methods* **2018**, *10* (36), 4430–4437. https://doi.org/10.1039/c8ay00736e.

(390) Ahmad, M. W.; Dey, B.; Kim, B. H.; Sarkhel, G.; Yang, D. J.; Safdar Hossain, S. K.; Kamal, T.; Choudhury, A. Bimetallic Copper-Cobalt MOFs Anchored Carbon Nanofibers Hybrid Mat Based Electrode for Simultaneous Determination of Dopamine and Tyramine. *Microchem. J.* **2023**, *193* (June), 109074. https://doi.org/10.1016/j.microc.2023.109074.

(391) Wei, X.; Guo, H.; Lu, Z.; Sun, L.; Pan, Z.; Liu, B.; Peng, L.; Yang, W. A Novel Electrochemical Sensor Based on DUT-67/ZnCo2O4-MWCNTs Modified Glassy Carbon Electrode for the Simultaneous Sensitive Detection of Dopamine and Uric Acid. *Colloids Surfaces A Physicochem. Eng. Asp.* **2023**, *674* (March), 131921. https://doi.org/10.1016/j.colsurfa.2023.131921.

(392) Şahin, B.; İlgün, G. Risk Factors of Deaths Related to Cardiovascular Diseases in World Health Organization (WHO) Member Countries. *Health Soc. Care Community* **2022**, *30* (1), 73–80. https://doi.org/https://doi.org/10.1111/hsc.13156.

(393) Gupta, A.; Sharma, S. K.; Pachauri, V.; Ingebrandt, S.; Singh, S.; Sharma, A. L.; Deep, A. Sensitive Impedimetric Detection of Troponin I with Metal-Organic Framework Composite Electrode. *RSC Adv.* **2021**, *11* (4), 2167–2174.

https://doi.org/10.1039/d0ra06665f.

(394) Yuan, Z.; Wang, L.; Chen, J.; Su, W.; Li, A.; Su, G.; Liu, P.; Zhou, X. Electrochemical Strategies for the Detection of CTnI. *Analyst* **2021**, *146* (18), 5474–5495. https://doi.org/10.1039/d1an00808k.

(395) Yola, M. L.; Atar, N. Amperometric Galectin-3 Immunosensor-Based Gold Nanoparticle-Functionalized Graphitic Carbon Nitride Nanosheets and Core-Shell Ti-MOF@COFs Composites. *Nanoscale* **2020**, *12* (38), 19824–19832. https://doi.org/10.1039/d0nr05614f.

(396) Ling, Y.; Chu, Y.; Gao, F.; Feng, Q.; Xie, H.; Shao, Y.; Wang, Q. Immunoaffinity-Induced Signal Depression of Cu-MOF-74 for Label-Free Electrochemical Detection of Cardiac Troponin I. *J. Phys. Chem. C* **2022**, *126* (22), 9416–9424. https://doi.org/10.1021/acs.jpcc.2c02455.

(397) Palanisamy, S.; Senthil Raja, D.; Subramani, B.; Wu, T.-H.; Wang, Y.-M. Label-Free Bimetallic in Situ-Grown 3D Nickel-Foam-Supported NH<inf>2</Inf>-MIL-88B(Fe<inf>2</Inf>Co)-MOF-Based Impedimetric Immunosensor for the Detection of Cardiac Troponin I. *ACS Appl. Mater. Interfaces* **2020**, *12* (29), 32468–32476. https://doi.org/10.1021/acsami.0c09086.

(398) Feng, S.; Yan, M.; Xue, Y.; Huang, J.; Yang, X. Electrochemical Immunosensor for Cardiac Troponin I Detection Based on Covalent Organic Framework and Enzyme-Catalyzed Signal Amplification. *Anal. Chem.* **2021**, *93* (40), 13572–13579. https://doi.org/10.1021/acs.analchem.1c02636.

(399) Dong, S.; Zhang, D.; Cui, H.; Huang, T. ZnO/Porous Carbon Composite from a Mixed-Ligand MOF for Ultrasensitive Electrochemical Immunosensing of C-Reactive Protein. *Sensors Actuators B Chem.* **2019**, *284*, 354–361. https://doi.org/https://doi.org/10.1016/j.snb.2018.12.150.

(400) Li, M.; Xia, X.; Meng, S.; Ma, Y.; Yang, T.; Yang, Y.; Hu, R. An Electrochemical Immunosensor Coupling a Bamboo-like Carbon Nanostructure Substrate with Toluidine Blue-Functionalized Cu(Ii)-MOFs as Signal Probes for a C-Reactive Protein Assay. *RSC Adv.* **2021**, *11* (12), 6699–6708. https://doi.org/10.1039/d0ra09496j.

(401) Liu, T.-Z.; Hu, R.; Zhang, X.; Zhang, K.-L.; Liu, Y.; Zhang, X.-B.; Bai, R.-Y.; Li, D.; Yang, Y.-H. Metal–Organic Framework Nanomaterials as Novel Signal Probes for Electron Transfer Mediated Ultrasensitive Electrochemical Immunoassay. *Anal. Chem.* **2016**, *88* (24), 12516–12523. https://doi.org/10.1021/acs.analchem.6b04191.

(402) Gupta, A.; Sharma, S. K.; Pachauri, V.; Ingebrandt, S.; Singh, S.; Sharma, A. L.; Deep, A. Sensitive Impedimetric Detection of Troponin I with Metal–Organic Framework Composite Electrode. *RSC Adv.* **2021**, *11* (4), 2167–2174. https://doi.org/10.1039/D0RA06665F.

(403) Ahmadi, A.; Khoshfetrat, S. M.; Mirzaeizadeh, Z.; Kabiri, S.; Rezaie, J.; Omidfar,

K. Electrochemical Immunosensor for Determination of Cardiac Troponin I Using Two-Dimensional Metal-Organic Framework/Fe3O4–COOH Nanosheet Composites Loaded with Thionine and PCTAB/DES Modified Electrode. *Talanta* **2022**, *237*, 122911. https://doi.org/https://doi.org/10.1016/j.talanta.2021.122911.

(404) Palanisamy, S.; Senthil Raja, D.; Subramani, B.; Wu, T.-H.; Wang, Y.-M. Label-Free Bimetallic in Situ-Grown 3D Nickel-Foam-Supported NH2-MIL-88B(Fe2Co)-MOF-Based Impedimetric Immunosensor for the Detection of Cardiac Troponin I. *ACS Appl. Mater. Interfaces* **2020**, *12* (29), 32468–32476. https://doi.org/10.1021/acsami.0c09086.

(405) Zhang, T.; Huang, C. H. Simultaneous Quantification of Peracetic Acid and Hydrogen Peroxide in Different Water Matrices Using HPLC-UV. *Chemosphere* **2020**, *257*, 127229. https://doi.org/10.1016/j.chemosphere.2020.127229.

(406) Mohan, B.; Dhiman, D.; Virender; Mehak; Priyanka; Sun, Q.; Jan, M.; Singh, G.; Raghav, N. Metal-Organic Frameworks (MOFs) Structural Properties and Electrochemical Detection Capability for Cancer Biomarkers. *Microchem. J.* **2023**, *193*, 108956. https://doi.org/https://doi.org/10.1016/j.microc.2023.108956.

(407) Mathew, G.; Daniel, M.; Peramaiah, K.; Ganesh, M. R.; Neppolian, B. Real-Time Electrochemical Quantification of H2O2 in Living Cancer Cells Using Bismuth Based MOF. *J. Electroanal. Chem.* **2022**, *914*. https://doi.org/10.1016/j.jelechem.2022.116255.

(408) Huang, W.; Xu, Y.; Sun, Y. Functionalized Graphene Fiber Modified With MOF-Derived Rime-Like Hierarchical Nanozyme for Electrochemical Biosensing of H2O2 in Cancer Cells. *Front. Chem.* **2022**, *10* (March), 1–11. https://doi.org/10.3389/fchem.2022.873187.

(409) Weizhou, Fan; Xiaohong, Liu; Jinsheng, Wu; Qian, Liu; Lan, Ding; Xiuhui, L. Electroanalysis - 2021 - Fan - Development of a Novel Silver- based Sensing Platform for Detecting Superoxide Anion Released.Pdf. Electroanalysis 2021. chrome-extension://efaidnbmnnnibpcajpcglclefindmkaj/https://analyticalsciencejournals.onlinelibrary.wiley.com/doi/pdfdirect/10.1002/elan.202100254.

(410) Li, J.; Lee, S. H.; Yoo, D. K.; Woo, H. C.; Jhung, S. H.; Jović, M.; Girault, H.; Lee, H. J. A Spatially Multiplexed Voltammetric Magneto-Sandwich Assay Involving Fe3O4/Fe-Based Metal-Organic Framework for Dual Liver Cancer Biomarkers. *Sensors Actuators B Chem.* **2023**, *380*, 133313. https://doi.org/https://doi.org/10.1016/j.snb.2023.133313.

(411) Zhang, Y.; Zhu, H.; Ying, Z.; Gao, X.; Chen, W.; Zhan, Y.; Feng, L.; Liu, C. C.; Dai, Y. Design and Application of Metal Organic Framework ZIF-90-ZnO-MoS2Nanohybrid for an Integrated Electrochemical Liquid Biopsy. *Nano Lett.* **2022**, *22* (16), 6833–6840. https://doi.org/10.1021/acs.nanolett.2c01613.

(412) Zhang, Y.; Li, N.; Xu, Y.; Yang, M.; Luo, X.; Hou, C.; Huo, D. An Ultra-Sensitive

Electrochemical Aptasensor Based on Co-MOF/ZIF-8 Nano-Thin-Film by the in-Situ Electrochemical Synthesis for Simultaneous Detection of Multiple Biomarkers of Breast Cancer. *Microchem. J.* **2023**, *187*, 108316. https://doi.org/https://doi.org/10.1016/j.microc.2022.108316.

(413) Zha, R.; Wu, R.; Zong, Y.; Wang, Z.; Wu, T.; Zhong, Y.; Liang, H.; Chen, L.; Li, C.; Wang, Y. A High Performance Dual-Mode Biosensor Based on Nd-MOF Nanosheets Functionalized with Ionic Liquid and Gold Nanoparticles for Sensing of CtDNA. *Talanta* **2023**, *258*, 124377. https://doi.org/https://doi.org/10.1016/j.talanta.2023.124377.

(414) Xia, Q.; Mu, Z.; Qing, M.; Zhou, J.; Bai, L. A Sandwich-Type Electrochemical Immunosensor for Sensitive Detection of HER2 Based on Dual Signal Amplification of La-MOF-PbO2 and PEI-MoS2NFs Composites. *Bioelectrochemistry* **2023**, *152*, 108431. https://doi.org/https://doi.org/10.1016/j.bioelechem.2023.108431.

(415) Xiang, L.; Cheng, W.; Zhang, J.; Li, X.; Khan, A.; Yi, Y.; Li, J. Signal-off Electrochemical Sensor for Matrix Metalloproteinase 9 Detection Based on Sacrificial FeMOF and Host-Guest Strategy. *Biosens. Bioelectron.* **2023**, *237*, 115455. https://doi.org/https://doi.org/10.1016/j.bios.2023.115455.

(416) Huang, X.; Deng, X.; Deng, Z.; Huang, C.; Zhu, X.; Sun, L. Simultaneous Detection of Two Tumor Markers Using Electrochemical Immunosensor Based on Ultrathin Metal–Organic Framework Derived Nanosheets as Redox Probes. *New J. Chem.* **2023**, *47* (24), 11651–11659. https://doi.org/10.1039/D3NJ01245J.

(417) Hu, R.; Zhong, S.; Liu, H.; Liu, Y.; Chen, H.; Hu, X. Laccase-Inspired Bi-Amino Acid MOFs with High Substrate Affinity: Catalytic Deposition Induced “Signal-down” Electrochemical Response towards PD-L1. *Sensors Actuators B Chem.* **2024**, *399*, 134773. https://doi.org/https://doi.org/10.1016/j.snb.2023.134773.

(418) Zhang, Y.; Xu, Y.; Li, N.; Ma, W.; Yang, M.; Hou, C.; Huo, D. An Ultra-Sensitive Dual-Signal Ratio Electrochemical Aptasensor Based on Functionalized Bimetallic MOF Nanocomplexes by the in-Situ Electrochemical Synthesis for Detect HER2. *Int. J. Hydrogen Energy* **2023**, *48* (63), 24548–24558. https://doi.org/https://doi.org/10.1016/j.ijhydene.2023.03.169.

(419) Vijayaraghavan, P.; Wang, Y. Y.; Palanisamy, S.; Lee, L. Y.; Chen, Y. K.; Tzou, S. C.; Yuan, S. S. F.; Wang, Y. M. Hierarchical Ensembles of FeCo Metal-Organic Frameworks Reinforced Nickel Foam as an Impedimetric Sensor for Detection of IL-1RA in Human Samples. *Chem. Eng. J.* **2023**, *458* (January), 141444. https://doi.org/10.1016/j.cej.2023.141444.

(420) Liu, F.; Geng, L.; Ye, F.; Zhao, S. MOF-Derivated MnO@C Nanocomposite with Bidirectional Electrocatalytic Ability as Signal Amplification for Dual-Signal Electrochemical Sensing of Cancer Biomarker. *Talanta* **2022**, *239*, 123150. https://doi.org/https://doi.org/10.1016/j.talanta.2021.123150.

(421) Sadrabadi, E. A.; Benvidi, A.; Azimzadeh, M.; Asgharnejad, L.; Dezfuli, A. S.; Khashayar, P. Novel Electrochemical Biosensor for Breast Cancer Detection, Based on a Nanocomposite of Carbon Nanofiber, Metal–Organic Framework, and Magnetic Graphene Oxide. *Bioelectrochemistry* **2024**, *155*, 108558.